Alma Mater Studiorum - Università di Bologna

DOTTORATO DI RICERCA IN

INGEGNERIA ELETTRONICA, TELECOMUNICAZIONI E TECNOLOGIE DELL'INFORMAZIONE

Ciclo 35

**Settore Concorsuale:** 09/F2 - TELECOMUNICAZIONI

**Settore Scientifico Disciplinare:** ING-INF/03 - TELECOMUNICAZIONI

# USER SCHEDULING FOR LOW EARTH ORBIT MULTI-USER MULTIPLE-INPUT-MULTIPLE-OUTPUT NON-TERRESTRIAL NETWORK SYSTEMS

**Presentata da:** Bilal Ahmad

**Coordinatore Dottorato**

Prof. Aldo Romani

**Supervisore**

Prof. Alessandro Vanelli-Coralli

**Co-Supervisore**

Prof. Alessandro Guidotti

Dr. Daniel Gaetano Rivello

**Esame finale anno 2023**

## Abstract

In rural and isolated areas without cellular coverage, Satellite Communication (SatCom) is the best candidate to complement terrestrial coverage. Thanks to this, future generations of Terrestrial Network (TN)'s are expected to make extensive use of Non-Terrestrial Network (NTN)'s for improving the coverage and capacity to truly achieve global connectivity. In addition, the next generations of wireless networks are anticipated to be able to connect an extremely large number of devices at high throughput with minimum latency. Due to its less demanding requirements in terms of power consumption and propagation latency compared to the Geostationary Earth Orbit (GEO) counterpart, Low Earth Orbit (LEO), based NTN systems are anticipated to be game changers to fulfill several different B5G and Sixth Generation (6G) use cases.

However, the main challenge for future generations of wireless networks will be to meet the growing demand for new services while dealing with the scarcity of frequency spectrum. As a result, it is critical to investigate more efficient methods of utilizing the limited bandwidth; and resource sharing is likely the only choice. The research community's focus has recently shifted towards the interference management and exploitation paradigm to meet the increasing data traffic demands. To increase the transmission data rates the recent trend is to adopt the Multi-beam (MB) architectures to obtain higher power flux density per beam and increase the spectrum's reuse factors. From the current State-of-the-Art literature, one possible way to reduce the Co-Channel Interference (CCI)/ Inter-beam Interference (IBI), is the exploitation of the available spectrum bandwidth, by adding unused or underutilized spectrum chunks via flexible spectrum usage paradigms e.g., Cognitive Radio solutions or by fully exploiting the spectrum by lowering the frequency reuse factors. In contrast to a Four-Color Frequency reuse (FR4C) scheme, in which orthogonality between adjacent

beams is ensured through the use of disjoint frequencies and polarizations, the Full Frequency reuse (FFR) of the spectrum has recently been considered.

Among others, Multi-User (MU)-Multiple-Input-Multiple-Output (MIMO) has become one of the NTN's key enablers. It can improve data rates and enhance spectral efficiency. In the Downlink (DL) and Feedspace (FS), LEO satellites with an on-board antenna array can offer service to numerous User Terminals (UTs) (VSAT or Handhelds) on-ground in FFR schemes by using cutting-edge digital beamforming techniques. Considering this setup, the adoption of an effective user scheduling approach is a critical aspect given the unusually high density of User terminals on the ground as compared to the on-board available satellite antennas. In particular, scheduling users in similar channel conditions might lead the channel matrix to be rank deficient and, thus, to poor performance. In this context, one possibility is that of exploiting clustering algorithms for scheduling in LEO MU-MIMO systems in which several users within the same group are simultaneously served by the satellite via Space Division Multiplexing (SDM) also known as digital beamforming or MU-MIMO techniques and then these different user groups are served in different time slots via Time Division Multiplexing (TDM). It is well known that the implementation of an ideal user grouping method is an NP-complete problem that can only be resolved through exhaustive searching.

With this in mind and the growing interest in NTN systems, novel techniques are needed to solve the complex user scheduling problem. This thesis addresses this problem by defining a user scheduling problem as an optimization problem and discusses several algorithms to solve it. In particular, focusing on the FS and user service link (i.e., DL) of a single MB-LEO satellite operating below 6 GHz, the user scheduling problem in the Frequency Division Duplex (FDD) mode is addressed. The proposed State-of-the-Art scheduling approaches are based on graph theory and the maximum clique algorithm. Both user scheduling and beamforming are addressed

jointly as they are inextricably linked because the interference between scheduled users is determined by the beamforming design, which is determined by the scheduled users in other beams. To boost the sum-rate capacity of the system, a heuristic optimization of the graph density—the ideal cluster size—is carried out. The capacity (Mbps), Signal-to-Interference-Plus-Noise-Ratio (SINR) [dB], and spectral efficiency (b/s/Hz) are the metrics used to assess performance. To verify the outcomes, the suggested graph-based techniques are compared with the well-known and well-established classical algorithms which include Position-based scheduler and Multiple Antenna Downlink Orthogonal clustering (MADOC). Furthermore, to address the issue of group number minimization i.e., maximizing the per-cluster sum-rate capacity, a novel strategy is proposed which is based on a low-complex graph-based iterative procedure with constant graph density and variable graph threshold value per-cluster. This solution significantly improves the sum-rate capacity, offers higher throughput, and allows a significant reduction in the variance of the cluster size distribution, thus improving the fairness among users and the overall performance.

*Part of this work has been supported by the H2020 project, Dynamic Spectrum Sharing, and Bandwidth-Efficient Techniques for High-Throughput MIMO Satellite Systems (DYNASAT), grant agreement 101004145.*

## Acknowledgements

First and foremost, I wish to thank my Supervisor, Professor Alessandro Vanelli-Coralli. He has been extremely supportive since the days he offered me a Ph.D. Position in his Research Lab (DIGICOMM). Although I joined the Ph.D. program extremely late due to some issues and when I reached Italy, it was COVID-19 lockdown. Because of his help and support all my issues got compensated. In fact, He is my role model and in the future, I want to be like him. My son who is now 5 years old calls him a "superpower". Not only academically but emotionally he mentored me. It is not only me, but my family has discovered a true gentleman with high moral grounds and someone who is extremely composed. But, it is also the fact that he is extremely challenging, critical, and qualitative when it comes to academics. I have always found him extremely busy, focused, and highly committed. I find myself extremely lucky that he is my supervisor and he has provided his guidance to me. This is my personal opinion and I believe that one has two names that are written with him/ her. One is the father's name, and the other is the Ph.D. Supervisor. I have no words to express what it means to me to have the name of Professor Alessandro Vanelli-Coralli in my academic journey. It is just an unbelievable feeling to me.

Next, I would like to thank Professor Alessandro Guidotti. Because of him, I had the opportunity to work on his developed State-of-the-Art simulator for the DYNASAT project. Also, his scientific contributions helped me a lot during my journey.

Then, I would like to thank Dr. Daniel Gaetano Riviello, who guided me. Because of him, I started with Graph Theory. Whenever I needed him, he was always there to help me out. He is someone who always comes up with new and exciting challenging ideas.

Also, A Special thanks to:

- all of those who taught me different courses during my Ph.D. journey and also the Ph.D. Coordinator and the DEI-Administration.
- my colleagues Carla Amatetti, M Rabih Dakkak, Riccardo Campana, and Bruno De Filippo. They all are like my family members.
- the person who has been amazing, a friend, and someone very excited to spend time with is Swapnil Sadashiv Shinde. He always supported me and accompanied me when I was depressed.
- Dr. Murtaza, who helped me out on various occasions. He is the one who was always available when I faced problems.

For my wife (Sehrish Malik), my son (Muhammad Shahwaiz Bilal), and my newly born daughter (Hazel Bilal), "I Love you all. You all are my life and this thesis is dedicated to you". I will do whatever I can to make you all feel happy and secure in the future so that you can live your dreams. Finally, for my parents and my three sisters, I believe that you will be very happy and proud of my achievements.

# Table of Contents

# List of Figures

# List of Tables

# Abbreviations

**3GPP** Third Generation Partnership Project

**5G** Fifth Generation

**6G** Sixth Generation

**BK** Bron-Kerbosh

**CCI** Co-Channel Interference

**CDF** Cummulative Distribution Function

**CoC** Coefficient of Correlation

**CoMP** Coordinated Multi-Point

**CPC** Centralized Precoding Computation

**CSI** Channel State Information

**CU** Centralized Unit

**DL** Downlink

**DPC** Distributed Precoding Computation

**DPC** Dirty Paper Coding

**DU** Distributed Unit

**FDD** Frequency Division Duplex

**FDM** Frequency Division Multiplexing

**FFR** Full Frequency reuse

**FR1** Frequency-range 1

**FR2** Frequency-range 2

**FR4C** Four-Color Frequency reuse

**FS** Feedspace

**GEO** Geostationary Earth Orbit

**GW** Gateway

**HTS** High Throughput Satellite

**IBI** Inter-beam Interference

**ISL** Inter-Satellite Link

**IUI** Inter-User Interference

**LEO** Low Earth Orbit

**LOS** Line of Sight

**MADOC** Multiple Antenna Downlink Orthogonal clustering

**MaxClqDyn** Maximum Clique Dyn

**MB** Multi-beam

**MIMO** Multiple-Input-Multiple-Output

**MISO** Multiple Input Single Output

**MMSE** Minimum Mean Square Error

**MPC** Maximum Power Constraint

**MU** Multi-User

**MUD** Multi-User Detection

**NOMA** Non Orthogonal Multiple Access

**NTN** Non-Terrestrial Network

**PAC** Per-Antenna Power Constraint

**SatCom** Satellite Communication

**SB** Single-beam

**SDM** Space Division Multiplexing

**SINR** Signal-to-Interference-Plus-Noise-Ratio

**SMUG** Sum Rate Maximization User Grouping Algorithm

**SNR** Signal-to-Noise-Ratio

**SPC** Sum Power Constraint

**SSP** Sub-Satellite Point

**TDD** Time Division Duplex

**TDM** Time Division Multiplexing

**TN** Terrestrial Network

**TR** Technical Report

**UL** Uplink

**UPA** Uniform Planar Array

**UTs** User Terminals

**VSAT** Very Small Aperture Terminal

**ZF** Zero-Forcing

# Chapter 1 - Introduction

## 1.1 Motivation

NTN systems are expected to play a significant role in future generations of wireless networks [1]. The primary motivator is that, due to their intrinsic characteristics, these systems can integrate and complement terrestrial coverage, thus extending the provision of data access to all geographical locations, where the terrestrial coverage is not available or financially viable [2], and also improves the network resiliency whenever the terrestrial network is experiencing a malfunctioning or total failure (e.g., natural or man-made disasters). NTN can also help with effective backhauling and improve Fifth Generation (5G) network management, synchronization, and signaling [3, 4]. With the approval of Third Generation Partnership Project (3GPP) Rel-17 and the inclusion of NTN systems in 5G-Advanced and 6G systems, the satellite industry is undergoing rapid growth, paving the way for global access to 6G services [5].

Various technological breakthroughs in the SatCom industry has revealed their potential for future communication systems. Satellites are extremely successful at delivering extensive coverage due to their high position above the earth. One satellite, depending on its elevation, can cover thousands of square kilometers, whereas one cellular antenna on Earth can only cover a few square kilometers.

This is why satellite is typically viewed as a better economical and practical alternative to bring coverage to places that would otherwise be completely unserved.

LEO technology began to take shape at the beginning of the 1990s, as the name implies, an orbit that is close to the Earth's surface. Smaller, lighter satellites orbiting at lower altitudes (between 180 km and 2,000 km) were intended to replace a few high-orbit satellites, particularly GEO orbits (at an elevation of about 36,000 km) where satellites have fixed positions with respect to the Earth. This would significantly lower the cost of the solution as the satellites would be less expensive to produce and launch. But, there are difficulties, both technical and economical.

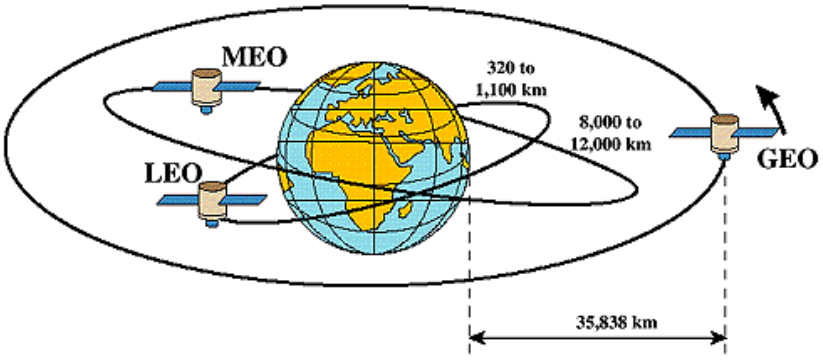


**Figure 1.1:** Communication Satellites [6].

The elevation that characterizes LEO has a direct impact on coverage. At an altitude of 36,000 km, a satellite's coverage area is 2.7 times larger than it is at a height of 1000 km. In GEO, three satellites are required to cover the entire planet; in LEO, a minimum of fifteen satellites are required. The satellites at this elevation are moving, thus more are required to provide continuous coverage.

Nonetheless, there are advantages to the LEO satellite constellation's lower altitude. The fact that satellites are closer to the Earth than GEO satellites means that the latency, which is one of the drawbacks of GEO satellites generally, is considerably decreased as well as the trip time between the ground and the satellite and the satellite and the ground. For real-time applications, such as voice, latency is crucial [7].

Frequency bands are of course of critical importance for any wireless communication system whether it is a TN, or a NTN. To increase the throughput and capacity, more spectrum is required. Previously, only a limited amount of spectrum was required to provide voice or messaging services. With the development of new data-intensive usages such as video consumption, and access to the cloud, holding a limited amount of spectrum is no longer an option and most players are fighting to get this access. The 5G technology supports two alternative frequency ranges, Frequency-range 1 (FR1) and Frequency-range 2 (FR2). FR1 bands are intended to carry the majority of the traffic for conventional mobile communications. The higher frequency bands in the FR2 range are intended to provide the 5G radio short-range, very high data rate capacity. The additional bandwidth of these higher frequency bands will be required to meet the expectations of the users in order to deliver the data at higher speeds. The FR1 or sub 6 GHz spectrum band has some special features, including guaranteed wide coverage for both indoor and outdoor use cases, increased capacity, support for up to 7 Gbps data rate, reduced sensitivity to obstruction and other environmental conditions, and readily available equipment that requires little in the way of

capital expenditure (CAPEX) and time. The FR1 band was initially intended to specify bands below 6 GHz, however, following World Radio Conference in 2019 (WRC19) where global spectrum allocations were agreed upon, the FR1 range was increased to 7.125 GHz [8]. Due to different atmospheric factors in the troposphere, the performance and availability of the future generations of High Throughput Satellite (HTS) operating in FR2 will be significantly reduced for the Line of Sight (LOS). Rainfall attenuation is the most important and prominent atmospheric influence, especially in the Ka-band. As a result, link budget modeling must strongly take into account the impact of rainfall attenuation. The transmitting and receiving gain of omnidirectional antennas designed for UTs on-ground is insufficient to meet the link budget due to the high frequency of the Ka-band and the considerable free space loss of electromagnetic waves. Therefore, satellite mobile services are often delivered by lower band satellites, and the Ka-band HTS is only appropriate for providing the fixed user services [1, 9].

The LEO business model can be presented with five essential components. On the cost side, the four elements are the cost related to the satellites, launching, ground stations, and UTs. The quantity of subscribers that will generate the revenue is the fifth factor. These components interrelate with each other with other variables that control their interdependency, such as spectrum assets, performance indicators, and the quality of service. Also, the huge geographical digital divide is non-negligible in conventional TNs caused by harsh terrain environments. In light of this, future B5G or even 6G integrated with space-based LEO constellations is expected to bridge the digital divide. This will be done by

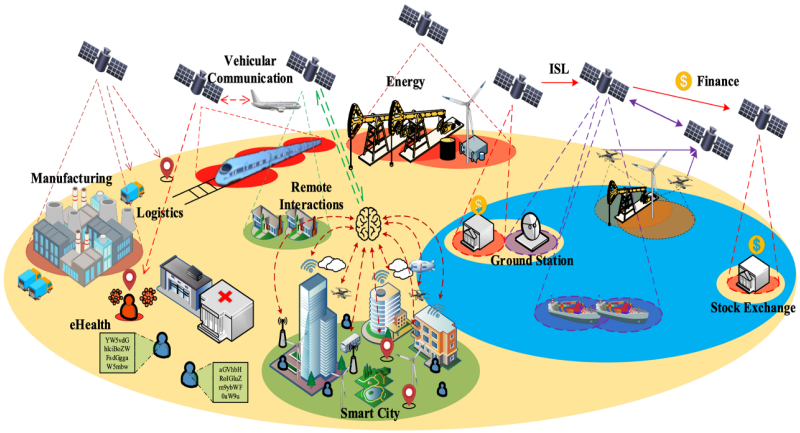


**Figure 1.2:** Ambitious vision of various vertical domains reshaped by LEO satellite constellations [10].

altering the existing vertical domains and presenting a wide range of options for emerging enterprises as depicted in Fig. 1.2 [10].

The expectation from the future generations of wireless telecommunication is to use SatCom technology at a reasonable cost. To better use the limited available frequency spectrum, one of the accomplishments in SatCom is the transition from Single-beam (SB) to MB transmission design, which provides numerous benefits. MB architectures, as opposed to SB architectures, enable spatially multiplexed communication by concurrently transmitting different data streams to geographically separated areas. Furthermore, available radio resources can be reused across beams, thus increasing the user bandwidth [11, 12]. Therefore it is extremely critical to focus on the increasing spectral efficiency in MB satellite systems in order to achieve the maximum performance w.r.t. limited satellite resources (power and bandwidth) [13].

However, the main challenge for future generations of TN systems will be to meet the growing demand for new services while dealing with the scarcity of frequency spectrum [14]. As a result, it is critical to investigate more efficient methods of utilizing the limited bandwidth, with resource sharing likely being the only option. The research community's focus has recently shifted toward the interference management and exploitation paradigm to meet the increasing data traffic demands. Interference is no longer avoided by design with the advent of precisely engineered transceiver architectures but is instead purposefully introduced and then mitigated or exploited. In the existing literature, it has been demonstrated that this paradigm shift can provide extraordinarily high benefits when compared to the interference avoidance strategy used by conventional systems [14–17].

Conceptually, adding more antennas at the satellite increases the system capacity, thus enhancing energy efficiency and significantly boosting the NTN systems' throughput [18–21]. The requirements of future satellite-based 6G's high transmission rates and extremely reliable communication can be well met by the MU-MIMO technology. However, this technology must deal with new issues including constrained system resources and dependable communication of dynamic users, which are brought on by a dramatic rise in the number of antennas, densification, and beam directionality. Designing algorithms that can address the issue of scarce system resources in the LEO-MU-MIMO system is therefore extremely crucial and challenging for NTN communications [22]. This thesis presents various novel solutions based on the graph theory framework to address the user

scheduling problem focusing on FS and the user service link i.e., DL of a single MB-LEO satellite operating below 6 GHz in FDD mode, oriented to improve the systems sum-rate capacity. Users are grouped together based on the dissimilarity metric and served by the satellite via SDM by means of Minimum Mean Square Error (MMSE) digital beamforming on a cluster basis. Clusters are then served in different time slots via TDM. Aggressive frequency i.e., FFR reuse of bandwidth, combined with CCI mitigation techniques, is being considered to improve spectral efficiency in the coverage area which is divided into several spot beams. Both User scheduling and beamforming are addressed jointly. A heuristic optimization of the graph density, that is the ideal cluster size, is performed to increase the system sum-rate capacity. The performance is measured in terms of capacity (Mbps), the SINR [dB], and the spectral efficiency (b/s/Hz). Furthermore, the proposed graph-based approach is compared to well-established classical algorithms to validate the results. To improve the results further finally, a low-complex graph-based iterative procedure with constant graph density is proposed. This novel scheduling approach aims to improve fairness among the users and overall performance. The extensive simulation results demonstrate that this significantly improves the sum-rate capacity, offers higher throughput, and allows a significant reduction in the variance of the cluster size distribution. To increase transmission data rates, MB transmission techniques have been widely used. In the following section, the possibility of adopting different existing solutions to IBI management is discussed.

## 1.2 Interference Management and the Exploitation of Advanced Transmission Techniques for MB-LEO MU-MIMO NTN Systems

LEO satellites launched in LEO orbit deliver stronger signals because they are closer to the earth. As a result, less power (roughly about 1 watt) is required for the transmission. Because of its proximity to the Earth, it has the smallest propagation delay (approximately 10 ms), when compared to other orbits. It can be utilized for real-time, time-sensitive applications because of the lower latency. Due to the higher Carrier to Noise (C/N) signal ratio, heavy reception equipment is not necessary. Moreover, smaller footprints allow for achieving better frequency reuse [23, 24].

To mimic the TN, operating in different frequency bands typically S or Ka-band (depending on the offered type of service and the channel propagation conditions) the current trend is the design shift from SB to MB architectures. In this context, the payload has a variety of feeds so that data can be broadcast simultaneously to various spot beams on the ground with a specific frequency reuse pattern. With such a setup, beams that are far enough apart from one another can efficiently reuse bandwidth.

In Fig. 1.3, an end-to-end MB system architecture from the gateway Gateway (GW) to the user terminals (UTs) is shown. It can be seen that the UTs communicate through the feeder link which is fed MB antenna pattern to receive and broadcast data. The feeder link's available bandwidth must be large enough to accommodate the frequency re-use strategy adopted for the user beams.

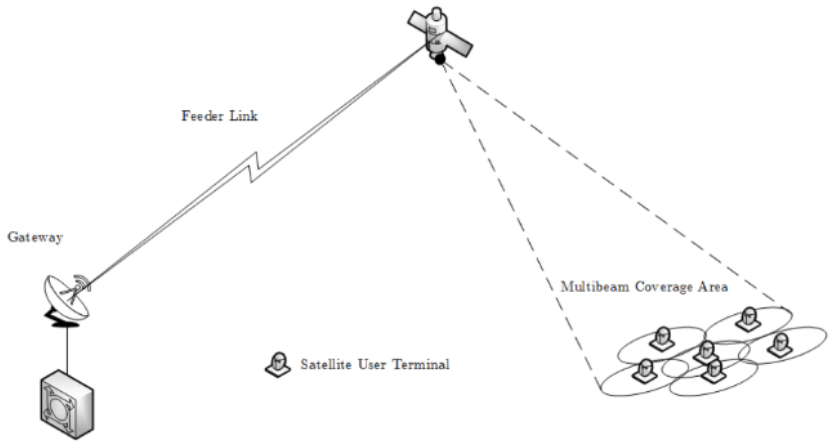


**Figure 1.3:** Architecture of Multi-beam SatCom System [25].

The satellite's projection of the beam-generating process on Earth enables adaptive coding and modulation (ACM) to adapt distinct information streams at different rates to the underlying channel conditions. Nevertheless, sharing the frequency among several spot beams causes CCI/ IBI between nearby ones. Since it is impossible to have completely isolated spot beams, a planned overlap between them is created, resulting in a regulated carrier-to-co-channel interference ratio (C/I).

As a result, through the antenna sidelobes of a specific beam, the transmit signal is partially radiated to the corresponding adjacent beams. The feasible SINR, which depends on the frequency reuse method and the UTs position, is degraded by the produced interference even when the received power levels of the adjacent beams are not as high as the intended one. Legacy SatCom systems use multi-color frequency reuse schemes to spatially reuse available resources while minimizing interference from beam side lobes. MB transmission techniques have

been widely used in SatCom systems to increase transmission data rates. To reduce CCI/ IBI, One possible way to reach it is the exploitation of the available spectrum bandwidth, by exploiting the unused or underutilized spectrum chunks via flexible spectrum usage paradigms (e.g., Cognitive Radio solutions [26–28]), or by fully exploiting the spectrum by lowering the frequency reuse factors. The frequency band is frequently divided into four sub-bands for high throughput satellite (HTS) systems so that near adjacent beams have disconnected frequency bands. By using orthogonal polarizations, the spot beams can be then separated to a greater extent. Higher antenna gain and frequency reuse capacity are the two major performance criteria that mobile satellite communication systems must meet. The beam size must be reduced in order to offer the edge of cell edge of coverage (EOC) directivity and the beam roll-off rate necessary to accomplish inter-beam isolation. Hence, many more beams and cells are required to cover a specific region. This results in reflectors and feed arrays that are much bigger and have a lot more radiating elements. While spatial frequency reuse employs the same frequency in more distant beams, it assigns different frequencies to neighbor beams. A consistent grid of beams must be used for this to be accomplished effectively. Fig. 1.4, illustrates the frequency reuse schemes with 3, 4, and 7 colors [29].

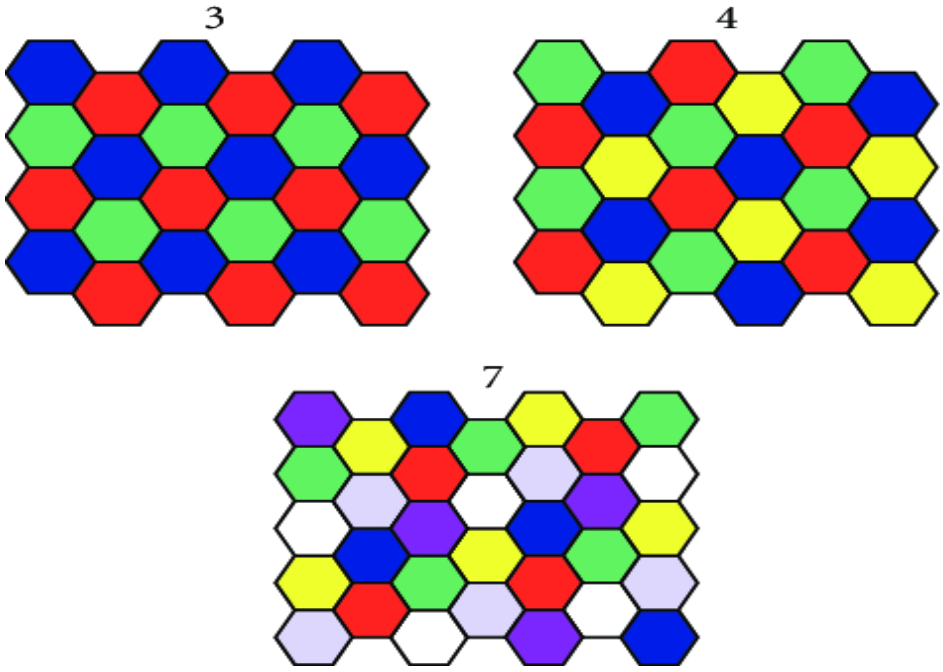


**Figure 1.4:** Frequency reuse schemes with 3, 4, and 7 colors [29].

One of the most widely adopted solutions for the future generations of HTS is to define a 4-color frequency reuse scheme FR4C, that enables frequency reuse with little interference from nearby spot beams. Each beam is given half of the bandwidth that is available and uses one of the two polarizations i.e., Right Hand Circular Polarization (RHCP) or Left Hand Circular Polarization (LHCP) as illustrated in Fig. 1.5 [30]. Due to the frequency reuse via orthogonal polarizations, a cluster of four beams benefits from an equivalent bandwidth (BW) equal to twice the bandwidth (BW) allocated to the satellite. Hence, the overall

bandwidth of the satellite system is equal to

$$\mathbf{B}_{Wtotal} = \frac{2\, N_b\, B_w}{N_c} \tag{1.1}$$

where $N_b$ = Number of Beams in the Satellite, $N_c$ = Number of colors, and $\mathbf{B}_{Wtotal}$= Total Bandwidth.

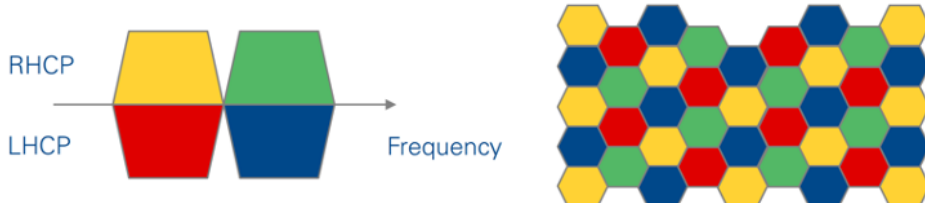


**Figure 1.5:** Example of a 4-color pattern and allocation of colors to multiple beams providing continuous coverage [30].

The capacity i.e., the total transmitted bit rate of the satellite is multiplied by a factor $\frac{2\, N_b}{N_c}$ known as the frequency reuse factor, allowing for significant capacity gains when compared to a single beam satellite. System capacity and an acceptable level of interference are traded off to determine the number of colors and the corresponding frequency reuse factor. Therefore, to improve the spectral efficiency of SatCom systems, more aggressive FFR schemes with reduced colors are adopted [31–35] but at the cost of an increased interference that must be controlled at the receiver and/or transmitter to achieve the required performance. For this thesis FFR is adopted as illustrated in Fig. 1.6.

Considerably, in FFR, IBI becomes a critical issue that must be addressed properly. In general, IBI management can be performed at either the transmitter

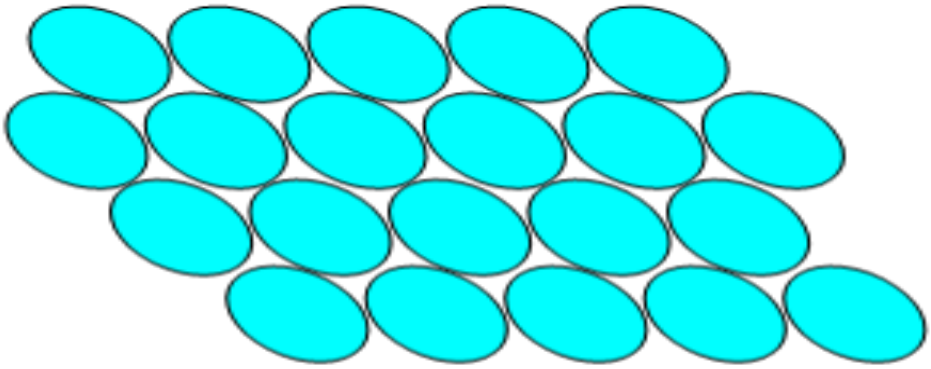

**Figure 1.6:** One-color frequency reuse FFR [25].

via precoding [4, 36–38] or at the receiver via Multi-User Detection (MUD). In the current literature, several bandwidth-efficient techniques for NTN systems are discussed which can be used at the transmitter and/or the receiver, some of which have been adapted from the literature on terrestrial networks. MU-MIMO cooperation techniques, such as Coordinated Multi-Point (CoMP) for 5G systems [39], Non Orthogonal Multiple Access (NOMA) for NTN systems [40], time-frequency packing for NTN systems [41], MUD at the receiver [42], etc. are a few examples. Also, the implementation of multiple spot beams allows the exploitation of the frequency reuse principle, thus leading to more efficient use of the spectrum [43] but with high CCI. The MB-LEO satellite transmits the signals to the beams on the surface of the Earth after they are generated at either one or several gateways. By decreasing the frequency reuse factor down to one, i.e., FFR schemes, the same spectrum resources are exploited for all beams simultaneously.

Fig. 1.7 represents a typical 71-beam GEO satellite coverage of Europe, which is adopted by the current broadcast and unicast systems.

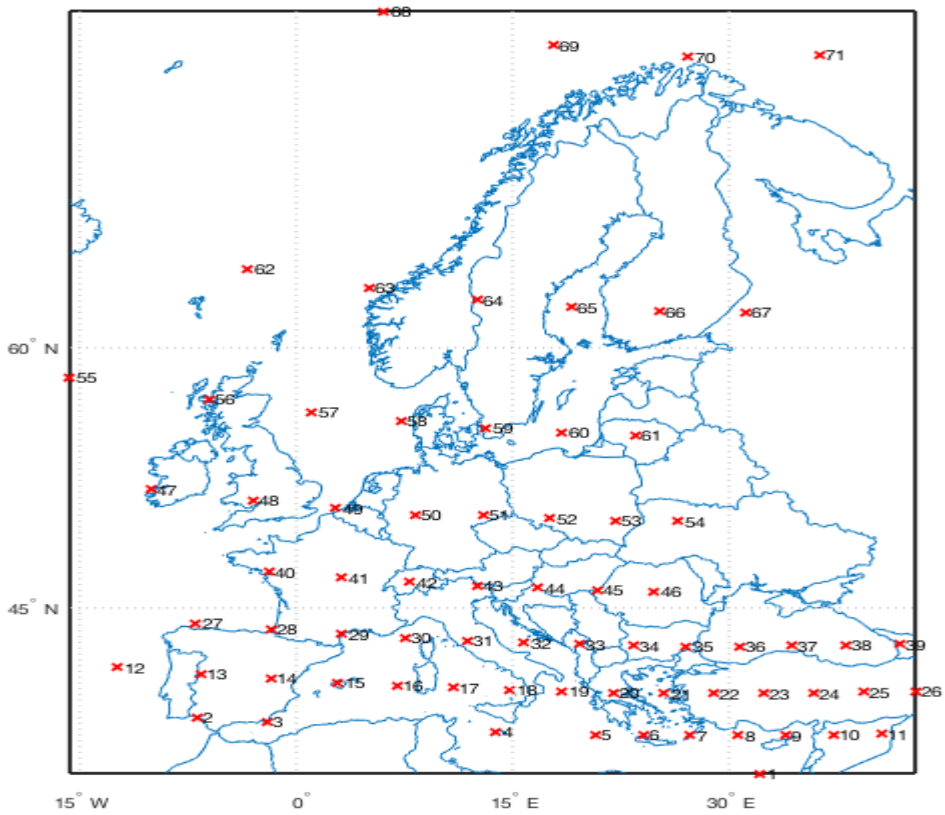


**Figure 1.7:** A Typical 71-Beam GEO Satellite Coverage of Europe with the red crosses identifies the beam centers [1].

In the existing literature, different precoding techniques have been extensively discussed, assessed, and evaluated as reported in [44–51] (and the references therein). Precoding is considered one of the key technologies in the MU-MIMO systems. It transforms the complexity system from the side of user terminals to the side of the satellite by using a strong signal processing technology at the transmitter side [52]. Typically, in a real wireless propagation environment, obtaining reliable Channel State Information (CSI) is difficult, as DL transmission performance is heavily dependent on CSI. Precoding technology can be used to

deal with imperfect CSI. Furthermore, MU-MIMO precoding technology plays a critical role in breaking down the system's performance by controlling the direction of the beams and directing them to a specific received terminal location [52]. Research related to TN's reveals, that when the number of antennas approaches infinity, the adoption of precoding technology in MU-MIMO systems eliminates the effects of interference and fading while increasing throughput and capacity [53]. The precoding algorithms are broadly classified as linear, non-linear, peak-to-average power ratio (PAPR), and machine learning based [54].

Although precoding techniques can improve performance, However, there must be a trade-off between computational complexity and performance reduction. For example, Dirty Paper Coding (DPC) achieves the best capacity [44], but due to its high computational complexity, it is still not widely used in existing practical systems. Due to its non-linearity, DPC has high computational complexity. Tomlinson-Harashima precoding [45], another non-linear precoding method, involves modular operation at both the transmitter and the receiver but is likewise impracticable for real-time implementation given the existing capacity of processors. Due to their low processing cost and close to the ideal performance, linear precoding and detection are more desirable in MB SatCom systems compared to non-linear DPC precoding and MUD [55].

Two widely adopted linear precoders in MB-LEO NTN systems are Zero-Forcing (ZF) and MMSE also known as R (regularized)-ZF [9, 56]. ZF is the most classical algorithm. The main idea is at the transmitting end first multiply the modulated signal $s$ by the inverse matrix of the channel matrix. To eliminate the

signal interference, the precoding processed signal is transmitted via the channel and multiplied by a channel matrix. The concept is expressed in mathematical terms and is comparable to $\mathbf{HW}_{ZF} = \mathbf{I}$, where $\mathbf{H}$ is the channel matrix, and $\mathbf{I}$ is the identity matrix. The pseudo-inverse of the channel matrix is calculated to produce the precoding matrix. To totally eradicate CCI. The number of antennas installed at the relay must be greater than the number of interferences [57]. The ZF precoding matrix has the following expression

$$\mathbf{W}_{ZF} = (\mathbf{H}^H\mathbf{H})^{-1}\mathbf{H}^H \tag{1.2}$$

By normalizing each column vector in the ZF precoding matrix, the precoding vector for a corresponding user can be obtained in a practical application. Equation 1.2 shows that the ZF precoding algorithm can eliminate interference from other users using the same frequency. This precoding technique, however, is considered ideal only when the additive noise is absent. In the event of low Signal-to-Noise-Ratio (SNR), the achieved system performance is suboptimal.

In the case of high SNR, ZF precoding is asymptotically optimal, but it does not take into account the effects of channel noise on system performance. As a result, MMSE precoding introduces a regularization parameter that considers the impact of noise and performs well in low SNR situations. MMSE precoding algorithm works similarly to the ZF precoding algorithm. In other words, the precoding matrix is calculated using the MMSE criterion, and noise and user interference are eliminated by suppressing the noise amplification. The MMSE

precoding matrix has the following expression

$$\mathbf{W}_{MMSE} = (\mathbf{H}^H\mathbf{H} + \alpha\mathbf{I}_k)^{-1}\mathbf{H}^H \tag{1.3}$$

It is obvious from Equation 1.3 that the MMSE precoder is essentially a ZF precoder which is regularized by a factor $\alpha$. For the case when $\alpha \to \infty$, Equation 1.3 represents a matched filter, and for $\alpha \to 0$, the same equation represents a ZF precoder. In comparison, the MMSE precoder, offers the best balance between interference suppression and noise augmentation while still partially eliminating the CCI [58]. A comprehensive overview of precoding techniques for MU-MIMO is presented in [54]. Below are the advantages and disadvantages of ZF, and MMSE precoding taken from the existing literature.

- *Advantages of ZF precoding*: Eliminates the Inter-User Interference (IUI) [59], Provides a tradeoff between performance and complexity [59], and performs close to the optimal performance in interference-limited systems [59, 60].

- *Disadvantages of ZF precoding*: Does not consider the noise effect [61], Exhibit a complicated matrix inversion process [62], Amplifies the Noise [54], Offers low performance for ill-conditioned channel [59, 60], and when the ratio of the number of transmit antennas to the number of received antennas reaches one, the ability to increase diversity gain is lost [62].

- *Advantages of MMSE precoding*: Offers a tradeoff between Maximal Ratio Transmission and ZF [60, 61], Performs better in Noisy environments and

considers the effect of Noise [62, 63], Eliminates the IUI [61, 62], and with a proper channel propagation model offers a near-optimal performance [64].

- *Disadvantages of MMSE precoding*: Complicated matrix inversion method when the number of transmit antennas is high [63], and when the ratio of the number of transmit antennas to the number of received antennas reaches one, the ability to increase diversity gain is lost [62].

Trend-wise, the incorporation of MU-MIMO technology into LEO-NTN systems happened relatively slower as compared to the terrestrial networks [65]. The use of the spatial dimension is one of the most important aspects of MU-MIMO as it improves performance significantly through array gain, spatial diversity, spatial multiplexing, and interference avoidance. MU-MIMO transmission for NTNs has recently attracted more attention because the LEO-NTN systems are anticipated to be included in the next wireless networks. Moreover, they have various advantages over their GEO counterparts, including significantly lower constraints for power consumption and transmission signal delays. To have a strong LOS path is common for a SatCom channel between the ground and a satellite. The LOS path is required for achieving a healthy link budget [24]. In a MU-MIMO scenario, however, the LOS nature of the channel and the long-range distance in the channel path can increase the spatial correlation between the channel paths. Extra spatial degrees of freedom are achieved by geometrical optimization. In order to achieve spatial orthogonality in the LOS SatCom channel, antenna separation depending on the wavelength is required, either in space or on the ground. Moreover, it is important to establish, that most of the

published work based on the DL precoding methods mainly depends on accurate and real-time instantaneous CSI [55, 66–69]. However, this is a hard obstacle since there is not only a significant propagation delay between the satellite and the UTs on-ground but also both the LEO satellites and UTs are moving.

Particularly for the Time Division Duplex (TDD) systems, it is not possible to acquire both correct and instantaneous CSI via the Uplink (UL) and DL reciprocity because when compared to the transmission delay the channels' coherence time is less. In contrast, the CSI at the satellite side is conveniently obtained by using FDD systems, and therefore this approach is widely used [70].

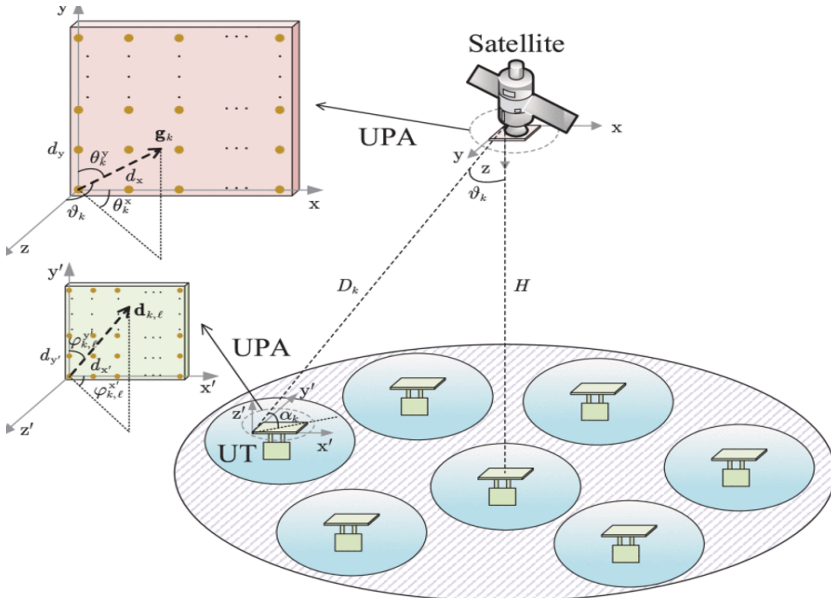


**Figure 1.8:** Illustration of the DL in FFR massive-MIMO LEO-NTN system [70].

Fig. 1.8, illustrates a MB LEO-NTN system adopted in [70], which takes into account the DL transmission over lower frequency bands, such as L/S/C bands, in FFR. As seen in Fig. 1.8, a single LEO satellite at an altitude of 'H'

provides service to the mobile UTs. It is anticipated that the satellite operates with a regenerative payload, thus allowing for on-board processing (OBP) of base-band signals. The amplitude and phase of each antenna element of the Uniform Planar Array (UPA)s can be digitally changed because both the satellite and the mobile UTs are equipped with digitally active UPAs. The MB satellite transmits the signals to the beams on the earth's surface, where the user terminals are located, denoted by the sky blue ellipses. The signals arrive from the operator network and the GW forwards them to the LEO satellite through the feeder link.

The hierarchical representation in Fig. 1.9 outlines the obstacles, implementation costs, and qualitative performance gain of the aforementioned bandwidth-efficient approaches and provides motivation for user scheduling algorithms, which is the scope of this thesis.

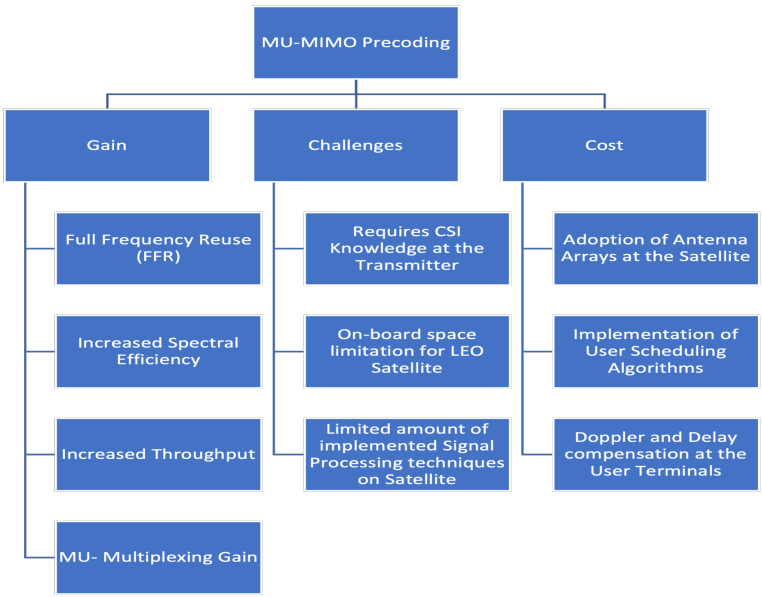


**Figure 1.9:** Qualitative Performance Gain, Challenges, and Implementation Cost of the Considered Bandwidth Efficient Techniques.

## 1.3 User Scheduling in LEO MU-MIMO NTN Systems

LEO satellite equipped with an on-board UPA can serve many UTs on-ground. Distributed with the extremely large number of UTs on-ground as compared to the antennas available on the satellite, the design of a proper user scheduling strategy becomes crucial for mainly two key reasons. First, the number of on-board antenna elements accessible on LEO satellites is significantly less than the number of users to be served. Second, users' instantaneous channels are not orthogonal to one another, which causes interference between users [71]. Thus, the objective of a proper user scheduling algorithm is to boost the overall throughput in unicast or multicast systems [72]. Moreover, an important aspect that needs attention is that interference between scheduled users is determined by the beamforming design, which is determined by the scheduled users in other beams. As a result, user scheduling and beamforming design are inextricably linked, and a joint design scheme for user scheduling and beamforming must be considered [73].

There is significantly published literature on user scheduling and beamforming design in the SatCom systems. Based on the perfect CSI availability and with the objective of throughput maximization, in [74] the precoding design of a MB SatCom system is investigated and a user scheduling and beamforming decoupling scheme is proposed. In [34], the robust multigroup multicast transmission scheme of the MB SatCom system is studied, and a low complexity beamforming algorithm together with the user grouping algorithm is proposed. This study

considers the impact of the CSI errors with the optimization objective to minimize the power. The multigroup multicast transmission design scheme of the frame-based multi-beam SatCom system is investigated in [75] and proposes a joint design scheme of the user scheduling and beamforming which is based on the perfect CSI, with the optimization objective of maximizing Spectrum Efficiency. The work in [1] addresses the user scheduling problem of a MB SatCom system. The user selection problem for multicast precoding is considered to be a clustering problem. Fixed-/ variable-size clustering algorithms are designed that groups users together and serve simultaneously via digital MU-glsmimo beamforming techniques. This work provides qualitative results in terms of overall sum-rate maximization. [76] addressed the joint scheduling and beamforming design problem for MU Multiple Input Single Output (MISO) DL channel with the perfect CSI, and the frame-based user grouping and scheduling algorithm has been proposed. The majority of the preceding research uses GEO satellites.

Discussing further, In general, for the NTN systems, the user scheduling methods are broadly classified as either user selection or user grouping [71, 77]. The former has either extremely limited or no relevance to SatCom systems because, from the satellite provider's point of view, all users are required to be served. Typically a 'user selection' method is implemented when the performance upper bound is required to be evaluated. With user selection schemes, a subset of users is selected which relies on certain channel conditions, for example, if only those users selected and served which are experiencing the best channel gains, then the remaining users will be starving due to the fact that the channel

from the satellite to the user on-ground is almost flat, as it is affected only by the long-term fading effects. Therefore, the focus of this work is based on the user grouping/ clustering algorithms in which all the users are served. Fig. 1.10 illustrates a MB LEO satellite with several users waiting to be served.

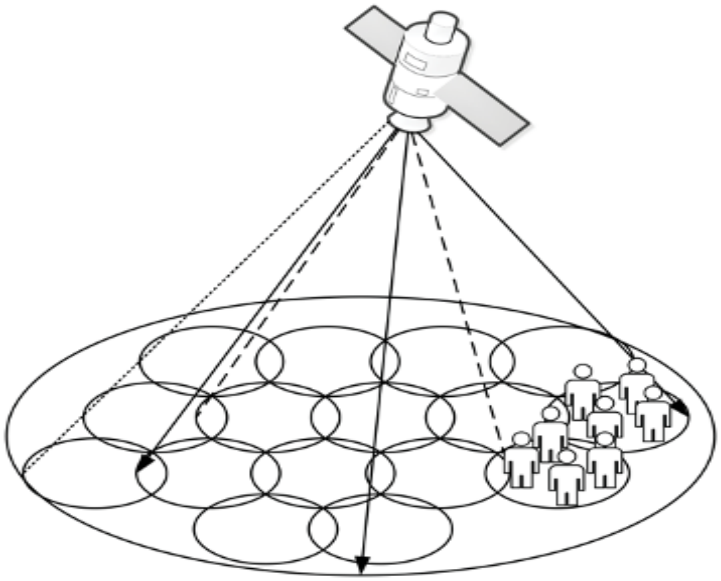

**Figure 1.10:** illustration of Multi-beam (MB) LEO Satellite [78].

In a user grouping algorithm, different users are multiplexed together into a cluster based on a decision policy/ grouping indicator. These different users are then served together by means of SDM via digital beamforming techniques in different time slots via TDM. Therefore, the design of an optimal user grouping strategy is known as a Non-deterministic Polynomial-Time (NP) hard problem. In the existing literature, to solve this problem, two approaches exist which are direct and indirect-based scheduling. In the former, the SINR for every user is computed first. The user 'u' is then allocated to the group that has the lowest impact on

the resulting SINR. This cannot be a practical strategy for hundreds of users per spot beam within a reasonable time. The Sum Rate Maximization User Grouping Algorithm (SMUG) [78], is a classical State-of-Art algorithm that is based on this approach and performs well when the total number of users in the system is very limited. The SMUG algorithm systematically chooses the users from the candidate user set based on the total number of time slots to optimize the current sum rate and ensure that the sum rate will increase in each time slot. The indirect method quantifies the spatial compatibility of two users in a MU-MIMO system by using a different metric of low computing complexity i.e., Coefficient of Correlation (CoC). [71] provides a comprehensive description of relevant measurements. One of the well-established algorithms based on an indirect approach is the MADOC [77]. For quantifying the spatial compatibility of two users, the CoC matrix is computed. This metric considers both the orthogonality and gains and it is therefore considered a reliable indicator to schedule one user without influencing the other user and to construct so-called $\epsilon$- orthogonal groups. The main idea is to group UTs together only if the CoC matrix, calculated for all combinations of UTs within a group, does not exceed a certain $\epsilon$-threshold [71].

The literature contains a wide variety of alternative metrics. Most of these metrics, however, either concentrate on the case of multiple antenna receivers or are unable to estimate the SINR with the same level of accuracy as the CoC in the unique circumstance of SatCom channels.

The clustering algorithms can be designed for both unicast and multicast precoding. For this thesis, we address the problem of user scheduling in a uni-

cast mode in which we schedule and group users into clusters that have channel vectors as mutually orthogonal as possible in order to spatially separate them. In contrast, for multicast precoding, the same symbol is sent to multiple users and for that reason, the same beamforming or precoding vector is used for all of them. In [1], two clustering algorithms for multicast precoding are established: one with fixed-size clusters aimed at limiting the impact of outlier users and the other with variable-size clusters based on the kmeans++ algorithm intended to minimize system outlier effects through proper cluster initialization. To maximize the overall system spectral efficiency, the authors suggested two new multiplexing techniques, which include grouping users who can be thought of as similar based on a certain similarity measure and treated. This is a cluster analysis problem where a set of objects (users) must be grouped so that objects in the same group (a cluster) have a closer similarity measure to those in other groups (based on a particular metric) (clusters).

The scheduling algorithm presented in [72] is referred to as a Position-based scheduler in which a beam lattice is first generated on-ground. One user per beam is randomly selected to form a cluster. As long as not all of the users in the beam have been served, the scheduler ensured that each user is served in only a one-time frame and that each beam's users are served. Both the bi-dimensional Euclidean distance between users [79, 80] and the concatenation of the real and imaginary parts of the channel coefficients vector [81] are taken into account for the similarity measure. For this thesis, the Position-based Scheduler [72] is considered a benchmark algorithm.

In the next section, the fascinating history of graph theory is first briefly presented. Then the graph formulation and the clique problems are explained to explain. We further attempt to justify why it is one of the most attractive and relevant solutions to address the user scheduling problem.

## 1.4 Graph-Theory and the Clique problem

### 1.4.1 History of Graph-Theory

In Prussia, Königsberg was a city on the Pregel River. The city, which included the island of Kneiphopf, was divided into four distinct landmasses by the river. As depicted in Fig. 1.11, seven bridges connected these four locations. City dwellers pondered whether it was conceivable to leave home, travel across each of the seven bridges precisely once, and then come back. In 1700, the Swiss mathematician Leonhard Euler learned about solving the puzzling Konigsberg seven bridges problem for the first time and the method recorded the graph theory in a written form [82].

A simple abstraction of the puzzle held the secret to Euler's answer. If the diagram of the city of Königsberg is re-done by converting each land mass into a vertex and each bridge into an edge that connects the land mass-corresponding vertices. A graph that encodes the required data is now achieved. Finding a "closed walk"—also known as an Eulerian circuit—in the graph that travels through each edge exactly once is the solution to the problem.

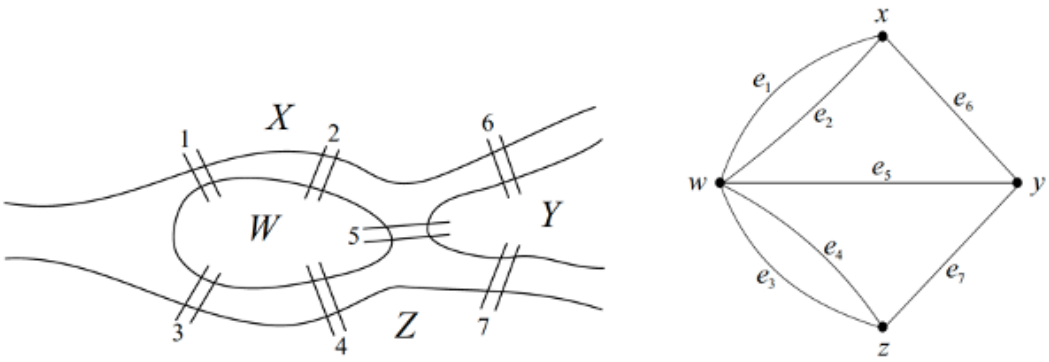


**Figure 1.11:** The Königsberg Bridge Problem.

James Joseph Sylvester later referred to this novel level of abstraction as "graphs" [83] presented in his 1878 Nature paper, which was necessary to implement the solution that Euler had given. Even though most of Konigsberg's bridges have been damaged since Euler's era but the associated theory and techniques have continued to develop. It was 1936, when the first book on graph theory was published. Roughly about 200 years, when Euler introduced the concept of graph theory, the first textbook on graph theory got published in 1936 [82, 84]. Graph theory is now regarded as a fundamental tool with huge utilities and well-known and well-established references. In recent times, graph theory is used in different research domains. Indeed, being a branch of discrete mathematics, graph theory is especially useful for resolving discrete equations with a clearly defined structure. This property makes it extremely promising to solve non-convex optimization problems.

### 1.4.2 Formulation of a Graph and the Clique problem

The fundamental step towards the formation of any graph is the formulation of the graph's adjacency matrix which is a square matrix and is used to represent a finite graph [84]. The matrix's components show whether or not a graph's vertex pairs are adjacent. The adopted approaches presented in this thesis for the user grouping problems are graph and clique based. In Karp's fundamental paper on computational complexity, Clique is one of the 21 NP-complete problems [85, 86], represented in Fig. 1.12. The Maximum Clique Problem is one of the most researched combinatorial issues.

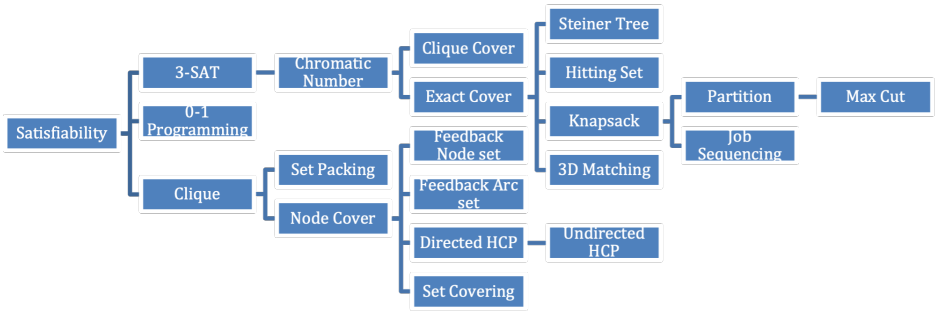


**Figure 1.12:** A Tree demonstrating 21 NP-Complete problems including Clique by Karp, with the edges denoting distinct reductions [85, 86].

### 1.4.3 Clique and its brief Introduction

In an undirected and unweighted graph $\mathcal{G}$, a clique is defined as a group of vertices where every two distinct vertices are adjacent (which means they share an edge), indicating that the induced sub-graph is complete. Cliques are widely adopted to solve various optimization problems. Cliques frequently reveal the observable characteristics of graphs. A clique, for instance, is a group of all dissimilar users, if nodes in the graph represent users and edges represents their relationships. A clique is a group of users who share a shared interest. The word clique was first used in 1949 in a study by Luce and Perry that examined the social network concept [87].

Even though it is NP-complete to determine if a clique of a specific size exists, various approaches are adopted in this thesis to find cliques. The investigated approaches are based on maximal and maximum clique findings. In the maximum clique problem, given a graph $\mathcal{G}$, one attempts to find the largest number of vertices, any two of which are adjacent.

When a clique cannot be expanded by adding a nearby vertex, it is said to be maximum, meaning it is not a subset of a more prominent clique. Since a maximum clique is the largest clique in a given graph, it concludes that it is also always maximal, while the opposite is not true. In graph-theoretic applications, such as fractional and non-fractional graph coloring, maximal cliques play a crucial role. A thorough examination of contemporary graph theory techniques, such

as flows and connectivity, the coloring problem, random graphs, and trees, can be found in [88, 89].

## 1.5 Contributions

The thesis has four main scientific contributions, each one is presented in an individual chapter. Part of this work has been funded by the "European Union (EU) Horizon-2020 Project, Dynamic Spectrum Sharing and Bandwidth-Efficient Techniques for High-Throughput MIMO Satellite Systems (DYNASAT)" under the Grant Agreement 101004145. The views expressed are those of the authors and do not necessarily represent the project. The Commission is not liable for any use that may be made of any of the information contained therein".

1. **Chapter 2 - System Characterization**: Importantly, to design and implement the user scheduling algorithms, the fundamental step is to have an appropriate system architecture along with the practical channel model. For this thesis, we considered the indirect-based scheduling algorithms due to the fact that the number of UTs considered to be scheduled is extremely large as compared to the on-board UPA at the satellite. For that, we first formulate a comprehensive system model which takes into account the FS and user service link (i.e., DL) of a single MB-LEO satellite operating below 6 GHz in the FDD mode. S-band has been considered, keeping in mind that till now the 3GPP only supports handhelds in lower bands. However, we have considered the Very Small Aperture Terminal (VSAT) terminals only for this thesis. The adopted channel model is completely aligned with

the 3GPP specifications. All the proposed scheduling algorithms in the following chapters will take into account the same channel model. For the grouping policy, the CoC matrix is in Chapter 3, and users' great circle distance in Chapter 4 is formulated and adopted.

2. **Chapter 3 - Joint Graph-based User Scheduling and Beamforming in LEO-MIMO SatCom Systems**:

   Based on the formulated system model in Chapter 2, here, a LEO-HTS MU-MIMO system is considered. To minimize inter-beam interference among the UTs, we propose a joint graph-based user scheduling and FS beamforming framework in the DL. First, we construct a graph where the vertices are the users and edges are based on a dissimilarity measure of their channels. Secondly, we design a low-complexity greedy user clustering strategy, in which we iteratively search for the maximum clique in the graph. Finally, a MMSE beamforming matrix is applied on a cluster basis with different power normalization schemes i.e., Sum Power Constraint (SPC), Maximum Power Constraint (MPC), and Per-Antenna Power Constraint (PAC). Heuristic optimization of the graph density, i.e., optimal cluster size, is performed to maximize the system capacity. The proposed scheduling algorithm is compared with a position-based scheduler, in which a beam lattice is generated on-ground and one user per beam is randomly selected to form a cluster. Results are presented in terms of achievable per-user capacity and show the superiority in performance of the proposed scheduler w.r.t. to the

position-based approach [72]. Our presented solution is based on FS and user-centric spot beams.

3. **Chapter 4 - Graph-based User Scheduling Algorithms for LEO-MIMO NTNs**: Extending our presented work in Chapter 3, We propose an iterative user scheduling procedure based on the maximum clique algorithm. As a grouping indicator, we have presented the channel CoC matrix in case of CSI availability at the scheduling phase, or the users' great circle distance in case only users' locations are known. As discussed in Chapter 1, user scheduling algorithms heavily rely on the availability of real-time CSI information. To tackle the scenarios where the CSI information is unavailable, a novel user scheduling framework is presented which is based on a graph adjacency matrix computed from the users' inter-distance matrix. For each cluster, a digital MMSE beamforming matrix allows to spatial separate the scheduled users and we have considered two power normalizations for the MMSE matrix: SPC, and MPC. To evaluate and confirm the improved performance with our proposed graph-based scheduling algorithm, we have compared our proposed results with a well-established classical MADOC algorithm [77]. We then found the optimal threshold values for both graph-based schedulers and for MADOC [77]. The results have been presented in terms of achievable per-user capacity and SINR and show an improvement in the performance of both graph-based schedulers i.e., CSI-based [90] and Distance-based w.r.t. MADOC [77].

4. **Chapter 5 - Improved Graph-based User Scheduling for Sum-Rate Maximization in LEO-NTN Systems**: One of the observations from the previously presented solutions i.e., CSI-based and Distance-based Maximum clique schedulers, was the formation of some of the user groups with extremely less number of users. For that reason, the clustering weights were assigned. To address the problem of group number minimization, in this work, we present a novel solution in which instead of having a fixed threshold value, a new strategy is proposed in which it is no longer required to find the optimal threshold value but differently, the optimal graph density is determined. Since the graph density is changed when the threshold value is changed because the actual number of edges is only determined with the fixed threshold values, therefore, finding the threshold for the requested graph density provided at the input and keeping the graph density constant at each pruning iteration is the problem statement that is solved by a well-known Bisection method. The results are compared w.r.t. the CSI-based maximum clique scheduler [90], the position-based scheduler [72], and MADOC [77]. Extensive simulation results reveal that with this novel solution, the sum-rate capacity is maximized and the total number of clusters is minimized as compared to [72, 77, 90].

5. **Chapter 6 - Conclusion**: Finally, the conclusion section summarizes the thesis and highlights the possible directions for future activities to further extend the subject.

# Chapter 2 - System Characterization

The content of this chapter is based on the following article;

*"D. G. Riviello, B. Ahmad, A. Guidotti, and A. Vanelli-Coralli, "Joint Graph-based User Scheduling and Beamforming in LEO-MIMO Satellite Communication Systems," 2022 11th Advanced Satellite Multimedia Systems Conference and the 17th Signal Processing for Space Communications Workshop (ASMS/SPSC), Graz, Austria, 2022".*

## 2.1 Introduction

As this thesis addresses the user scheduling and beamforming problem jointly, it is therefore essentially required to formulate a system model. In this Chapter, For simplicity, we first provide the streamlined architecture, with a focus on the FS and user service link (i.e., DL) of a single MB-LEO satellite operating below 6 GHz, and in the FDD mode.

MIMO rely on beamforming/ precoding. The three main components SatCom systems as illustrated in Fig. 2.1 consist of an on-ground segment made up of GW stations and control facilities. We have considered a single GW managing the users' CSI; an on-board segment, made up of the satellite; and a user segment made up of handheld or stationary UTs. For simulations, we have considered the

VSAT terminals. Within a certain range of the allotted spectrum, these three components send and receive signals. As indicated in Fig. 2.1, the forward link is the end-to-end connection that is from the GW to the UTs via satellite, while the return link is the end-to-end connection that runs in the reverse direction. Last but not least, the user link designates the connection between the satellite and the UTs. GW and satellite are represented by the feeder link. Typically, radio frequencies are used by both the feeder link and the user link.FDD is considered because of the propagation delays that make the TDD obsolete. The system and modeling features of SatCom systems are briefly discussed in this section as preliminaries.

## 2.2 Notations

Throughout this thesis, and if not otherwise specified, the following notation is used: boldface lower case and boldface upper case characters denote vectors and matrices, respectively, $(\cdot)^\intercal$ denotes the matrix transposition operator, $(\cdot)^H$ denotes the matrix conjugate transposition operator, $[\mathbf{A}]_{i,j}$ denotes the entry in the $i$-th row and in the $j$-th column of the matrix $\mathbf{A}$, $\mathrm{tr}(\mathbf{A})$ denotes the trace of the matrix $\mathbf{A}$. The diag operator, when applied to a vector, i.e., $\mathbf{D} = \mathrm{diag}(\mathbf{a})$ constructs a diagonal matrix $\mathbf{D}$, whose main diagonal coincides with $\mathbf{a}$, otherwise, when the diag operator is applied to a matrix, i.e., $\mathbf{d} = \mathrm{diag}(\mathbf{A})$, extracts the main diagonal of matrix $\mathbf{A}$ into the column vector $\mathbf{d}$.

## 2.3 Preliminaries

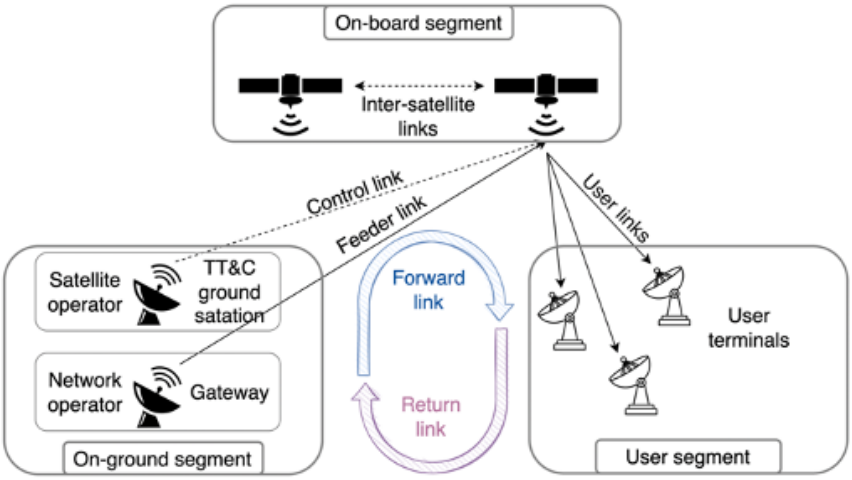


**Figure 2.1:** SatCom Architecture [91].

1. *On-ground segment*: As represented in Fig. 2.1, the satellite operator and the network operator jointly control and maintain the on-ground segment of a SatCom system. Telemetry, tracking, and control (TT&C) stations are deployed by satellite operators to monitor the satellite subsystems, maintain the proper orbits and configurations, and deal with upgrades and malfunctions. To handle network access and backhauling, on the other hand, the network operator runs and maintains the GW stations. Additional information regarding the on-ground segment is provided in [91].

2. *On-board segment*: The MB-LEO satellite, which has an altitude range of 600 Km, is considered here.

3. *User-segment*: VSAT, as described in 3GPP Technical Report (TR) 38.821 [92], is taken into account. Some of the pictures presented in this thesis have handhelds which will be considered for future work. Additionally, with reference to 3GPP TS 22.261 [93], these terminals can be stationary or move at various speeds. Even while all combinations are possible, some of them would not be taken into account in the numerical assessment because they are unreasonable (such as VSAT terminals operating at pedestrian speeds) or are not currently anticipated by the 3GPP (e.g., VSAT for public safety). Also, VSAT terminals are taken into account in order to have a performance benchmark to comprehend the effects of directional radiation patterns with large gains on the performance of MU-MIMO.

## 2.4 Space-segment and User-centric Spot-beams

A Single MB-LEO MU-MIMO satellite equipped with an on-board UPA is considered here with a focus on feed space (not in the beam space) and DL. The antenna array consists of $N$ radiating elements that provide connectivity to a total of $K$ single-antenna uniformly distributed on-ground users employing $S \leq N$ beams. The users are simultaneously served on the same spectral resources i.e., FFR with a single GW managing the users' CSI. The beamforming matrix is computed on the feed space as it offers to have user-centric spot beams. Additionally, it is assumed, that the LEO satellite always maintains a logical link with an on-ground gNB. To do this, the satellite is considered to be either directly

connected to an on-ground GW or to be connected via other LEO satellites in the constellation via Inter-Satellite Link (ISL)'s.

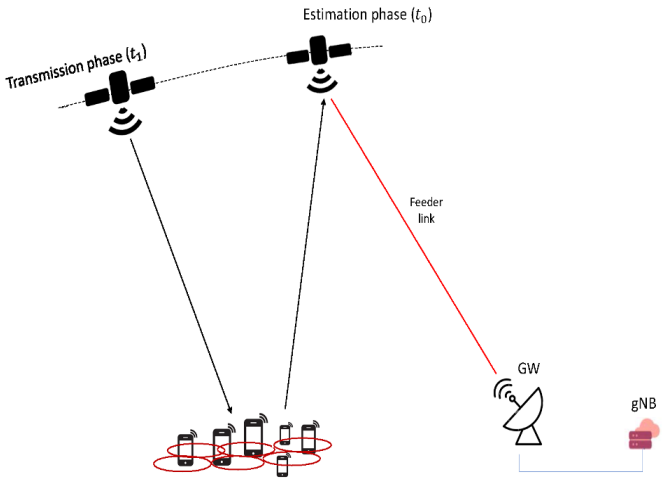


**Figure 2.2:** System Architecture with LEO

The estimation of the CSI provided by the UTs is necessary for both beamforming and scheduling. In reference to Fig. 2.2, the users compute the CSI values at time instant $t_0$; the gNB subsequently computes the scheduling and beamforming matrices for each group of users, which are then actually employed to send the beamformed symbols to the users at time instant $t_1$. The misalignment between the channel on which the scheduling and beamforming matrices are computed and the actual channel through which the transmission occurs is introduced by the latency $\Delta t = t_1 - t_0$ between the channel estimation phase and the transmission phase, which affects the system performance. This delay can be calculated as follows;

$$\Delta t = t_{ut,max} + 2t_{feeder} + t_p + t_{ad} \tag{2.1}$$

where

i $t_{ut,max}$ is the maximum delay for the UTs requesting connectivity in the coverage area

ii $t_{feeder}$ is the delay on the feeder link, considered twice since the estimates are to be sent to the GW on the return link, and then the beamformed symbols are sent on the forward link to the satellite

iii $t_p$ is the processing delay needed to compute the beamforming matrix

iv $t_{ad}$ includes any additional delay

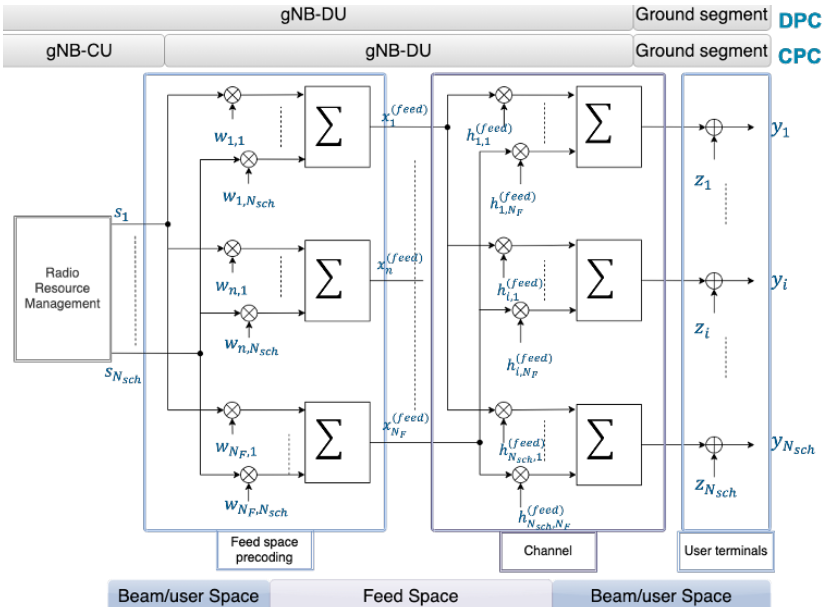


**Figure 2.3:** Block Diagram of Feed space precoding

Fig. 2.3, provides a block diagram where it can be noticed

1. with Centralized Precoding Computation (CPC), precoding is computed at the gNB-Centralized Unit (CU) on-ground and then applied on-board at the gNB-Distributed Unit (DU)

2. with Distributed Precoding Computation (DPC), precoding is both computed and applied to the symbols on-board at the gNB-DU

In the case of CPC, the precoding and scheduling matrices are computed locally. All users within the service area must provide information, and all gNBs CUs maintaining the logical connections with the onboard gNBs DUs must provide information to a single network entity in order to apply the appropriate algorithms. This entity can be one of the gNB-CUs. Here, the users' data is provided to the satellite constellations to compute the scheduling and precoding matrices, which are subsequently transmitted to the satellites (either directly or through the ISLs) to broadcast the precoded symbols.

For the DPC, The computation of the scheduling and precoding matrices is implemented on-board in this instance using the functional split. A reference gNB-DU that does these computations and gathers data from all satellites is required in the constellation since the entity executing these computations must be distinct. The precoded symbols are transmitted by the other satellites in the constellation using the matrices, which have been computed. Clearly, this technique offers a large latency advantage but demands a more sophisticated payload that can include scheduling and precoding algorithms.

The On-Board Beamforming (OBBF) strategy, which involves applying the precoding coefficients to the users' onboard symbols, is taken into consideration

in both of the aforementioned alternatives. It should be noted that this differs from the computation of the coefficients, which can be done using CPC or DPC.

## 2.5 UPA Antenna Model

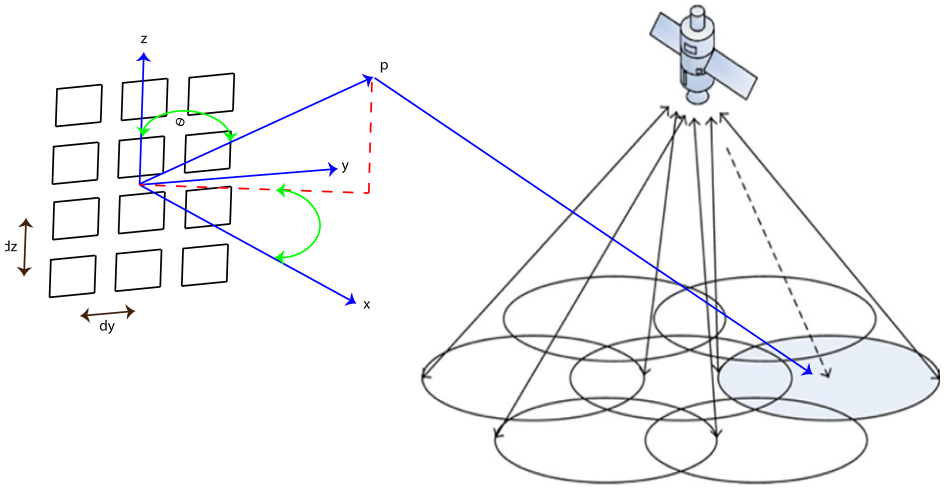


**Figure 2.4:** Multi-beam Antenna Array Model [94].

As represented in Fig. 2.4, by default the antenna boresight directions are defined by the direction of the Sub Satellite Point (SSP). The point $P$ is the position of the user terminal on the ground. The user directions are identified by $(\vartheta, \varphi)$ angles where the boresight direction is (0,0).

Now, the direction cosines for the considered user are defined as

$$u = \frac{P_y}{\|P\|} = \sin\vartheta \sin\varphi \tag{2.2}$$

$$v = \frac{P_z}{\|P\|} = \cos\vartheta \tag{2.3}$$

The total array response of the UPA in the generic direction $(\vartheta_i, \varphi_i)$ can be expressed as a Kronecker product of the array responses of the 2 Uniform Linear Arrays (ULAs) lying on the $y$- and $z$-axis [72]. We first define the $1 \times N_H$ Steering vector (SV) of the ULA along the $y$-axis $\mathbf{a}_H(\theta_i, \varphi_i)$ and the $1 \times N_V$ SV of the ULA along the $z$-axis $\mathbf{a}_V(\theta_i)$:

$$\mathbf{a}_H(\vartheta_i,\varphi_i) = \left[1, e^{jk_0 d_H \sin\vartheta_i \sin\varphi_i}, \ldots, e^{jk_0 d_H (N_H-1) \sin\vartheta_i \sin\varphi_i}\right] \tag{2.4}$$

$$\mathbf{a}_V(\vartheta_i) = \left[1, e^{jk_0 d_V \cos\vartheta_i}, \ldots, e^{jk_0 d_V (N_V-1) \cos\vartheta_i}\right]. \tag{2.5}$$

Where $k_0 = 2\pi\lambda$ is the wave number, $N_H, N_V$ denotes the number of array elements on the horizontal ($y$-axis) and vertical ($z$-axis) directions with $N = N_H \cdot N_V$ and $d_H, d_V$ denote the distance between adjacent array elements on the $y$-and $z$-axis respectively. We assume that the array is equipped with directive antenna elements, whose radiation pattern is denoted by $g_E(\vartheta_i, \varphi_i)$. Finally, we can express the $(1 \times N)$ SV of the UPA at the satellite targeted for the $i$-th user as the Kronecker product of the 2 SVs along each axis multiplied by the element radiation pattern:

$$\mathbf{a}(\vartheta_i, \varphi_i) = g_E(\vartheta_i, \varphi_i)\, \mathbf{a}_H(\vartheta_i, \varphi_i) \otimes \mathbf{a}_V(\vartheta_i) \tag{2.6}$$

## 2.6 The Channel Matrix

The presented Channel Matrix computation for a single LEO satellite is based on the parameters provided by 3GPP [92].

The CSI vector at feed level $\hat{\mathbf{h}}_i$ represents the channel between the $N$ radiating elements and the generic $i$-th on-ground UT, with $i = 1, \ldots, K$, can be written as

$$\hat{\mathbf{h}}_i = G_i^{(rx)} \frac{\lambda}{4\pi d_i} \sqrt{\frac{L_i}{\kappa B T_i}} e^{-j\frac{2\pi}{\lambda} d_i} \mathbf{a}(\vartheta_i, \varphi_i) \tag{2.7}$$

in which

i $d_i$ is the slant range between the generic $i$-th user and the satellite

ii $\lambda$ is the wavelength

iii $\kappa B T_i$ denotes the equivalent thermal noise power, with $\kappa$ being the Boltzmann constant

iv $B$ the user bandwidth (assumed to be the same for all users), and $T_i$ the equivalent noise temperature of the $i$-th UT

v $L_i$ denotes all the additional losses per user, such as atmospheric, antenna, and cable losses.

vi $G_i^{(rx)}$ denotes the receiving antenna gain for the $i$-th UT

The additional losses are computed as $L_i = L_{sha,i} + L_{atm,i} + L_{sci,i}$ where $L_{sha,i}$ represents the log-normal shadow fading term, $L_{atm,i}$ the atmospheric loss, and $L_{sci,i}$ the scintillation, these terms are computed as per 3GPP TR 38.821 [92].

Collecting all of the $K$ CSI vectors, it is possible to build a $K \times N$ complex channel matrix at the system level

$$\hat{\mathbf{H}} = [\hat{\mathbf{H}}_1^{\mathbf{T}}, \hat{\mathbf{H}}_2^{\mathbf{T}}, ..., \hat{\mathbf{H}}_k^{\mathbf{T}}]^{\mathbf{T}}$$

where the generic $k$-th row contains the CSI vector of the $k$-th user and the generic $n$-th column contains the channel coefficients from the $n$-th on-board feed towards the $K$ on-ground users.

## 2.7 User Scheduling Framework for Graph and Maximum Clique-based Algorithms

The User Scheduling framework is based on unicast mode as illustrated in Fig. 2.5.

Given the set of all users to be scheduled, denoted with $\mathcal{U} = \{U_1, U_2, \ldots, U_K\}$, the Radio Resource Management (RRM) algorithm defines a possible users' partitioning $\{\mathcal{C}_1, \mathcal{C}_2, \ldots, \mathcal{C}_P\}$ where $\mathcal{C}_p \subseteq \mathcal{U}$ is defined as cluster and $|\mathcal{C}_p| = K_p$ is defined as the cardinality of the $p$-th cluster. Clusters are not necessarily disjoint sets of users, clearly $|\mathcal{C}_1 \cup \mathcal{C}_2 \cup \ldots \cup \mathcal{C}_P| = K$. It is assumed further that $T_{tot} = \sum_{p=1}^{P} |\mathcal{C}_p| \geq K$ time frames are available at the RRM, then for each time frame, the RRM selects the subset of users belonging to cluster $\mathcal{C}_p$ to be

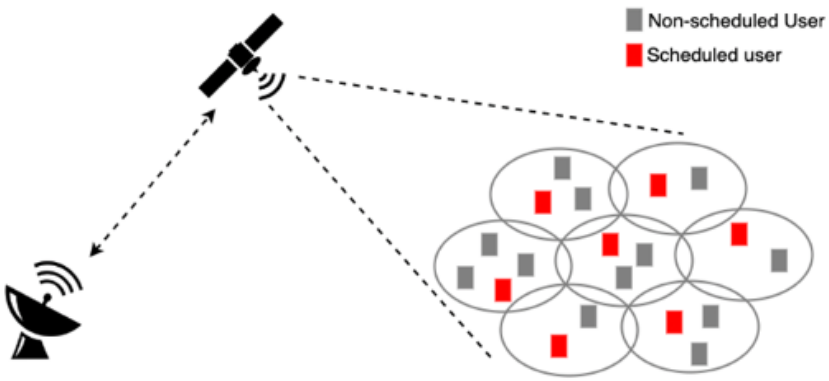


**Figure 2.5:** User Scheduling in unicast mode [91].

served, leading to a $K_p \times N$ complex scheduled channel matrix $\mathbf{H}_p = \mathcal{F}(\mathbf{H})$, where $\mathcal{F}(\cdot)$ denotes the RRM scheduling function, which is a sub-matrix of $\mathbf{H}$, i.e., $\mathbf{H}_p \subseteq \mathbf{H}$, which contains only the rows of the scheduled users in the $p$-th cluster. The selected beamforming algorithm computes for each cluster a $N \times K_p$ complex beamforming matrix $\mathbf{W}_p = [\mathbf{w}_1^{(p)}, \mathbf{w}_2^{(p)}, \ldots, \mathbf{w}_{K_p}^{(p)}]$ , where $\mathbf{w}_i^{(p)}$ denotes the $N \times 1$ beamformer designed for the $i$-th user in the $p$-th cluster. The matrix $\mathbf{W}_p$ projects the $K_p$ dimensional column vectors $\mathbf{s}_p = [s_1, s_2, ..., s_{K_p}]^{\mathbf{T}}$ containing the unit-variance user symbols onto the $N$-dimensional space defined by the antenna feeds.

Hence, in the feed space, the computation of the beamforming matrix allows for the generation of a dedicated beam toward each user direction. The signal received by the $i$-th user in the $p$-th cluster can be expressed as follows:

$$y_k^{(p)} = \mathbf{h}_k \mathbf{w}_k^{(p)} s_k + \sum_{\substack{i=1 \\ i \neq k}}^{K_p} \mathbf{h}_k \mathbf{w}_i^{(p)} s_i + z_k^{(p)} \tag{2.8}$$

where $z_k^{(p)}$ is a circularly symmetric Gaussian random variable with zero mean and unit variance. The $K_p$-dimensional vector of received symbols in the $p$-th cluster is:

$$\mathbf{y}_p = \mathbf{H}_p \mathbf{W}_p \mathbf{s}_p + \mathbf{z}_p \tag{2.9}$$

It shall be noted that, as previously discussed, the estimated channel matrix $\hat{\mathbf{H}}$ at time $t_0$ is used to compute the scheduling and the beamforming matrices $\mathbf{W}_p$ in the estimation phase, while the beamformed symbols are sent to the users at a time instant $t_0 + \Delta t$, in which the scheduled channel matrices and vectors are different and denoted as $\mathbf{H}_p$ and $\mathbf{h}_k$, respectively.

The SINR for user $k$ belonging to cluster $p$ can be computed as

$$\mathrm{SINR}_k^{(p)} = \frac{\left\| \mathbf{h}_k \mathbf{w}_k^{(p)} \right\|^2}{1 + \sum_{\substack{i=1 \\ i \neq k}}^{K_p} \left\| \mathbf{h}_k \mathbf{w}_i^{(p)} \right\|^2} \tag{2.10}$$

To design a fair-proportional scheduler, given a total amount of $T_{tot}$ time frames, each cluster is assigned a number of time frames equal to the cardinality of the cluster $K_p$, i.e., $T_p = K_p = |\mathcal{C}_p|$. Therefore, the per-user achievable capacity can be computed as:

$$C_k = B \sum_{\substack{p \\ U_k \in \mathcal{C}_p}} \gamma_p \log_2 \left(1 + \mathrm{SINR}_k^{(p)}\right) \tag{2.11}$$

where

$$\gamma_p = \frac{|\mathcal{C}_p|}{\sum_{p=1}^{P} |\mathcal{C}_p|} = \frac{K_p}{T_{tot}} \tag{2.12}$$

denotes the cluster weight.

## 2.8 The Beamforming Matrix

The MMSE precoder is designed to solve the beamforming problem. The beamforming matrix $\mathbf{W}_p$, which is computed on a cluster basis and given by

$$\mathbf{W}_p = (\hat{\mathbf{H}}_p^H \hat{\mathbf{H}}_p + \alpha \mathbf{I}_N)^{-1} \hat{\mathbf{H}}_p^H \tag{2.13}$$

where $\mathbf{I}_N$ indicates the $N \times N$ identity matrix and $\alpha$ is the vector of regularization factor for each of the users to be served and it has been subjected to different discussions in the literature related to its optimal value. In [67], identified the optimal value to be $1/SNR_K$ in which the channel matrix is not normalized to the noise power. In this thesis, the normalization has been introduced given by $\alpha = \frac{N}{P_t}$, with $P_t$ as the total available power on board.

From Equation 2.13, it can be noticed that the MMSE precoding matrix is based on the knowledge at the transmitter side (gNB-CU or gNB-DU for CPC and DPC, respectively) of the channel CSI vectors. This leads to two critical

challenges in the implementation of MMSE solutions in a satellite system, both leading to a misalignment between the channel matrix that is used to compute the Equation 2.13, and the channel matrix that actually represents the channel when the transmission occurs

A) the latency between the moment in which the user estimates their CSI and the moment in which these are exploited to compute the MMSE matrix since both the satellite and the users might not be fixed and

B) estimation errors at the user terminal, leading to non-ideal CSI vectors even in a completely fixed scenario. Another aspect worth to be mentioned is that Equation 2.13 leads to a large dimension of the Gram matrix $\hat{\mathbf{H}}_p^H \hat{\mathbf{H}}_p$ when precoding is implemented in the feed space. The Gram Matrix in this case is $N_F \times N_F$ Here, the MMSE precoding matrix is implemented on the feed space. However, the most important and fundamental step is related to performing proper power normalization.

## 2.9 The Power Normalizations

The total power emitted by the satellite is actually represented by the Frobenius norm of the MMSE precoding matrix, and it is obvious that this value must be upper bound by the total power available [1].

### 2.9.1 Sum-Power Constraint (SPC)

It ensures that the total amount of power allotted by the precoding matrix is equal to the amount that is actually available $P_t$, and maintains the orthogo-

nality between the columns of the precoding matrix. However, no regulation of the power allotted to each antenna or stream is applied. Driving the onboard High Power Amplifiers (HPAs) close to or above the saturation level could result in performance deterioration by introducing unwanted non-linear effects [72].

$$\tilde{\mathbf{W}}_p = \frac{\sqrt{P_t}\mathbf{W}_p}{\sqrt{\mathrm{tr}(\mathbf{W}_p\mathbf{W}_p^H)}} \tag{2.14}$$

### 2.9.2 Maximum-Power Constraint (MPC)

With $K{=}N_F$ for feed space precoding, it is guaranteed that the overall power is upper bounded by $P_t$ while also making sure that none of the onboard antennas use more power than is permitted. The orthogonality of the precoding matrix columns is maintained in the SPC technique. This strategy could, however, result in a performance decrease in terms of the sum capacity because just one antenna is emitting at maximum power while the others have drastically reduced emissions [72].

$$\tilde{\mathbf{W}}_p = \frac{\sqrt{P_t}\mathbf{W}_p}{\sqrt{N\ \max_j \left[\mathbf{W}_p\mathbf{W}_p^H\right]_{j,j}}} \tag{2.15}$$

### 2.9.3 Per-Antenna Power Constraint (PAC)

With $K{=}N_F$, for the feed space precoding, adopting this method, each antenna to transmit at the same power level is allowed while guaranteeing that the total amount of power available is not surpassed. The precoding matrix's individual rows' independent normalization causes a performance decrease in terms

of interference cancellation [72].

$$\tilde{\mathbf{W}}_p = \sqrt{\frac{P_t}{N}} \left(\text{diag}\left(\text{diag}\left(\mathbf{W}_p \mathbf{W}_p^H\right)\right)\right)^{-\frac{1}{2}} \mathbf{W}_p \tag{2.16}$$

The extensive simulation results in the following chapters will demonstrate that MMSE with SPC is the optimal precoding algorithm in terms of maximizing the system capacity, which is inferred from the aforementioned arguments. This method obviously requires knowledge of the CSI vectors at the gateway side, and any misalignment caused by inaccurate estimates or delays can seriously affect the performance. [77] emphasizes that the dedicated power amplifiers used by each satellite feed in SatCom prevent instantaneous power sharing across the $N_F$ feeds. Therefore, PAC rather than SPC, which is frequently employed in precoder designs based on information theoretic deductions, must be applied when the precoding matrix is determined.

# Chapter 3 - Joint Graph-based User Scheduling and Beamforming in LEO-MIMO SatCom Systems

The content of this chapter is based on the following article;

*"D. G. Riviello, B. Ahmad, A. Guidotti, and A. Vanelli-Coralli, "Joint Graph-based User Scheduling and Beamforming in LEO-MIMO Satellite Communication Systems," 2022 11th Advanced Satellite Multimedia Systems Conference and the 17th Signal Processing for Space Communications Workshop (ASMS/SPSC), Graz, Austria, 2022".*

## 3.1 Introduction

Modern State-of-the-Art user scheduling algorithms either employ 'direct-based' or 'indirect-based' user grouping/clustering algorithms [71]. When it comes to the former, only a subset of users can be scheduled [78]. The sum rate capacity $\gamma C$ for a particular user subset would change as a result of the addition of a new user. This change can be broken down into two parts: the incremental increase $C_{gain}$ in sum rate capacity and the incremental decrease in capacity $C_{loss}$ as a result of the new user interfering with the existing users. The effect of the new user on the sum rate capacity would be favorable if the gain outweighed the loss and vice versa.

In contrast, the indirect method quantifies the spatial compatibility of two users in a MU-MIMO system using a different metric of low computing complexity. [71] provides a thorough description of relevant measurements. To reliably predict the channel capacity or throughput, appropriate decision criteria must be chosen in accordance with the adopted channel model e.g., we use the CoC matrix because the aim is to maximize the system performance while minimizing the spatial correlation among users per cluster. It has been comprehensively explained in [71, 77, 95] that a capacity-optimal LOS MIMO satellite channel exhibits identical eigenvalues of the matrix $\mathbf{HH}^H$ eigenvalues. This indicates that the ideal $\mathbf{HH}^H$ has a diagonal structure and is therefore orthogonal. The signal phase relationships at the receiving antennas rely on the users' locations on the ground. Moreover, the orthogonality depends on the users' positions, and to obtain an orthogonal channel matrix, the spacing between the receivers on Earth must be adequate. Combining these factors, it is obvious that the appropriate metric that is considered as a grouping indicator for user scheduling must consider both the orthogonality of the channel matrix $\mathbf{H}$ and the channel gains experienced by each user. The CoC matrix is represented by $\mathbf{\Psi}$, explained in the Equation 3.1 is an extremely effective metric since it takes into consideration both the orthogonality and gains [71, 77]. The separation between the on-ground users should be sufficient enough to provide an orthogonal channel matrix. $\mathbf{\Psi}$ is considered a reliable indicator for the scheduler to evaluate how efficiently can the generic user $i$ be provided with the data without interfering with the generic user $j$ and vice versa. There exist other grouping indicators comprehensively explained in [71, 77] but

typically for the scenarios where the number of users is significantly large, they are limited because of the processing delays.

$$[\mathbf{\Psi}]_{i,j} = \frac{\left|\hat{\mathbf{h}}_i \hat{\mathbf{h}}_j^H\right|}{\left\|\hat{\mathbf{h}}_i\right\| \left\|\hat{\mathbf{h}}_j\right\|} \tag{3.1}$$

This work presents a joint graph-based user scheduling and feed space beamforming framework for LEO-MIMO NTN systems, which is based on the comprehensive system model described in Chapter 2. The focus remains on indirect-based scheduling algorithms, in which different users are clustered together which is based on a decision policy. When choosing which users to be grouped and scheduled concurrently in a cluster, it is essential to have a reliable grouping indicator. Once the users are identified for a cluster, the LEO satellite serves the cluster's users simultaneously through SDM. Then, using TDM, these diverse clusters are distributed across various time slots. With this method, all users are served and not a subset of users.

## 3.2 Graph-based User Scheduling

The clique problem and the graph theory are introduced in this section. First, Graph theory definitions and notations are provided for the formulation of the clique problems. Following that, several graph-based precise and effective algorithms for finding maximal and maximum cliques are presented, and their computational complexities are examined.

Graphs are defined as mathematical structures that are used to represent and model the pairwise relationship between objects. The two main components in a graph $\mathcal{G}$ are nodes (also known as vertices) $\mathcal{V}$ and edges $\mathcal{E}$ (a line or a link that connects two nodes). The edge set is represented as $\mathcal{E} \subset \mathcal{V} \times \mathcal{V}$. Moreover, in an undirected graph, the edge links two vertices symmetrically. In this chapter, to address the user scheduling problem, the same concept has been adopted where users constitute the vertices of the graph, and edges are based on a dissimilarity measure of their channels. The overall graph structure is considered to be unweighted and undirected.

A Clique $\mathcal{C}$ of $\mathcal{G}$ is a subset of $\mathcal{V}$ such that every two vertices in $\mathcal{C}$ are adjacent. i.e. $\forall_{u,v} \in \mathcal{C}, \{u, v\} \in \mathcal{E}$.

In reference to the Equation 3.1, in which, $[\mathbf{\Psi}]_{i,j} \in [0, 1]$. The set of edges $\mathcal{E}$ of the $\mathcal{G}$ graph is identified by the graph's adjacency matrix $\mathbf{A}$, whose entries are defined as

$$[\mathbf{A}]_{i,j} = \begin{cases} 1, & [\mathbf{\Psi}]_{i,j} \leq \delta_{th} \\ 0, & [\mathbf{\Psi}]_{i,j} > \delta_{th} \end{cases} \tag{3.2}$$

where $\delta_{th}$ denotes a properly designed threshold Equivalently,
$\mathcal{E} = \{\{U_i, U_j\} \,|\, [\mathbf{A}]_{i,j} = 1\}$ where
$\{U_i, U_j\}$ are unordered pairs of vertices. If an element of $\mathbf{A}$ is equal to 0, it means $\mathbf{h}_i$ and $\mathbf{h}_j$ are considered to be co-linear and there is no edge between $U_i$ and $U_j$ while if an element of $\mathbf{A}$ is equal to 1, it means that $\mathbf{h}_i$ and $\mathbf{h}_j$ are considered to be orthogonal, i.e., there is an edge between $U_i$ and $U_j$ and they can belong to the same cluster (or they can be co-scheduled). Based on these premises, a clique $\mathcal{Q}$

of the graph $\mathcal{G}$ represents a set of users with mutually uncorrelated channels, and therefore, co-scheduled. Selecting the proper threshold $\delta_{th}$ plays a crucial role in the scheduler design as it determines the density of the graph $D(\mathcal{G})$, defined as the ratio of the number of edges $|\mathcal{E}|$ concerning the maximum possible edge

$$D(\mathcal{G}) = \frac{2|\mathcal{E}|}{|\mathcal{V}|\left(|\mathcal{V}|-1\right)} \tag{3.3}$$

The following section explains how the clique issue manifests the user scheduling problem.

## 3.3 Clique-based User Scheduling

For our considered scenario $\mathcal{G}$=($\mathcal{V}$,$\mathcal{E}$), The total vertices are the total number of users in the system with vertex set $\mathcal{V} = \{1, 2, ..., K\}$ and the edges are based on a dissimilarity measure of their channels. A clique denotes, a group of those users who are orthogonal with each other. Because we want to schedule dissimilar users together to avoid co-channel interference. First, an overview of all the considered algorithms is provided and finally, the adopted approach which is based on the maximum clique is justified by explaining the system limitations and computational complexity.

### 3.3.1 The Maximal Clique Algorithms

A maximal clique in a graph cannot be expanded by adding more neighboring vertices without endangering its connecting property, i.e., it is not a subset of a more prominent clique. In a maximal clique algorithm, all possible cliques

are identified.

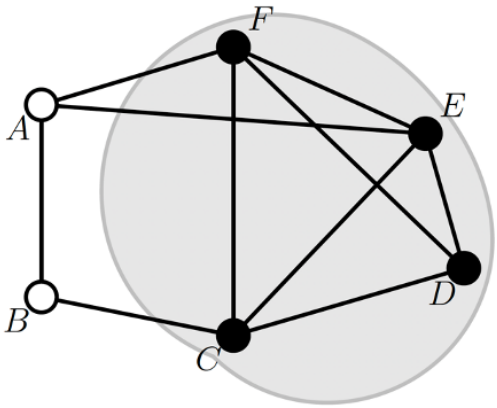


**Figure 3.1:** Representation of Cliques

Fig. 3.1, illustrates a graph that has several maximal and one maximum clique. The vertices $\{C, D, E, F\}$ participate in the maximum clique of the graph. However, there are several other maximal cliques e.g. $\{C, D, E\}$, $\{C, E, F\}$ etc.

One of the well-known and well-established algorithms to find all the maximal cliques is Bron-Kerbosh (BK) [96]. Below are the three different versions of the BK algorithm that was adopted initially for the work.

#### 3.3.1.1 The classical Bron-Kerbosh Algorithm

In an undirected graph, the BK algorithm is an enumeration algorithm for finding the maximal cliques [96]. This means that it lists all vertices with the two qualities that every pair of vertices in a listed subset is connected by an edge and that no listed subset may have any extra vertices added to it while maintaining its

full connectivity. Dutch researchers Coenraad Bron and Joep Kerbosch developed the BK algorithm, and they published a description of it in 1973 [97].

The three sets considered are $\{R\}$,$\{P\}$ and $\{X\}$. Initially, $R$ and $X$ are set to be an empty set , and $P$ contains all the vertices of the graph. $P$, has the set of potential candidates, $R$ is the interim result, and $X$ is the excluded set. The neighbors of the vertex $V$ are indicated by $N(v)$. The implementation of the algorithm is

A User $U$ represented by a vertex $V$ is chosen from $P$ to expand. Its non-neighbors are removed from $P$ and $X$ and then $v$ is added to $R$. The operation is then repeated using a different vertex from the new $P$ collection. The process is repeated until $P$ is no longer filled. If $X$ is empty once $P$ is empty, then the contents of $R$ are reported as a new maximal clique; if it isn't, then $R$ comprises a subset of an already discovered clique.

#### 3.3.1.2 BK Algorithm with Pivoting

Since the classical Bron-Kerbosh algorithm performs a recursive call for every clique, whether it is maximum or not, the basic version of the algorithm, as described above, is not quick and it is, therefore, insufficient when applied to graphs with a very large number of non-maximal cliques [98]. Bron and Kerbosch developed a variation of the approach incorporating a "pivot vertex" $u$, picked from $P$ ($as$P$\cup$X), to save time and enable the algorithm to backtrack more quickly in branches of the search that do not contain maximal cliques.

#### 3.3.1.3 BK Algorithm with Vertex Ordering

By arranging the sequence of the recursive calls carefully to reduce the sizes of the sets $P$ of candidate vertices within each recursive call, one alternative approach to improving the BK algorithm's fundamental form avoids pivoting at the highest level of recursion [99].

### 3.3.2 Vertex Removal

Creating cliques for some vertex $v \in \mathcal{V}$ of a graph $\mathcal{G}(\mathcal{V}, \mathcal{E})$ from the cliques of an included graph $\mathcal{G} - \{v\}$ is the foundation of the vertex removal method. Explaining differently, the technique gradually adds vertices to the newly discovered cliques while maintaining the list of all previously identified smaller cliques [100–102]. This approach typically results in the early identification of minimal maximal cliques. This method does, however, have a big drawback in that it requires a lot of memory to store all previously discovered cliques. To ensure that the detected cliques are maximal, each new clique must be compared to every clique that has been previously identified.

### 3.3.3 Backtracking- (Depth-First and Breadth-First Search)

The backtracking approach constructs a tree of probable cliques or solutions, then traverses iteratively using depth-first search. Because the method precludes the formation of repeating cliques, it does not require storing any past solutions to test maximality [103]. The backtracking approach, which is frequently used in real-world applications [104–118], only needs polynomial storage capac-

ity, in contrast to the exponential storage space needed by the vertex removal method [119]. However, backtracking shows that the cliques are not found in a predetermined order and that cliques of different sizes are found quasi-random. On the other hand, the backtracking approach has the major advantage of avoiding some search tree branches that don't produce new cliques.

The breadth-first search algorithm, as its name suggests, employs a systematic breadth-first search routine, similar to the backtracking method, to browse the tree of probable solutions. By listing maximal cliques in a non-decreasing size order, the breadth-first search distinguishes itself from the depth-first search [119]. However, because all cliques must be stored in memory to test the maximality, it has the same storage space disadvantage as vertex removal.

### 3.3.4 MaxClqDyn (Maximum Clique Algorithm)

For this work, this algorithm has been implemented and adopted to find the maximum clique i.e., the largest maximum clique is the Maximum Clique Dyn (MaxClqDyn) algorithm [120]. The MaxClqDyn algorithm is used to find the largest clique in an undirected graph. It is based on a basic algorithm (Max. Clique algorithm) that finds the maximum clique of bounded size. The bound is discovered by employing an improved coloring algorithm. The MaxClqDyn algorithm extends the Max. Clique algorithm with dynamically varying bounds. Janez Konc created this algorithm, the description is available in [98]. MaxClqDyn is an enhanced approximation coloring technique also known as a color-sort

algorithm. This improves the algorithm and shortens the time to find the maximum clique.

Hence, this approach differentiates maximal clique algorithms from maximum clique algorithms. The maximum clique methods discover a maximum clique, but the maximal search looks for all maximal cliques in a graph. As a result, maximum clique methods become around a factor of two faster.

### 3.3.5 Improvements in the Maximum Clique Algorithm

The two main improvements implemented for the MaxClqDyn algorithm are

1. An enhanced approximation coloring approach is adopted, that keeps the candidate set $\{R\}$ vertices in the preferable decreasing order according to their degrees. This is based on the understanding that assigning vertices to color classes—which throws the order off—is only necessary above a certain threshold. The time and number of steps necessary to find a maximum clique are both continuously decreased by this concept

2. To boost the identification of the largest clique a much tighter, more computationally expensive upper constraint is imposed on a portion of the search area. As a result, it dynamically toggles the sorting on/off during the execution of the algorithm by re-sorting the vertices in $R$ by their degrees sorted on the lower branches of the search tree

### 3.3.6 Complexity Analysis of discussed Clique Algorithms

Even though the maximum clique algorithms and hence, their versions, are easy to define, they are difficult to solve. Graph-theoretical approaches, especially those that enumerate all cliques, are usually memory-intensive and require appropriate data sharing across several processors in parallel implementations since a network with $n$ nodes may have as many as $3^{n/3}$ maximal cliques [103]. In addition, the memory requirement grows exponentially with graph size and, for modern applications, can be terabyte-scale. In the worst-case situation, the maximal clique algorithms including the BK algorithm require $\mathcal{O}(3^{n/3})$ time, where n is the number of vertices and $\mathcal{O}(n^2)$ time in auxiliary space.

The clique issue is identified as one of Karp's 21 NP-complete issues [86]. Additionally, the problem is impenetrable and hard to approximate [103]. [121, 122] provides a comprehensive investigation of the approximation complexity and the connection between combinatorics and graph theory issues using numerous examples.

For a graph $\mathcal{G}$ with $n$ nodes, the complexity of optimum algorithms scales as $\mathcal{O}(\beta^n)$ for some value of $1 < \beta \leq 2$. For instance, a brute force technique would list and check every potential clique, resulting in an overall complexity of $n^2 2^n = \mathcal{O}(2^n)$. For information on how to skilfully leverage the unique structure of the problem to decrease the difficulty of the solution from $2^n$ to $n$, where $1 < \beta \leq 2$, see the approaches in [123–127] in which a large number of graphs

with varying properties were averaged to determine the complexity, which was determined by extensive simulations and mentioned in Tab. 3.1.

**Table 3.1:** Maximum-clique Algorithms with their found Complexities

| **Reference** | **Authors** | **Complexity** |
|---|---|---|
| [123] | R. E. Tarjan and A. E. Trojanowski | $1.261^n$ |
| [124] | T. Jian | $1.235^n$ |
| [125] | J. M. Robson | $1.211^n$ |
| [126] | F. V. Fomin, F. Grandoni and D. Kratsch | $1.221^n$ |
| [127] | N. Bourgeois, B. Escoffier, V. T. Paschos and J. M. M. van Rooij | $1.212^n$ |

## 3.4 Maximum Clique-based User Scheduling Algorithm

Instead of identifying all the maximal cliques, which has a huge time complexity and for a system where a large number of users are considered to be served is almost impossible, a clustering framework based on finding the maximum clique with a modified version of MaxClqDyn algorithm is adopted here.

The proposed user scheduling algorithm is a greedy iterative procedure that aims at minimizing the total number of $P$, given an optimized threshold $\delta_{th}$. This is accomplished by

1. maximizing the size of each cluster by iteratively finding the maximum clique of the updated graph

2. creating disjoint sets of scheduled users, i.e., $\mathcal{C}_i \cap \mathcal{C}_j = \varnothing,\ \forall i, j$, which also minimizes $T_{tot}$, i.e., $T_{tot} = K$

**Algorithm 1** Iterative clique-based user scheduling algorithm

**Require:** Channel matrix $\mathbf{H}$, threshold $\delta_{th}$
**Ensure:** Cluster sets $\mathcal{C}_p$ and cluster weights $\gamma_p$ for $p = 1, \ldots, P$

Compute channel correlation distance matrix $\mathbf{\Psi}$
Compute adjacency matrix $\mathbf{A}$
Initialize remaining set of vertices with all users $\mathcal{R} = \mathcal{U}$
Create graph $\mathcal{G}(\mathcal{R}, \mathcal{E})$
Initialize $p = 1$
**while** $\mathcal{R} \neq \varnothing$ **do**
    $\mathcal{Q}_{\max} = \text{MaxClqDyn}(\mathcal{G})$
    $\mathcal{C}_p \leftarrow \mathcal{Q}_{\max}$
    $K_p \leftarrow |\mathcal{C}_p|$
    **for all** $U_i \in \mathcal{Q}_{\max}$ **do**
        **for all** $U_j \in \mathcal{R}$ **do**
            $\mathcal{E} = \mathcal{E} - \{U_i, U_j\}$
        **end for**
    **end for**
    $\mathcal{R} \leftarrow \mathcal{R} - \mathcal{Q}_{\max}$
    $p \leftarrow p + 1$
**end while**
$T_{tot} \leftarrow \sum_{p=1}^{P} K_p$
**for** p:=1 TO P **do**
    $\gamma_p \leftarrow \frac{K_p}{T_{tot}}$
**end for**

As shown in Algorithm 1, the iterative procedure searches for the maximum clique $\mathcal{Q}_{\max}$ in the graph and declares it as a cluster; at each step, the nodes in $\mathcal{Q}_{\max}$ and any edges connected to them are removed, the graph is updated after

pruning. The procedure is repeated until there are no more vertices in the graph. Fairness is guaranteed among users by setting the cluster weight $\gamma_p = \frac{K_p}{K}$, i.e., the fraction of the overall resource assigned to $\mathcal{C}_p$, which could be a fraction of the total available bandwidth in the Frequency Division Multiplexing (FDM) or a fraction of the total time slots in TDM.

## 3.5 Position-based Scheduler

The Position-based scheduler is based on the beam space precoding and has been considered a benchmark scheduler for this work. The satellite payload is thought to be transparent and equipped with $N_B$ co-located transmitting antennas, resulting in $N_B$ on-ground beams. A beam lattice is generated on the ground and one user per beam is Randomly selected to form a cluster. The scheduler ensures that all the system users are served at a minimum of once. The algorithm does not have a problem with unfixed cluster sizes. CSI, which is considered to be ideal is controlled by a single system Gateway in order to deal with the aggressive frequency reuse strategy GW which makes this solution CSI-based. Utilizing linear precoding techniques, the CSI is used to calculate the precoding weights. It considers MMSE precoding. TDM is used to serve users in the $N_B$ on-ground beams during each time frame. Further details can be found in [72].

## 3.6 Results and Discussion

In this section, the outcomes of the extensive numerical simulations with the parameter setup provided in Tab.3.4 are presented.

### 3.6.1 System Configurations for single MB-LEO satellite Scenario Generation

The assessment is performed in full buffer conditions, i.e., infinite traffic demand. A single LEO satellite at a distance of 600 km from the earth is considered. The users are uniformly distributed with the density of 0.05 users/$\text{Km}^2$, on average, the number of users $K = 2850$. The satellite is equipped with a UPA of $32 \times 32$ feeds. The user terminals are fixed and their receiver antenna gains $G_{\max}^{(rx)}$ is set to 39.7 dBi. The propagation scenario is the LOS model based on TR 38.821 and TR 38.811 [92, 93]. In all tests, the performance of the maximum clique-based scheduler is compared against a position-based scheduler [72], in which a beam lattice is generated on the ground and one user per beam is randomly selected to form a cluster, as it is depicted in Fig. 3.2 for a tier 5 beam lattice consisting of 91 beams.

Tab. 3.2, reports and describes the auxiliary parameters that are determined based on the setup of the system.

- *Beam Edge Gain*: Unless otherwise provided, this parameter, which sets the radiation pattern value at the beam edge with respect to the beam center, is fixed at $\Delta G_{edge}$=-3 dB
- *Satellite Altitude*: The satellite's altitude above ground level, $h_{sat}$
- *SSP Coordinates*: Coordinates for the Sub-Satellite Point (SSP)'s of the satellites' latitude and longitude

- *Satellite Antenna Array*: Parameters necessary for defining each satellite's onboard antenna array. The amount of radiating elements on the horizontal and vertical array axes is included i.e., $N_H$ and $N_V$, respectively

    1. The horizontal and vertical spacing of the elements, $d_H = 0.55\lambda$ and $d_V = 0.55\lambda$, respectively, with $\lambda$ being the signal wavelength
    2. The radiating element gain, $G_{el}[dBi] = 5.3dBi$
    3. The 3 dB bandwidth of the single element on the array horizontal and vertical axis, $\widetilde{\vartheta}_{3dB} = 90^\circ$ and $\widetilde{\varphi}_{3dB} = 90^\circ$, respectively
    4. The front-to-back ratio on the array horizontal and vertical axis, $A_m =$ 30 dB and $SLA_m$=30 dB, respectively

- *User Terminal Antenna Parameters*: Depending on the type of receiver, the antenna arrangement is shown in Tables 3.2, and 3.3 [128] and defined in TR 38.821 [92] is taken into account. However, we are assuming an overall antenna gain of 0 dBi for these receivers because the two array components at the receiver yield a 3 dBi antenna gain. It should be noted that TR 38.821 [92] mandates that a 3 dB polarization loss must be considered for handhelds. We have Considered VSAT for simulations and not handhelds Tab. 3.3.

Based on Tables 3.2 and 3.3 [128], the following additional data can be obtained

1. *Satellite Field of View (FoV)*: Angular field of view of the satellite computed by

**Table 3.2:** Ancillary and Derived Parameters and Allowed ranges.

| **Parameters** | **Range/ Description** |
|---|---|
| Beam edge gain | Less than 0 dB |
| Satellite altitude | Approximately 600 Km |
| SSP coordinates | Global Latitude and Longitude coordinates |
| Satellite antenna array | Parameters defining the planar antenna array on-board each satellite |
| UT antenna parameters | Parameters defining the UT receiver antenna as per TR 38.821 |

**Table 3.3:** Receiving Antenna Parameters.

| **Parameters** | **VSAT** | **Handheld** |
|---|---|---|
| Antenna type | Directional, with 60 cm diameter (TR 38.811) | Omnidirectional with 2 radiating elements |
| Polarisation | Circular | Linear |
| RX antenna gain | 39.7 dBi | 0 dBi per element |
| Antenna temperature | 150 K | 290 K |
| Noise figure | 1.2 dB | 7 dB |

$$\rho = \sin^{-1}\left(\frac{R_E}{R_E + h_{sat}}\right) \; [deg] \tag{3.4}$$

where $R_E$=6371 km is the Earth radius assuming a spherical Earth model

2. *Total on-board Power*: Total power available onboard each satellite for the transmission, computed as

$$P_t\,[dB] = P_{t,dens}\,[dB] + 10\log_{10} B_{UE} \tag{3.5}$$

Regarding the overall power, it is important to take into account that the linear polarization causes the handheld terminals to undergo a 3 dB polarization loss; however, since there are two radiating elements, this loss is compensated in accordance with TR 38.821 [92]. Therefore, both VSAT and handhelds are covered by Equation 3.5.

3. *Noise Power*: Total noise power at the receiver is defined as

$$P_N\,[dB] = N_f\,[dB] + 10\log_{10}\left(T_0\,[K] + \left(T_a\,[K] - T_0\,[K]\right)^{-0.1N_f[dB]}\right) \quad (3.6)$$

where $T_0$=290 K is the reference ambient temperature

4. *Satellite Antenna Gain*: Maximum antenna gain from the onboard array is defined as

$$G_{max}^{(tx)} = G_{el} + 10\log_{10} n_H n_V \approx 35.4\ dBi \quad (3.7)$$

For simulations, the MB scenario is created for a single LEO-MU-MIMO satellite. The first step is the identification of the beam radius based on the following procedure:

A single beam below the SSP is generated in $(u, v)$ coordinates. Let us denote by $\mathbf{p}$ the the $M \times 2$ array of $(u, v)$ coordinates for the considered directions, i.e., $\mathbf{p}_i = [u_i, v_i]$ with $(u_i, v_i)$ being the coordinates of the i-th direction. Based on the antenna model and the MU-MIMO design in Chapter. 2, the radiation pattern in the i-th direction, when beamforming is not yet implemented, is obtained as:

$$g^{(tx)}(u_i, v_i) = g_E(u_i, v_i) \sum_{n=1}^{n_H n_V} g_n(u_i, v_i) = g_E(u_i, v_i) \sum_{n=1}^{n_H n_V} e^{jk_0 \mathbf{r}_n \bullet \mathbf{p}_i} \tag{3.8}$$

with $\mathbf{r}_n$ being the position of the n-th antenna array element on its plane. The $n_H$,$n_V$-dimensional unit-norm beamforming vector in the direction of the SSP, $(0, 0)$, is given by

$$\mathbf{b} = \frac{1}{\sqrt{n_H n_V}} \sum_{n=1}^{n_H n_V} e^{jk_0 \mathbf{r}_n \bullet \mathbf{c}_i} \tag{3.9}$$

Thus, the radiation pattern in the i-th direction when beamforming is implemented to obtain a beam directed toward the SSP can be written as

$$g_{bf}^{(tx)}(u_i, v_i) = g_E(u_i, v_i) \sum_{n=1}^{n_H n_V} g_n(u_i, v_i) b_n^*(u_i, v_i) = \mathbf{g}_{feed}(u_i, v_i) \mathbf{b}^H \tag{3.10}$$

**Table 3.4:** Simulation parameters.

| **Parameter** | **Value** |
|---|---|
| Carrier frequency | 2 GHz |
| System band | S (30 MHz) |
| Beamforming space | feed |
| Receiver type | VSAT |
| Receiver antenna gain | 39.7 dBi |
| Noise figure | 1.2 dB |
| Propagation scenario | Line of Sight |
| System scenario | urban |
| Total on-board power density, $P_{t,\text{dens}}$ | 4 dBW/MHz |
| Number of tiers | 5 |
| User density | 0.05 user/km$^2$ |
| The cluster size for position-based scheduler | 91 |
| Number of transmitters $N$ | 1024 ($32 \times 32$ UPA) |
| Monte Carlo iterations | 100 |

where $\mathbf{g}_{feed}(u_i, v_i)$, with $g_{feed,n}(u_i, v_i) = g_E(u_i, v_i)\, g_n(u_i, v_i)$, is the $n_H$,$n_V$-dimensional row vector of array radiation patterns in the i-th direction and H denotes the Hermitian operator.

The beamwidth, $\vartheta_{edge}$, is obtained by first finding the coordinates of the directions at which the above radiation pattern is $\Delta G_{edge}$ dB below the value at the beam boresight direction:

$$\{(u, v) : 20\, log_{10}\, |g_{bf}^{(tx)}| - G_{max}^{(tx)} \leq -\Delta G_{edge}\} \tag{3.11}$$

then, since many coordinates will satisfy this condition (basically all directions outside the desired beam footprint), the angle is obtained as the angle between the beam center direction SSP and the direction at which we obtain the value of $20 \log_{10} \left| g_{bf}^{(tx)}(u, v) \right| - G_{max}^{(tx)}$ that is the closest to $-\Delta G_{edge}$.

Once $\vartheta_{edge}$ is known, the beam lattice is built with the procedure reported in TR 38.821 [92]. In particular, the Adjacent Beam Spacing (ABS) in $(u, v)$ coordinates is defined as

$$ABS = \sqrt{3} \sin \vartheta_{edge} \tag{3.12}$$

This value defines the beam radius on the $(u, v)$ plane that can be used to generate the desired hexagonal beam lattice with $n_{tier}$ tiers. As an example, let us assume to operate in S-band, thus implying that $f_c$=2 GHz and $\lambda$=0.1499 m, and the antenna model in Chapter 2, with $n_H$=$n_V$=32. The procedure defined by Equations 3.8, 3.9, and 3.10 leads to $\vartheta_{edge}$=1.4325° and, thus, ABS=0.0433.

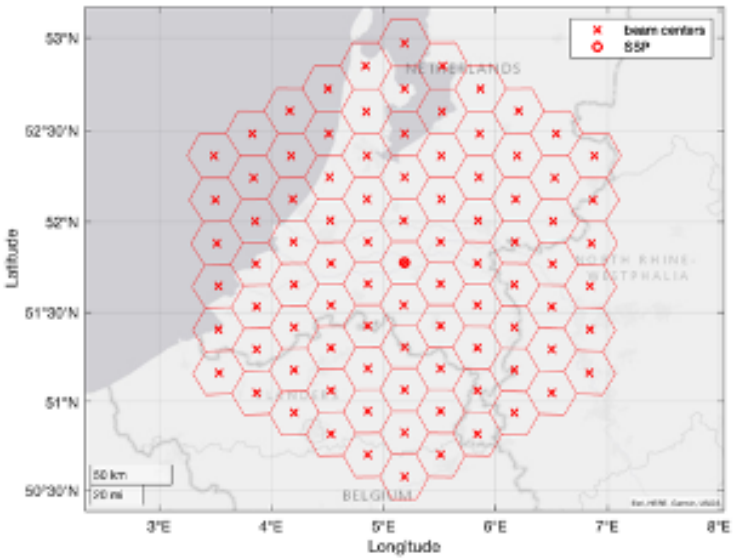


**Figure 3.2:** Tier 5 beam lattice for position-based scheduler and a standalone satellite.

Fig. 3.2, shows the beam lattice obtained with this procedure for a satellite with SSP located at 5.1863°E and 51.7757°N, in which $n_{tier}$=5 tiers around the SSP were generated.

Within the presented scenario, A heuristic optimization (i.e., by extensive simulations) of the graph threshold value $\delta_{th}$ which maximizes the average per-user capacity is first performed. The graph threshold $\delta_{th}$ determines the density of the graph, and therefore the size of the maximum clique at each iteration, i.e., $K_p$. In particular, the aim is towards finding a trade-off between the minimization of the total time slots $T_{tot}$ (maximization of the cluster size $K_p$), and the maximization of the average per-cluster SINR, $\frac{1}{K_p}\sum_{k=1}^{K_p}\text{SINR}_k^{(p)}$, which depends on the interference rejection capability of the per-cluster MMSE beamforming matrix $\mathbf{W}_p$, i.e., the ability to separate users only in the spatial domain.

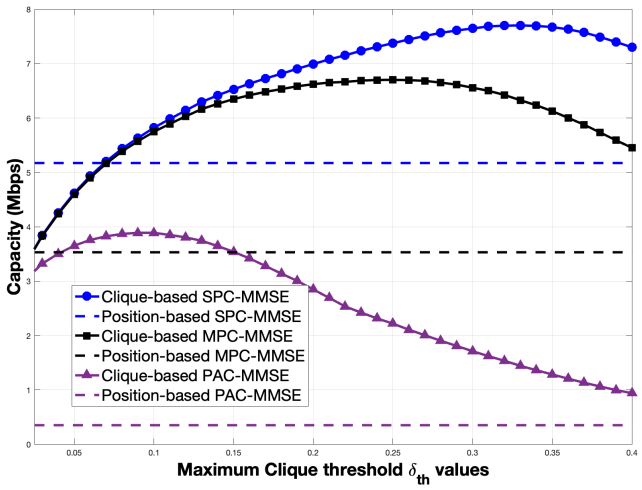


**Figure 3.3:** Graph threshold $\delta_{th}$ optimization for average per-user capacity maximization.

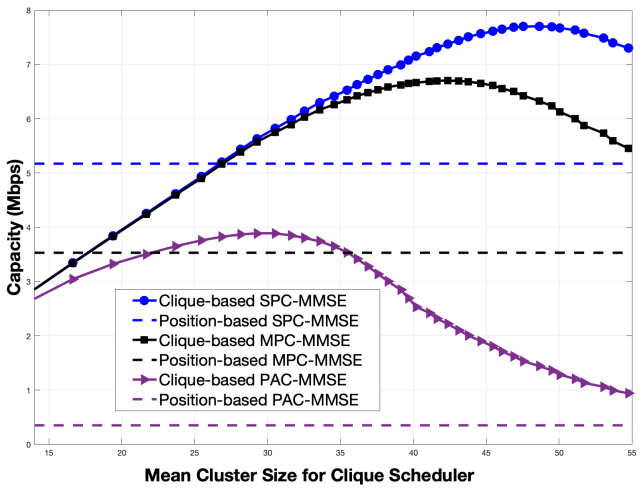


**Figure 3.4:** Clique-based scheduler mean cluster size vs. average per-user capacity.

Clearly, this capability decreases as the number of users increases within a cluster. The results of the graph threshold optimization are shown in Fig. 3.3 and Fig. 3.4. The average per-user capacity has been computed with a per-cluster MMSE beamforming matrix with SPC, MPC, and PAC normalizations, respectively.

Tab. 3.5, demonstrates the considered threshold values for the per-cluster capacity (Mbps) computation with all the three power normalizations i.e., SPC, MPC, and PAC with MMSE. The optimized threshold value $\delta_{th} = 0.33$ for SPC-MMSE, where the maximum value of capacity i.e., 7.71 Mbps is obtained. It can be further observed that the optimized threshold value $\delta_{th} = 0.25$ for MPC-MMSE with a maximum capacity of 6.70 Mbps, and finally for the PAC-MMSE, the optimized $\delta_{th} = 0.09$ with the maximum capacity of 3.9 Mbps. All the values are approximated and rounded off. Fig. 3.4 reports the mean cluster size as a function of the capacity. By recalling that in position-based scheduling the cluster size remains fixed, $K_p = 91$, $\forall p$, it can be noted that the clique-based scheduler produces clusters of smaller size, suggesting that interference management in a Tier 5 beam lattice becomes more problematic. With regards to the maximum clique-based scheduler, SPC and MPC normalizations allow a larger cluster size w.r.t. PAC, which has a reduced interference rejection capability since it disrupts the MMSE solution.

**Table 3.5:** Power Normalizations, Optimized Threshold values with their respective average cluster size, Capacity (Mbps), SINR [dB] and Spectral Efficiency i.e., Rate (b/s/Hz)

| MMSE- | Optimized $\delta_{th}$ | Average Cluster Size | Capacity (Mbps) | SINR [dB] | Spectral Efficiency (b/s/Hz) |
|---|---|---|---|---|---|
| SPC | 0.33 | 47 | 7.71 | 37.4 | 12.41 |
| MPC | 0.25 | 42 | 6.70 | 37.71 | 12.53 |
| PAC | 0.09 | 28 | 3.9 | 31.2 | 10.4 |

After the determination of maximum clique-based scheduler threshold optimization values for the three considered power normalizations with MMSE beamforming and average cluster size analysis, the Cummulative Distribution Function (CDF)s of the users' Capacity (Mbps), SINR [dB], and Rate (b/s/Hz) for both the maximum clique-based and position schedulers are obtained.

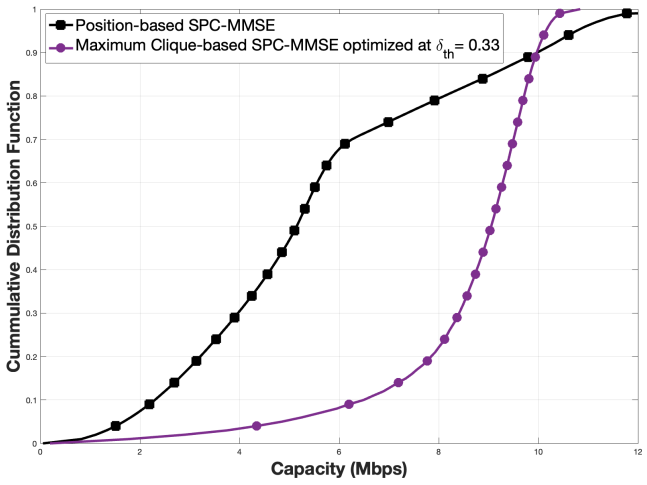


**Figure 3.5:** CDF of users' Capacity (Mbps) with graph threshold $\delta_{th} = 0.33$ optimized for SPC-MMSE

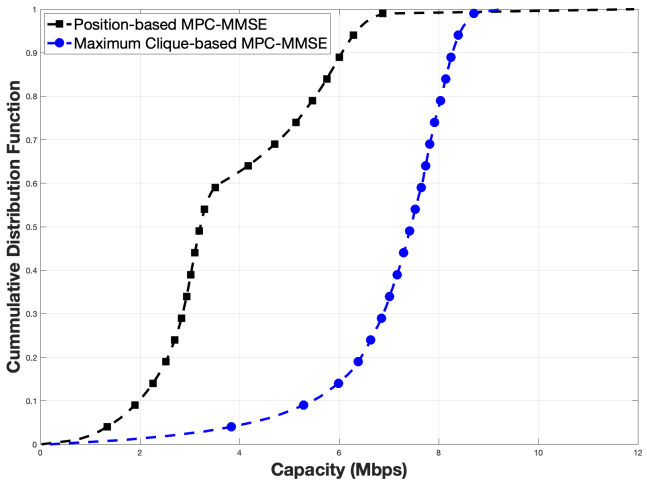


**Figure 3.6:** CDF of users' Capacity with graph threshold $\delta_{th} = 0.25$ optimized for MPC-MMSE

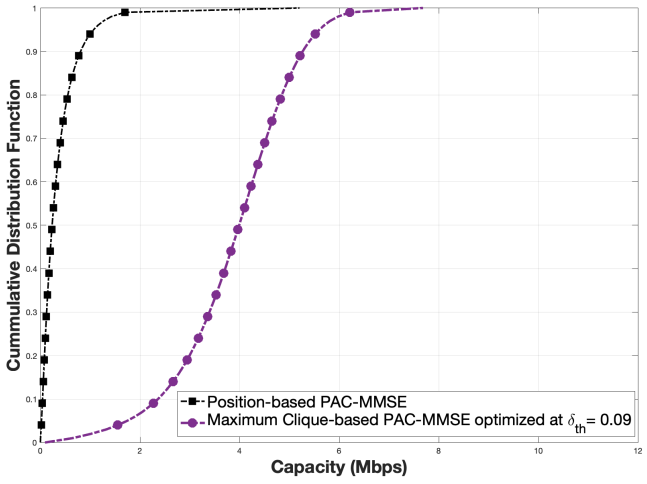


**Figure 3.7:** CDF of users' Capacity with graph threshold $\delta_{th} = 0.10$ optimized for MPC-MMSE

Figs.3.5, 3.6, and 3.7, illustrates the CDF of users' Capacity (Mbps) of the maximum-clique-based scheduler with graph threshold values of $\delta_{th} = 0.33$, $\delta_{th} = 0.25$ and $\delta_{th} = 0.09$ optimized for (SPC, MPC, and PAC)- MMSE w.r.t. the position-based scheduler. For SPC-MMSE and MPC-MMSE with $\delta_{th} = 0.33$, the maximum-clique-based scheduler shows an improvement in the average per-user Capacity of about 3.5 Mbps for both the normalization. For $\delta_{th} = 0.25$ the improvement for SPC and MPC w.r.t. the position-based scheduler is 3.6 and 3 Mbps approximately.

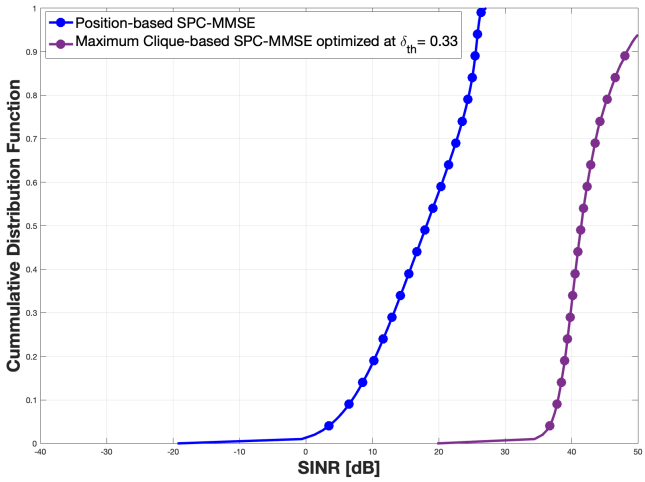


**Figure 3.8:** CDF of users' SINR with graph threshold $\delta_{th} = 0.33$ optimized for SPC-MMSE

Figs. 3.8, 3.9, and 3.10, illustrates CDF of users' SINR with graph threshold $\delta_{th} = 0.33$ optimized for SPC-MMSE, $\delta_{th} = 0.25$ optimized for MPC-MMSE, and $\delta_{th} = 0.09$ optimized for PAC-MMSE. The improvements in the maximum clique-based scheduler w.r.t. the position-based scheduler with $\delta_{th} = 0.33$ opti-

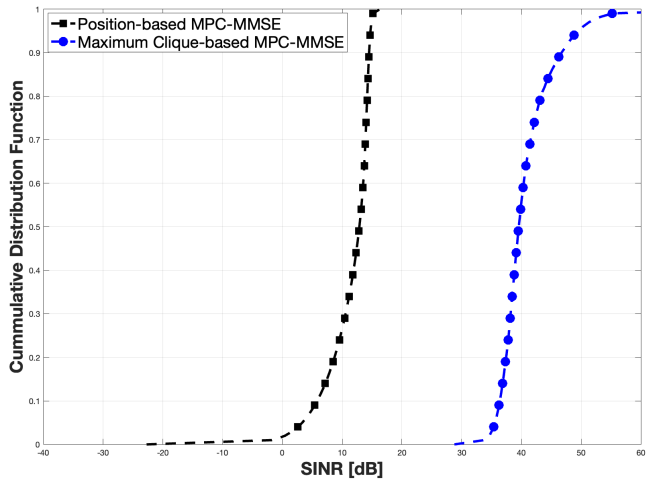


**Figure 3.9:** CDF of users' SINR5 with graph threshold $\delta_{th} = 0.25$ optimized for MPC-MMSE

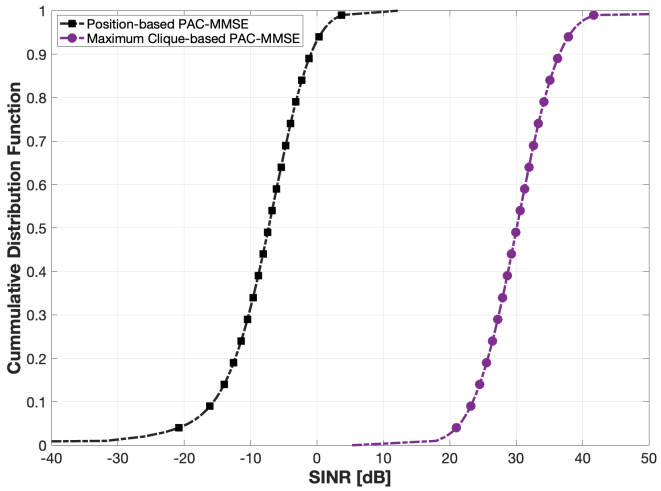


**Figure 3.10:** CDF of users' SINR with graph threshold $\delta_{th} = 0.33$, $\delta_{th} = 0.25$ and $\delta_{th} = 0.09$ optimized for (SPC, MPC, and PAC)- MMSE

mized for SPC-MMSE are approximately 20 [dB], 20 [dB], and 11 [dB] respectively.

Finally, Fig. 3.11, illustrates the CDF of users' spectral efficiency i.e., Rate(b/s/Hz) with the graph threshold value of $\delta_{th} = 0.33$ and optimized for SPC-MMSE. The improvements produced by the maximum clique-based scheduler w.r.t. the position-based scheduler with $\delta_{th} = 0.33$ optimized for SPC-MMSE are approximately 7 (b/s/Hz), 7 (b/s/Hz), and 2 (b/s/Hz) for the three considered power normalizations.

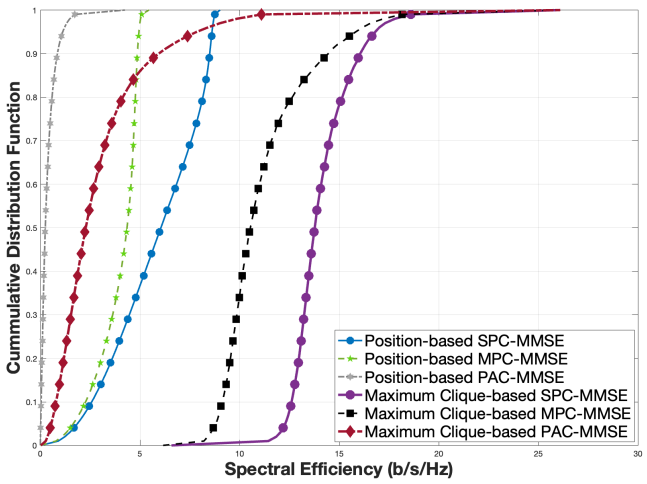


**Figure 3.11:** CDF of users' Rate(b/s/Hz) with graph threshold value of $\delta_{th} = 0.33$, optimized for SPC-MMSE

## 3.7 Conclusion

For this Chapter, a greedy iterative user scheduling procedure based on the maximum clique algorithm is proposed. A comprehensive analysis was performed considering both the maximal and maximum clique-based approaches along with their complexity analysis. Finally, to reduce the computational complexity and to perform user scheduling in an effective and efficient way the adopted maximum clique-based approach was further improved by relaxing the upper bound values and color sorting. This executed the maximum clique much quicker. The performances i.e., Capacity (Mbps), SINR [dB], and Spectral Efficiency i.e., Rate (b/s/Hz) of the maximum clique-based scheduler are compared against a position-based approach [72] for a single LEO satellite MU-MIMO system. For each time slot, a digital MMSE beamforming matrix allows to spatial separate the scheduled users and we considered three power normalizations for the beamforming matrix: SPC, MPC, and PAC. The results have been presented in terms of achievable per-user capacity and SINR and they show that the performance for clique-based scheduling is highly improved as compared to position-based scheduling. However, this scheduling framework is limited to the situations where the CSI is available.

# Chapter 4 - Graph-based User Scheduling Algorithms for LEO-MIMO Non-Terrestrial Networks

The content of this chapter is based on the following article;

*"B. Ahmad, D. G. Riviello, A. Guidotti, and A. Vanelli-Coralli, "Graph-based User Scheduling Algorithms for Non-Terrestrial Networks," Joint European Conference on Networks and Communications & 6G Summit (EuCNC), Gothenburg, Sweden, 2023"*

## 4.1 Introduction

In Chapter 3, we have proposed a Graph-based maximum clique algorithm to address the problem of user scheduling in the DL and on the feed space of the MU-MIMO LEO-NTN system. The results revealed high-performance gains w.r.t. the position-based scheduler [72]. However, that proposed solution was limited to scenarios where instantaneous and real-time CSI is available.

In order to address those situations where there is the absence of CSI, we performed a comprehensive study and constructed a graph adjacency matrix based on users' inter-distance which is computed from the users' great circle distance with the help of Haversine formula. The user scheduling is then performed

via the same maximum clique approach as presented in the previous Chapter. This novel user scheduling framework makes the solution viable for scenarios where there is an absence of CSI in the scheduling phase. However, to schedule the whole set of users we assume that the CSI is available at the transmission phase on a cluster basis because the MMSE beamforming requires the CSI.

After the computation of the graphs adjacency matrix, users are clustered together based on a dissimilarity metric and served by the satellite via SDM by means of MMSE on a cluster basis. After then, user groups are served in consecutive time slots using TDM.

In the graph representation, a UT is represented by each vertex in the graph network, and each vertex's edges are determined by one of the two possible dissimilarity metrics because we considered both CoC and users' inter-distance matrices for the comparison. The clustering issue is modeled in this manner

1. an edge in the graph between 2 users exists if their CoC, as defined in [77] is below a certain threshold

2. an edge in the graph between 2 users exists if their great-circle distance is above a certain threshold

It is apparent that the second method only needs to know the locations of the users, but the first scheduling methodology necessitates the availability of CSI at the transmitter during the scheduling phase. Once the graph has been created, each step of the process uses the efficient MaxClqDyn algorithm to identify the largest fully connected subgraph in the graph, also known as the maximum clique

diameter (MCD). The vertices in that clique are assigned to clusters, removed from the network, and the procedure is repeated until there are no more users to schedule.

As in [90], a Heuristic optimization of the ideal cluster size is carried out to maximize the system's sum-rate capacity. To further validate the results, the graph-based maximum-clique scheduler is compared with the well-established algorithm i.e., MADOC [77]. MADOC, make use of the CoC matrix computed from the Equation 3.1 which is used as a group policy and to assemble so-called $\epsilon$-orthogonal user groups, this means that the CoC calculated for all combinations of users inside a cluster does not exceed a certain threshold $\epsilon$. The optimal value for the$\epsilon$- threshold of MADOC depends on the scenario characteristics and hence, it has been newly identified w.r.t. [77]. The algorithm aims to consider fairness among all the users while maximizing the system throughput.

Results are presented in terms of achievable per-user capacity and show the superiority in performance of the proposed schedulers w.r.t. MADOC. By proposing a low-complexity graph-based user scheduling framework for MU-MIMO LEO NTN systems, the earlier work in [90] is further advanced. Each cluster's SDM is performed via FS MMSE beamforming.

In addition, the beamforming matrix power normalization using the SPC, and MPC approaches are considered [55]. The graph thresholds are heuristically optimized for both techniques in order to maximize the system's overall capacity. To confirm the study, the findings are compared with the MADOC algorithm [77]

and a position-based scheduler [72], which forms a beam lattice on the ground and clusters one user per beam at random.

## 4.2 Graph-based user scheduling

We denote with $\mathcal{G} = (\mathcal{V}, \mathcal{E})$ an undirected and unweighted graph with vertex set $\mathcal{V}$ and edge set $\mathcal{E}$. A clique $\mathcal{Q}$ of $\mathcal{G}$ is a subset of the vertices, $\mathcal{Q} \subseteq \mathcal{V}$, such that every two distinct vertices are adjacent, i.e., $\mathcal{Q}$ is a complete subgraph.

In our MU-MIMO LEO NTN scenario, the set of vertices $\mathcal{V}$ coincides with the set of users $\mathcal{U}$, and the edge set is constructed based on a dissimilarity measure. In case of no CSI availability at the transmitter at the scheduling phase, when only users' positions are known, we can adopt as a dissimilarity measure the users' great circle distance. Given the latitudes, $\phi_i$ and $\phi_j$ of the users $i$ and $j$, respectively, and $\lambda_i$ and $\lambda_j$ their respective longitudes, their great circle distance can be computed through the Haversine formula. Given two places' longitudes and latitudes, the Haversine formula calculates their great-circle separation. The law of haversines, which relates the sides and angles of spherical triangles, is a more broad formula in spherical trigonometry that is significant in satellite navigation [129].

Defining first

$$h = \sin^2\left(\frac{\phi_j - \phi_i}{2}\right) + \cos\phi_i \cdot \cos\phi_j \cdot \sin^2\left(\frac{\lambda_j - \lambda_i}{2}\right) \tag{4.1}$$

then

$$[\mathbf{\Gamma}]_{i,j} = 2r \arcsin\left(\sqrt{h}\right) \tag{4.2}$$

We can define now the corresponding adjacency matrix $\mathbf{A}$ as:

$$[\mathbf{A}]_{i,j} = \begin{cases} 1, & [\mathbf{\Gamma}]_{i,j} \geq \delta_D \\ 0, & [\mathbf{\Gamma}]_{i,j} < \delta_D \end{cases} \tag{4.3}$$

where $\delta_D$ is again a properly designed threshold. If an element of $\mathbf{A}$ is equal to 1, the great-circle distance and therefore the angular distance between $U_i$ and $U_j$ is such that their directions $(\vartheta_i, \varphi_i)$ and $(\vartheta_j, \varphi_j)$ can be spatially separated by means of MMSE digital beamforming, and they can belong to the same cluster (or they can be co-scheduled), while if an element of $\mathbf{A}$ is equal to 0, the directions of $U_i$ and $U_j$ are considered to be too close to be spatially distinguished by the beamformer.

The threshold determines an upper bound on the size of a clique and therefore the optimal number of users that can be efficiently multiplexed in the space domain by MMSE beamforming within a cluster.

As illustrated in Algorithm 2, the iterative procedure searches for the maximum clique $\mathcal{Q}_{\max}$ in the graph and declares it as a cluster; at each step, the nodes in $\mathcal{Q}_{\max}$ and any edges connected to them are removed, the graph is updated after pruning. The procedure is repeated until there are no more vertices in the graph. Fairness is guaranteed among users by setting the cluster weight $\gamma_p = \frac{K_p}{K}$, i.e., the fraction of the overall resource assigned to $\mathcal{C}_p$, which could be a

fraction of the total available bandwidth in FDM or a fraction of the total time slots in TDM as described in Chapter 3.

**Algorithm 2** Iterative clique-based user scheduling algorithm

**Require:** Channel matrix $\mathbf{H}$, threshold $\delta_D$
**Ensure:** Cluster sets $\mathcal{C}_p$ and cluster weights $\gamma_p$ for $p = 1, \ldots, P$

Compute users' great circle distance matrix $[\mathbf{\Gamma}]_{i,j}$
Compute adjacency matrix $\mathbf{A}$
Initialize remaining set of vertices with all users $\mathcal{R} = \mathcal{U}$
Create graph $\mathcal{G}(\mathcal{R}, \mathcal{E})$
Initialize $p = 1$
**while** $\mathcal{R} \neq \varnothing$ **do**
    $\mathcal{Q}_{\max} = \text{MaxCliqueDyn}(\mathcal{G})$
    $\mathcal{C}_p \leftarrow \mathcal{Q}_{\max}$
    $K_p \leftarrow |\mathcal{C}_p|$
    **for all** $U_i \in \mathcal{Q}_{\max}$ **do**
        **for all** $U_j \in \mathcal{R}$ **do**
            $\mathcal{E} = \mathcal{E} - \{U_i, U_j\}$
        **end for**
    **end for**
    $\mathcal{R} \leftarrow \mathcal{R} - \mathcal{Q}_{\max}$
    $p \leftarrow p + 1$
**end while**
$T_{tot} \leftarrow \sum_{p=1}^{P} K_p$
**for** p:=1 **to** P **do**
    $\gamma_p \leftarrow \frac{K_p}{T_{tot}}$
**end for**

## 4.3 Simulation setup and results

In this section, the outcomes of the extensive numerical simulations with the parameters specified in Tab. 4.1 are presented. The assessment has been performed in full buffer conditions. A single LEO satellite is considered at a distance of 600 Km from the earth. On average the total number of users is $K_T = 5700$ much larger than what is considered in Chapter 3. The satellite is equipped with a UPA of $32 \times 32$ feeds. The user terminals are fixed and their receiver antenna gains $G_{\max}^{(rx)}$ is set to 39.7 dBi. The propagation scenario is the LOS based on TR 38.811 and TR 38.821 [92, 93].

**Table 4.1:** Simulation parameters

| **Parameter** | **Value** |
|---|---|
| Carrier frequency | 2 GHz |
| System band | S (30 MHz) |
| Beamforming space | feed |
| Receiver type | VSAT |
| Receiver antenna gain | 39.7 dBi |
| Noise figure | 1.2 dB |
| Propagation scenario | Line of Sight |
| System scenario | urban |
| Total on-board power density, $P_{t,\text{dens}}$ | 4 dBW/MHz |
| Number of tiers | 5 |
| User density | 0.1 user/km$^2$ |
| The cluster size for position-based scheduler | 91 |
| Number of transmitters $N$ | 1024 ($32 \times 32$ UPA) |
| Monte Carlo iterations | 100 |

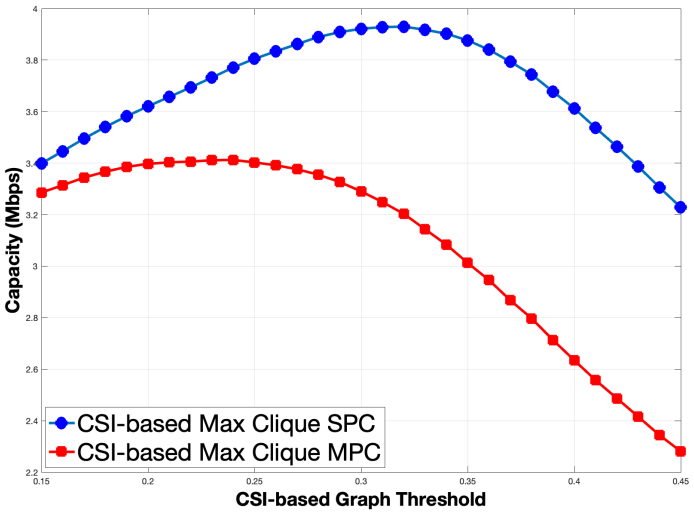


**Figure 4.1:** CSI-based Max Clique Scheduler.

Aiming at maximizing the average per-user capacity, a heuristic optimization of thresholds $\delta_C$, $\epsilon$, and $\delta_D$ for CSI-based Max clique, MADOC, and distance-based Max clique schedulers are performed, respectively, as illustrated in Figs. 4.1, 4.2, and 4.3 for both MMSE with the SPC and MPC power normalization. In particular, the trade-off between the maximization of the cluster size $K_p$ (minimization of the number of clusters), and the maximization of the average per-cluster SINR, $\frac{1}{K_p}\sum_{k=1}^{K_p}\mathrm{SINR}_k^{(p)}$ are examined, which depends on the interference rejection capability of the per-cluster MMSE beamforming matrix $\mathbf{W}_p$, i.e., the ability to separate users only in the spatial domain.

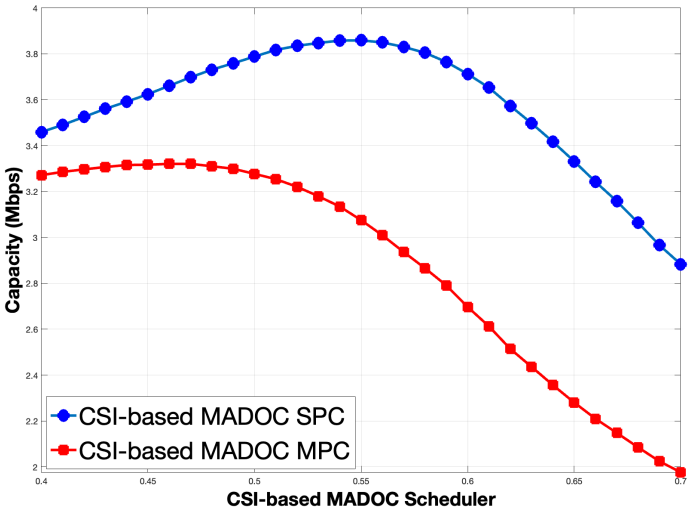


**Figure 4.2:** CSI-based MADOC Scheduler.

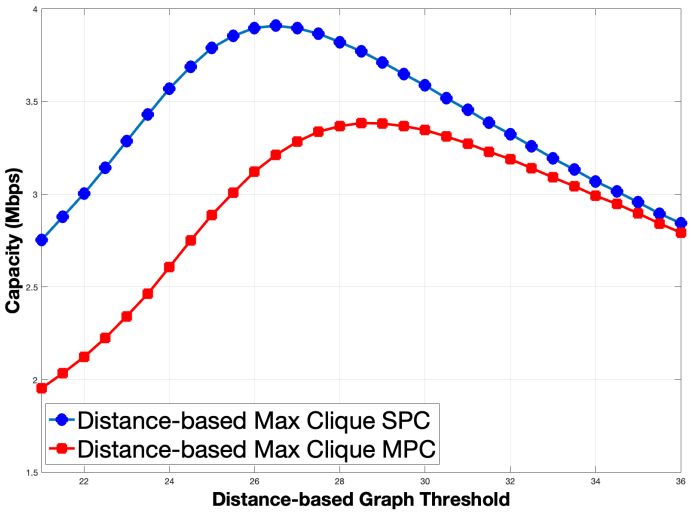


**Figure 4.3:** Distance-based Max Clique Scheduler.

Tab. 4.2, reports for each scheduler the obtained optimal threshold, the mean cluster size, and the average per-user capacity, which has been computed with a per-cluster MMSE beamforming matrix with SPC and MPC normalization.

**Table 4.2:** Simulation Results for Threshold Optimization

| Parameters | | CSI-based Max clique | CSI-based MADOC | Distance-based Max clique | Position-based random |
|---|---|---|---|---|---|
| Optimized threshold | SPC | 0.32 | 0.55 | 26.50 | - |
| | MPC | 0.24 | 0.47 | 28.50 | - |
| Mean cluster size | SPC | 51 | 59.4 | 52.3 | 91 |
| | MPC | 44 | 50 | 46 | 91 |
| Capacity (Mbps) | SPC | 3.92 | 3.85 | 3.90 | 2.58 |
| | MPC | 3.41 | 3.32 | 3.38 | 1.77 |

Recalling that in the simulated scenario, with a Tier 5 beam lattice, the cluster size for the position-based random scheduler remains constant $K_p = 91 \, \forall p$. Fig. 4.4, shows the average per-user capacity as a function of the mean cluster size, it can be noticed that both graph-based schedulers outperform MADOC and that in general CSI normalization can offer a larger user group size w.r.t. MPC. It is worth remarking that also a non-CSI-based technique, i.e. the distance-based Max clique scheduler, can be highly competitive, although CSI knowledge at the transmitter will be required at the transmission phase but on a cluster level.

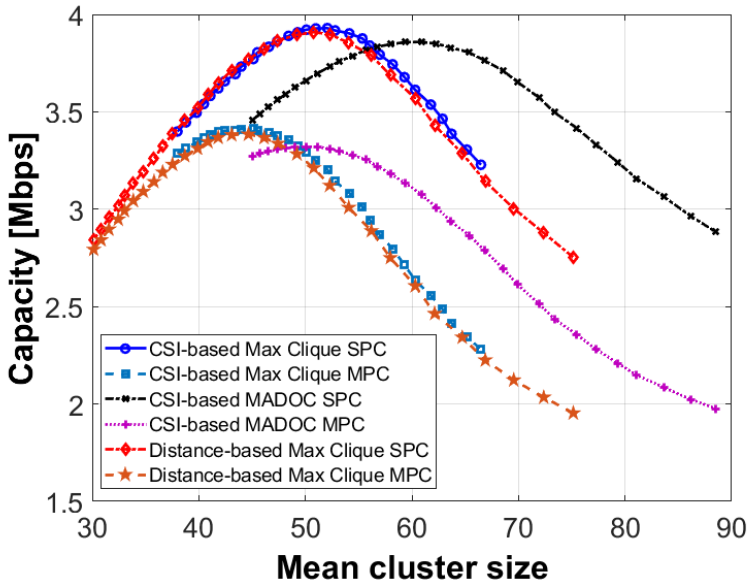


**Figure 4.4:** Mean cluster size vs. capacity for graph-based and MADOC schedulers.

In Fig. 4.5, the CDF of the user's capacity for all the considered schedulers is provided. The CSI-based (distance-based) Max clique scheduler shows an improvement w.r.t. MADOC in terms of the average per-user capacity of approximately 0.15 (0.14) Mbps for SPC and 0.12 (0.1) Mbps for MPC. The improvement of both graph-based schedulers w.r.t. the positon-based random scheduler [90] is above 1.6 Mbps for SPC and above 1.8 Mbps for MPC. Finally, Fig. 4.6 shows the CDF of users' SINR and further demonstrates the very high performance of both graph-based schedulers w.r.t position-based, with a slight improvement also w.r.t. to MADOC.

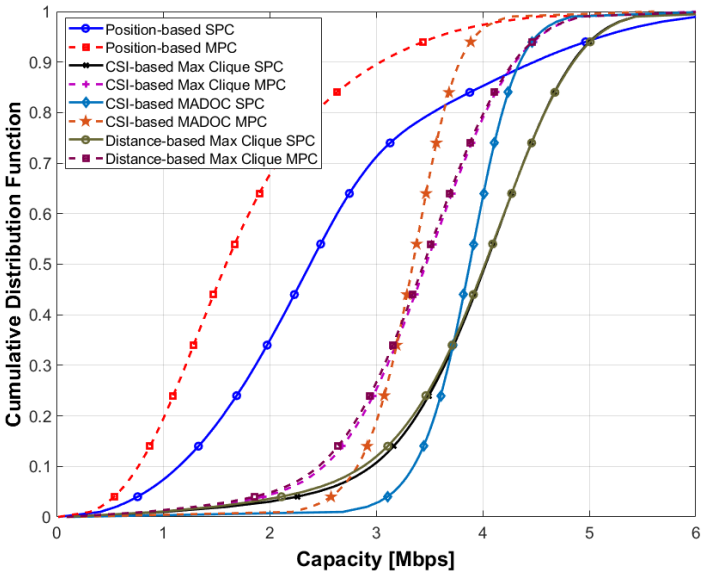


**Figure 4.5:** CDF of users' capacity.

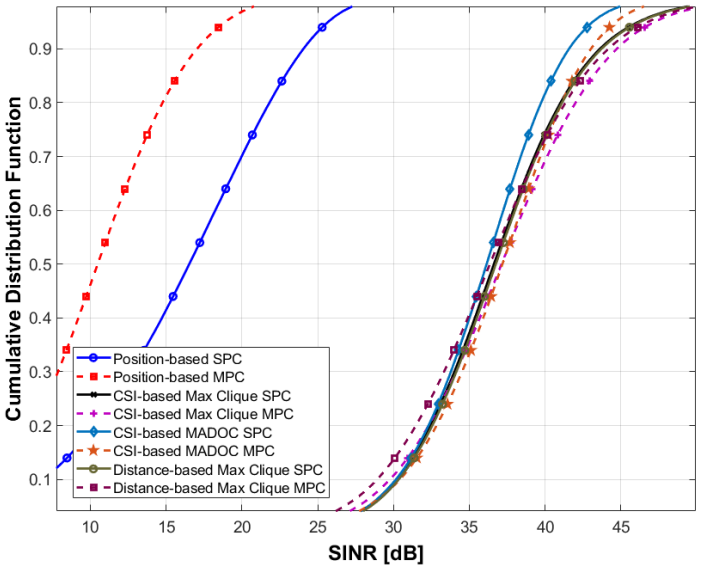


**Figure 4.6:** CDF of users' SINR.

## 4.4 Conclusion

For this work, we have proposed an iterative user scheduling procedure based on the maximum-clique algorithm that extended the previously presented work from Chapter 2 and considers the users' great circle distance for the formulation of the graph's adjacency matrix. This adaptation makes the maximum clique algorithm perform in the situation where there is no CSI availability with the consideration that CSI knowledge at the transmitter will be required at the transmission phase but on a cluster level.

Furthermore, a high user density is adopted as compared to the previous chapter to test whether the maximum clique approach is suitable or not for a high user density. The heuristic optimization was performed for both the CSI-based and Distance-based scenarios. For each cluster, a digital MMSE beamforming matrix is allowed to spatial separate the scheduled users, and two power normalizations are considered for the MMSE matrix: SPC and MPC.

Although, the extensive simulation results revealed that the maximum clique algorithm is highly capable and performance-oriented still to further validate the analysis effort was made to re-implement the MADOC scheduler. The optimal threshold values for both graph-based schedulers and MADOC were found and the results have been presented in terms of achievable per-user capacity and SINR and show an improvement in the performance of both graph-based schedulers w.r.t. the MADOC.

# Chapter 5 - Improved Graph-based User Scheduling for Sum-Rate Maximization in LEO-NTN Systems

The content of this chapter is based on the following article;

*"B. Ahmad, D. G. Riviello, A. Guidotti and A. Vanelli-Coralli, "Improved Graph-based User Scheduling for Sum-Rate Maximization in LEO-NTN Systems," The 48th IEEE International Conference on Acoustics, Speech, & Signal Processing (ICASSP), Rhodes, Greece, 2023"*

*"Part of this work has been funded by the 6G-NTN project, which received funding from the Smart Networks and Services Joint Undertaking (SNS JU) under the European Union's Horizon Europe research and innovation programme under Grant Agreement No 101096479. The views expressed are those of the authors and do not necessarily represent the project. The Commission is not liable for any use that may be made of any of the information contained therein."*

## 5.1 Introduction

In the previous two Chapters, we presented two distinct user scheduling methods based on graph theory and the maximum clique algorithm. In Chapter 3, a CSI-based method was described in which the CoC matrix was constructed to

compute the graph's adjacency matrix from Equation 3.2. Differently, in Chapter 4 the adjacency matrix was calculated from the users' great circle distance using Equation 4.3. However, in both approaches, a heuristic optimization was carried out to find the optimized threshold values $\delta_{th}$ for different power normalizations which are computed from Equations 2.14, 2.15, and 2.16. The scheduling algorithm provided in Algorithms 1, and 2 were tested for various threshold values $\delta_{th}$ such that the optimized threshold value is determined. After that For each cluster, a digital MMSE beamforming matrix is applied to spatially separate the users.

Evaluating [77], While implementing MADOC algorithm, in the initialization phase of user scheduling the total number of users $K_{tot}$ was divided by the total number of feeds $N_F$ to obtain the total number of time slots. After that, the first user of each group was assigned on the basis of the users with the highest channel gains. But it can be observed that when the actual algorithm is executed, some of the clusters generated have an extremely less number of users. The same issue was identified with the CSI-based maximum clique scheduler [90] and distance-based maximum clique scheduler since the graph gets pruned at each iteration but with improved per-user capacity as compared to MADOC. Tab. 4.2 lists the comparison of three different schedulers.

To address the issue of group number minimization, in this work, we propose a novel approach that aims to decrease the variance of the cluster size distribution. The adopted approach is that, instead of having a fixed threshold value and performing threshold optimization, the optimal graph density is determined.

It has been already explained that selecting the proper threshold $\delta_{th}$ plays a vital role in the scheduler design as it determines the density of the graph $D(\mathcal{G})$ which can be computed from Equation 3.3. It is already established that the graph density changes as the threshold value vary since the actual number of edges is only determined with the fixed threshold value. The proposed algorithm has still the same structure as Algorithms 1, and 2 i.e. the iterative procedure for each step

i search for the maximum clique in the graph

ii declares it as a cluster

iii prunes the graph until there are no more users to be scheduled

Now differently from the previous threshold optimization approaches, in this newly proposed novel user scheduling framework, a target graph density value $\alpha_t$ is required as input of the Algorithm 3, instead of a graph threshold $\delta_{th}$. At the beginning of the iterative procedure and after each pruning, a new graph threshold value, which produces the input target graph density, needs to be computed. To find the threshold for the requested graph density provided at the input and keep the graph density constant at each pruning iteration is the problem statement. To solve this, the simplest and most dependable iterative technique for solving nonlinear equations is the Bisection Method. This approach is commonly referred to as binary cutting/ chopping or the half-interval approach. The bisection method is a root-finding method in mathematics that can be applied to any continuous function for which two values with opposite signs are known.

The method entails repeatedly bisecting the interval defined by these values and then selecting the sub-interval in which the function changes sign, implying that it contains a root. In general, the concept of finding the root is explained in [130].

The bisection method can be used to solve the equation $f(x) = 0$ for the real variable $x$, where $f$ is a continuous function defined on the interval $[a, b]$ and $f(a)$ and $f(b)$ have opposite signs. In this case, $a$ and $b$ are said to bracket a root because the continuous function $f$, according to the intermediate value theorem, must have at least one root in the interval $(a, b)$. As a result, it can be determined which portion of the interval contains the root by determining the function's sign at the midpoint. Therefore to know the threshold for the requested graph density the Bisection method is used after each pruning iteration as provided in Algorithm 3.

## 5.2 User Scheduling with Constant Graph Density

### 5.2.1 Objectives

In [77], the paper, considered three major aspects for the development of the MADOC algorithm with the emphasis given on Group Number Minimization. As each additional user group requires a separate time slot since the user groups are divided via TDM, this suggests that all groups are provided less frequently, which lowers the data rate that is available to each group. Therefore, the number of groups must be kept to a minimum in order to establish the foundation for high data rates for each group. The number of users per group should be increased

as a result. The results in Tab. 4.2, lists the Mean cluster size along with other parameters for three different scheduling algorithms for the considered simulation parameters in Tab. 4.1. This work is aimed to minimize the number of total slots with the graph-based maximum clique algorithm.

### 5.2.2 Proposed User Scheduling Algorithm

We denote with $\mathcal{G} = (\mathcal{V}, \mathcal{E})$ an undirected and unweighted graph with vertex set $\mathcal{V}$ and edge set $\mathcal{E}$. A clique $\mathcal{Q}$ of $\mathcal{G}$ is a subset of the vertices, $\mathcal{Q} \subseteq \mathcal{V}$, such that every two distinct vertices are adjacent, i.e., $\mathcal{Q}$ is a complete subgraph. In our considered LEO-NTN MIMO scenario, the set of vertices $\mathcal{V}$ coincides with the set of users $\mathcal{U}$ and the edge set is constructed based on the channel Coefficient of Correlation (CoC) [71, 77, 90], defined as

$$[\mathbf{\Psi}]_{i,j} = \frac{\left|\mathbf{h}_i \mathbf{h}_j^H\right|}{\|\mathbf{h}_i\| \, \|\mathbf{h}_j\|} \tag{5.1}$$

where $[\mathbf{\Psi}]_{i,j} \in [0, 1]$. The set of edges $\mathcal{E}$ of the $\mathcal{G}$ graph is completely determined by its adjacency matrix $\mathbf{A}$, whose entries are defined as:

$$[\mathbf{A}]_{i,j} = \begin{cases} 1, & [\mathbf{\Psi}]_{i,j} \leq \delta_{th} \\ 0, & [\mathbf{\Psi}]_{i,j} > \delta_{th} \end{cases} \tag{5.2}$$

where $\delta_{th}$ denotes the graph threshold. An edge between $U_i$ and $U_j$ implies that their channels $\mathbf{h}_i$ and $\mathbf{h}_j$ are considered nearly orthogonal and therefore they can be co-scheduled. The graph threshold determines the density of the graph

$D(\mathbf{\Psi}, \delta_{th})$ which can be computed as

$$D(\mathbf{\Psi}, \delta_{th}) = \frac{2|\mathcal{E}|}{|\mathcal{V}|\left(|\mathcal{V}|-1\right)} = \frac{1}{2}\sum_{i=1}^{K}\sum_{j=1}^{K}[\mathbf{A}]_{i,j} \tag{5.3}$$

**Algorithm 3** Improved Max Clique scheduler with constant graph density.

**Require:** Set of users $\mathcal{U}$, channel CoC matrix $\mathbf{\Psi}$ and target graph density $\epsilon_t$
Initialize $p = 1$ and $K = |\mathcal{U}|$
**while** $\mathcal{U} \neq \varnothing$ **do**
  $\delta_{th} = BisectionMethod$ ($\mathbf{\Psi}$, 0, 1, $\epsilon_t$, $tol$, $I_{\max}$)
  Compute $\mathbf{A}$ as in (3.2)
  $\mathcal{Q}_{\max} = MaxCliqueDyn\mathbf{A}$
  $\mathcal{C}_p \leftarrow \mathcal{Q}_{\max}$ and $K_p \leftarrow |\mathcal{C}_p|$
  Remove all rows and columns of $\mathbf{\Psi}$ associated with users in $\mathcal{Q}_{\max}$
  $\mathcal{U} \leftarrow \mathcal{U} - \mathcal{Q}_{\max}$ and $K \leftarrow K - K_p$
  $p \leftarrow p + 1$
**end while**
**PROCEDURE** $BisectionMethod$ ($\mathbf{\Psi}$, 0, 1, $\epsilon_t$, $tol$, $I_{\max}$)
$c = \frac{a+b}{2}$ and $i = 0$
**while** $|f(\mathbf{\Psi}, c)| > tol$ & $i < I_{\max}$ **do**
  **if** $f(\mathbf{\Psi}, b) \cdot f(\mathbf{\Psi}, c) < 0$ **then**
    $a = c$
  **else**
    $b = c$
  **end if**
  $c = \frac{a+b}{2}$
  $i \rightarrow i + 1$
**end while**
**return** c
**ENDPROCEDURE**

As illustrated in Algorithm 3, we design a greedy iterative algorithm that aims at minimizing the total number of clusters $P$ and maximizing the total sum-rate capacity. Similarly to [90], the iterative procedure searches for the maximum clique $\mathcal{Q}_{\max}$ in the graph through the efficient MaxCliqueDyn algorithm [120] and declares it as a cluster; at each step the nodes in $\mathcal{Q}_{\max}$ and any edges connected to them are removed. The main novelty in the new algorithm is how the graph is updated after each pruning. In [90], since a constant graph threshold value is set at the beginning of the procedure, only graph pruning is implemented at each step.

Here instead we first set a constant target graph density value $\epsilon_t$, then at each step (both at the beginning and after each pruning), we search for the threshold $\delta_{th}$ such that $D(\mathbf{\Psi}, \delta_{th}) = \epsilon_t$. To obtain the respective threshold value for the required target density $\epsilon_t$, we aim at finding the root of the function $f(\mathbf{\Psi}, \delta_{th}) = D(\mathbf{\Psi}, \delta_{th}) - \epsilon_t$ through the bisection method [130]. Within this method, the root to be found is initially bounded between 0 and 1, the search interval is repeatedly halved until convergence is reached through the parameter *tol*. Finally, the parameter $I_{\max}$ limits iterations to prevent infinite loops.

### 5.3 Results and Discussion

The simulation parameters are exactly the same as listed in Tab. 3.4 from Chapter 3. Again, the assessment is performed in full buffer conditions, i.e., infinite traffic demand. A single LEO Satellite at a distance of 600 km from the Earth is considered. The users are uniformly distributed with the density of 0.05 users/Km$^2$, on average, the number of users $K = 2850$. The satellite is equipped with a UPA of $32 \times 32$ feeds. The user terminals are fixed and their receiver antenna gains $G_{\max}^{(rx)}$ is set to 39.7 dBi. The propagation scenario is the LOS based on TR 38.821 and TR 38.811 [92, 93]. In all simulations, the performance of the improved maximum (Max) clique-based algorithm with constant graph density is compared against our original Max clique scheduler [90] and MADOC [77].

Aiming at maximizing the total sum-rate capacity, we performed a heuristic optimization of the graph density for the improved Max clique, and we obtained optimized thresholds for the original Max clique [90] and MADOC [77] for

(SPC, and MPC)-MMSE power normalizations as shown in Tab. 5.1. It is evident that the improved Max clique offers the highest average per-cluster sum-rate capacity (Gbps), and mean cluster size as compared to the other schedulers, with a very large improvement in both indicators w.r.t. the original Max clique.

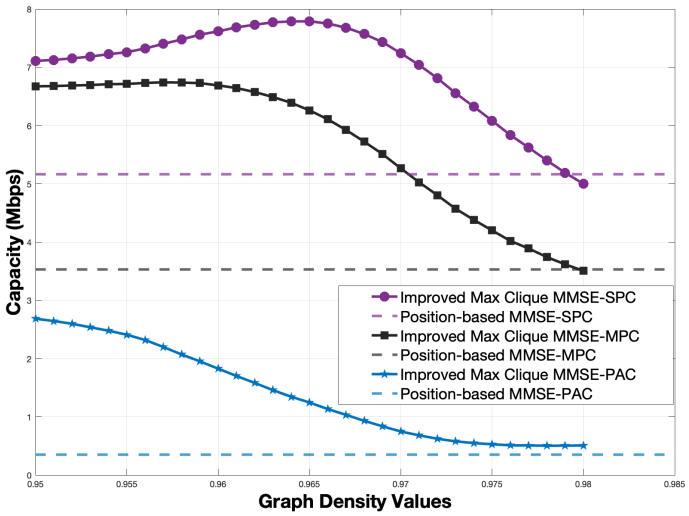


**Figure 5.1:** Improved Max Clique Threshold Optimization.

Within the presented scenario, we first performed a heuristic optimization (i.e., by extensive simulations) of the graph density values $D(\mathcal{G})$ which maximizes the average per-user capacity. The points where the graph densities intersect with the respective graph threshold $\delta_{th}$ values were determined by using the bisection method, and also, the size of the maximum clique at each iteration, i.e., $K_p$. Clearly, this capability decreases as the number of users increases within a cluster. The results of the graph with constant densities and variable threshold values optimization are shown in Fig. 5.1 and 5.2. The average per-user capacity has

been computed with a per-cluster MMSE beamforming matrix with SPC, MPC, and PAC normalizations, respectively.

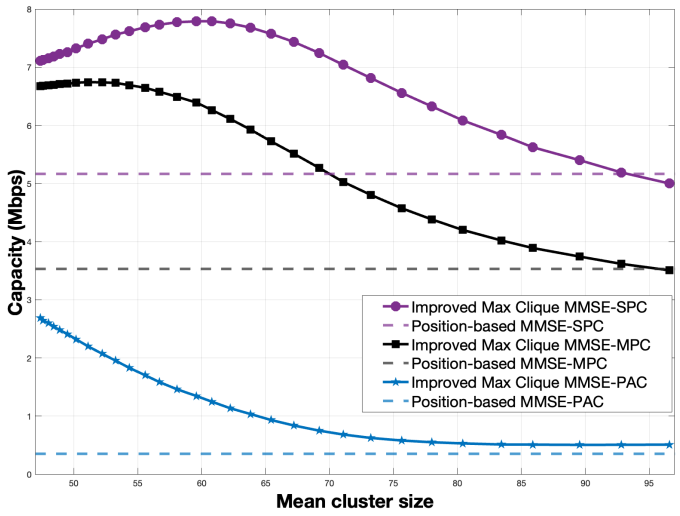


**Figure 5.2:** Improved Max Clique algorithm Mean Cluster Size vs. Capacity.

Fig. 5.2, shows the average per-user capacity as a function of the mean cluster size, it can be noticed that the Improved Max Clique scheduler which takes into account the constant graph density with variable threshold values accommodates a much larger number of users per-cluster as compared to CSI-based maximum clique scheduler [90]. In general, SPC normalization can offer a larger user group size w.r.t. MPC.

It is evident from Tab. 5.1, that not only the improved cluster sizes achieved from the newly proposed Improved Max Clique scheduler but also a high gain is achieved in terms of capacity (Mbps) as compared to both the CSI-based max-

**Table 5.1:** Simulation results for graph density optimization.

| Parameters | | Original Max clique | MADOC | Improved Max clique |
|---|---|---|---|---|
| Optimized threshold graph density | SPC | 0.32 | 0.58 | 0.965 |
| | MPC | 0.27 | 0.51 | 0.957 |
| Mean cluster size | SPC | 46.37 | 56.34 | 59.42 |
| | MPC | 42.81 | 48.56 | 50.29 |
| Sum-rate capacity (Gbps) | SPC | 17.93 | 21.17 | 21.49 |
| | MPC | 15.82 | 18.19 | 18.64 |

imum clique scheduler [90], and the position-based [72] scheduler. Furthermore, the improved cluster sizes result in the minimization of the time slots.

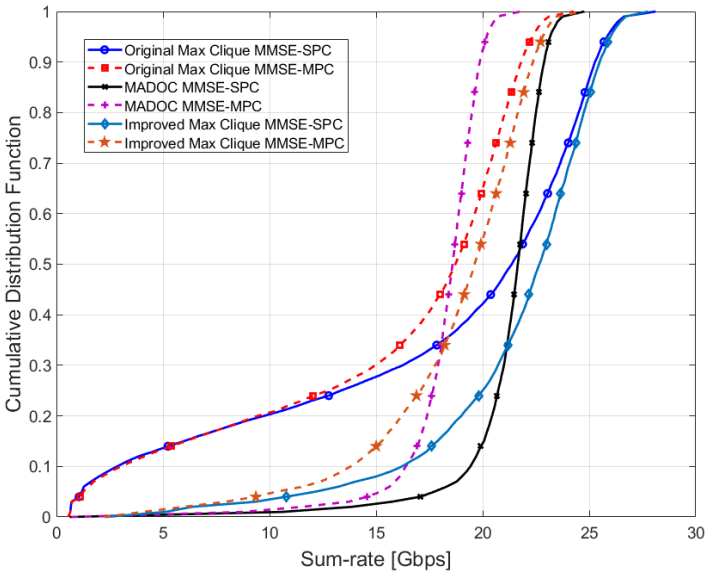


**Figure 5.3:** CDF of the per-cluster sum-rate capacity.

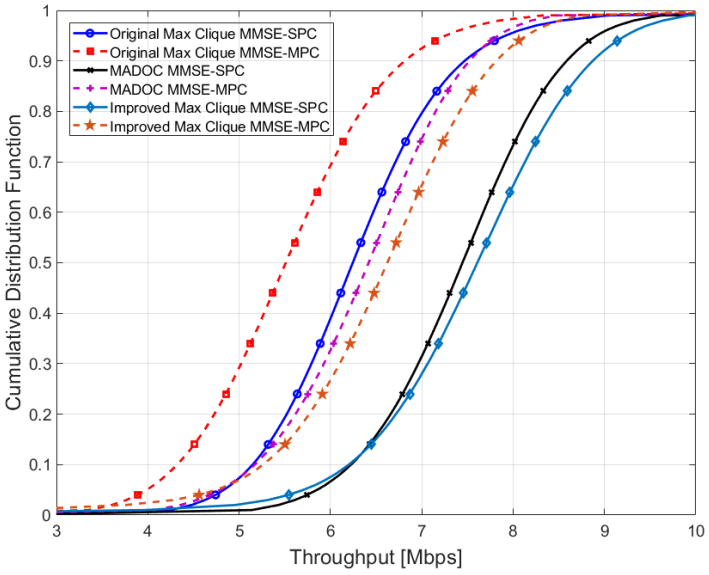


**Figure 5.4:** CDF of the user throughput.

In Fig. 5.3, the CDF of the per-cluster sum-rate capacity for all the considered schedulers is shown. Only 8% of the clusters experience less than 15 Gbps with the improved Max clique for MMSE-SPC, whereas the percentage increases to 28% with the original max clique. Fig. 5.4 shows the CDF of the users' throughput. It can be noticed that on average the throughput with the improved Max clique with MMSE-glsmpc is increased by 0.2 Mbps w.r.t. MADOC [77], and 1.4 Mbps when compared with the CSI-based scheduler [90]. To further validate the results, we present the histograms for both the improved and the original Max Clique schedulers. It can be observed that Fig. 5.6 shows a significant reduction in the cluster size variance, as opposed to Fig. 5.5.

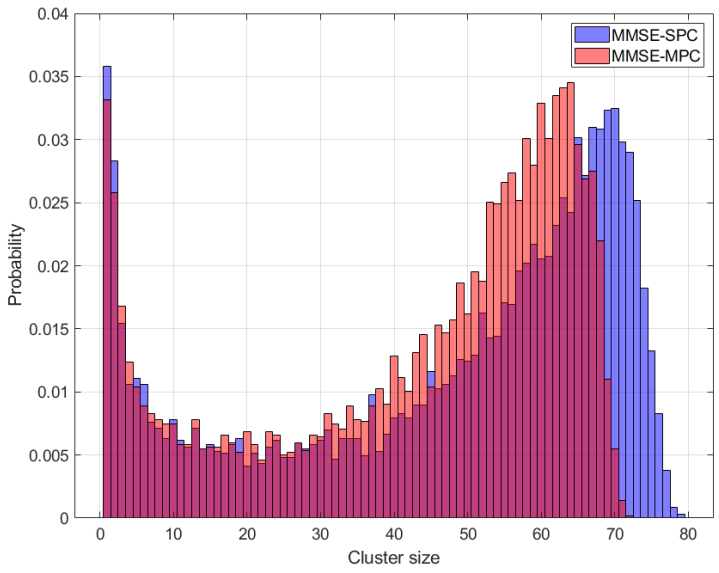


**Figure 5.5:** Original Max Clique.

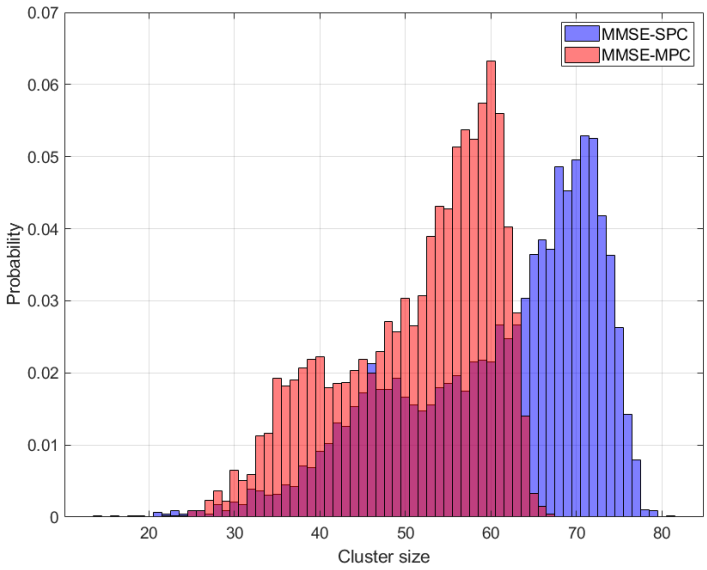


**Figure 5.6:** Improved Max Clique.

## 5.4 Conclusion

Here, we have proposed a novel solution that aimed to maximize the cluster mean size. A heuristic optimization (i.e., by extensive simulations) of the graph density values which maximizes the average per-user capacity is performed. The points where the graph densities intersect with the respective graph threshold values were determined by using the bisection method, and, also, the size of the maximum clique at each iteration. The results of the graph with Improved Max Clique Scheduler (i.e., maximum clique algorithm with constant density and variable threshold values) reveal that the per-user capacity (Mbps) is not compromised w.r.t. the CSI-based and Distance-based maximum clique schedulers, as well as the sum-rate capacity, is highly improved and the problem of group num-

ber minimization is also addressed. Results are presented in terms of per-cluster sum-rate capacity and user throughput. The presented novel solution overcomes the issue of group number minimization w.r.t. CSI-based maximum clique scheduler [90], Distance-based maximum clique scheduler (presented in Chapter 4) and MADOC [77]. and significantly improves the overall performance of the system with much lower computational complexity.

# Chapter 6 - Conclusion

The thesis focuses on indirect-based user scheduling algorithms for MB-LEO MU-MIMO NTN systems based on graph theory. Because of the unusually high density of UTs on the ground in relation to the available satellite antennas, users are organized into various clusters to facilitate scheduling based on a reliable grouping indicator: After the users within each cluster have been multiplexed and served together via SDM, also known as digital beamforming or MU-MIMO techniques, TDM is used to serve the various user clusters on different time slots. Implementing an ideal user grouping method is an NP-complete problem that can only be solved by exhaustive searching.

First, in Chapter 2, a comprehensive system model is presented. For the appropriate user scheduling algorithms to be implemented it is extremely important to have a practical channel model. Various aspects like space segment and spot beams setup, Antenna array model, Computation of beamforming matrix, user scheduling framework in the unicast, and the power normalizations i.e., SPC, MPC, and PAC are also comprehensively discussed along with their equations. This Chapter is considered to be the foundation for all the following chapters.

In Chapter 3, we proposed a greedy iterative user scheduling procedure based on the maximum clique algorithm for this work a thorough examination

was carried out, taking into account both the maximal and maximum clique-based approaches along with the complexity analysis. Finally, the maximum clique-based approach was adopted to reduce computational complexity and perform user scheduling in an effective and efficient manner, and the adopted algorithm was further improved by relaxing the upper bound values to find the maximum clique and by color sorting. For a single MB satellite MU-MIMO system, the maximum clique-based scheduler Capacity (Mbps), SINR [dB], and Spectral Efficiency (b/s/Hz) are compared to a position-based approach. A digital MMSE beamforming matrix allows us to spatially separate the scheduled users for each time slot, and we considered three power normalizations for the beamforming matrix: SPC, MPC, and PAC. The results are presented in terms of achievable per-user capacity, SINR, and spectral efficiency, and they reveal that clique-based scheduling performs significantly better than position-based scheduling [72]. Furthermore, the proposed algorithm requires the instantaneous availability of CSI.

In Chapter 4, we proposed an iterative user scheduling procedure based on the maximum-clique algorithm and extended the work provided in the previous chapter by taking the users' great circle distance into account when forming the graph's adjacency matrix. This modification allows the maximum clique algorithm to perform in situations where there is no CSI availability with the consideration that CSI knowledge at the transmitter will be required during the transmission phase, but on a cluster level. Also, a high user density was adopted to determine whether or not the maximum clique approach is appropriate for a high user density. Both the CSI-based and the distance-based scenarios were op-

timized. A digital MMSE beamforming matrix was implemented for each cluster to spatially separate the scheduled users, and two power normalizations are considered for the MMSE matrix: SPC and MPC. Despite the fact that extensive simulation results revealed that the maximum clique algorithm is highly capable and performance-oriented, an effort was made to re-implement the MADOC scheduler to further validate the analysis. The optimal threshold values for both graph-based schedulers (CSI, and Distance-based), and MADOC were optimized, and the results were presented in terms of achievable per-user capacity and SINR, demonstrating an improvement in the performance of both graph-based schedulers in comparison to the MADOC [77].

In Chapter 5, we proposed a user-scheduling framework that aimed to maximize the mean cluster size. From the mean-cluster size optimization results for the CSI-based maximum clique algorithm, Distance-based maximum clique algorithm, and MADOC, it was observed while analyzing the cluster distributions that these schedulers can generate clusters of very small sizes since the cluster size decreases as the graph gets pruned at each iteration. Therefore, we propose this new novel approach in an attempt to decrease the variance of the cluster size distribution. Instead of having a fixed threshold value and performing threshold optimization, the optimal graph density is determined. A heuristic optimization (i.e., by extensive simulations) of the graph density values which maximizes the average per-user capacity is performed. The points where the graph densities intersect with the respective graph threshold values were determined by using the bisection method, and, also, the size of the maximum clique at each iteration.

Not only this proposed scheduler solves the issue of group number minimization w.r.t. all the previous schedulers that are presented in Chapters 3 and 4, but also the performance has not been compromised.

## 6.1 Future work

The following represents different dimensions that need to be evaluated in the future

- For simplicity, we considered a single MB LEO satellite without the users' moment taken into account. There is a need to perform an analysis and evaluate the presented graph-based user scheduling techniques which consider the swarm of LEO satellites and the user's moments

- In this thesis, in all the presented contributions, the user scheduling was addressed on a uniform distribution of users. Although the maximum clique and graph-based approach performed very well when we considered a much larger number of users $K_T = 5700$ in Chapter 4, as compared to $K_T = 2850$ in Chapter. 3 but still there is a need to perform analysis on the realistic user distribution. One of our future works foresees the evaluation of these graph-based user scheduling techniques on the non-uniform distribution of users. We aim to present this work to
  *"B. De Filippo, B. Ahmad, D. G. Riviello, A. Guidotti, and A. Vanelli-Coralli, "Non-Uniform User Distribution in Non-Terrestrial Networks with Application to User Scheduling," IEEE GLOBECOM, Malaysia, 2023"*

- The considered Maximum Clique algorithm i.e., Max Clique Dyn algorithm is a branch and bound algorithm with color sorting and an improved version but it is not a fully optimal solution, and evaluating the exact computational complexity analysis is difficult. In the future, we desire to present a clique algorithm that is exact and less computationally expensive

- The introduction of subarrays in the satellite to obtain much more directive beams is also a very interesting topic and can be worthwhile to be considered.

# References


[1] Alessandro Guidotti and Alessandro Vanelli-Coralli. Clustering strategies for multicast precoding in multi-beam satellite systems. *CoRR*, abs/1804.03891, 2018.

[2] Alessandro Di Mezza, Alessandro Vanelli Coralli, Alessandro Guidotti, Tommaso Foggi, Giulio Colavolpe, and Guido Montorsi. 5g4space: Adaptation of 5g radio access technology for satcom. In *2019 International Symposium on Advanced Electrical and Communication Technologies (ISAECT)*, pages 1–3, 2019.

[3] Oltjon Kodheli, Eva Lagunas, Nicola Maturo, Shree Krishna Sharma, Bhavani Shankar, Jesus Fabian Mendoza Montoya, Juan Carlos Merlano Duncan, Danilo Spano, Symeon Chatzinotas, Steven Kisseleff, Jorge Querol, Lei Lei, Thang X. Vu, and George Goussetis. Satellite communications in the new space era: A survey and future challenges. *IEEE Communications Surveys & Tutorials*, 23(1):70–109, 2021.

[4] Alessandro Guidotti, Alessandro Vanelli-Coralli, Matteo Conti, Stefano Andrenacci, Symeon Chatzinotas, Nicola Maturo, Barry Evans, Adegbenga Awoseyila, Alessandro Ugolini, Tommaso Foggi, Lorenzo Gaudio, Nader Alagha, and Stefano Cioni. Architectures and key technical challenges for 5g systems incorporating satellites. *IEEE Transactions on Vehicular Technology*, 68(3):2624–2639, 2019.

[5] Ikbal Chammakhi Msadaa, Sajeh Zairi, and Amine Dhraief. Non-terrestrial networks in a nutshell. *IEEE Internet of Things Magazine*, 5(2):168–174, 2022.

[6] William Stalling. *Wireless communications and networks*. Pearson Prentice Hall, 2005.

[7] European Commission. Low-earth orbit satellites: Spectrum access. Survey, EC, 2017.

[8] 3GPP. 5g; nr; base station (bs) radio transmission and reception (release 16). Rec. TS 38.104 version 16.4.0, 3GPP, July 2020.

[9] Mingchuan Yang, Xinye Shao, Guanchang Xue, Botao Liu, and Yanyong Su. Regularized zero-forcing dirty paper precoding in a high-throughput satellite communication system. *Electronics*, 11(19), 2022.

[10] Shicong et all. Liu. Leo satellite constellations for 5g and beyond: How will they reshape vertical domains? *IEEE Communications Magazine*, 59(7):30–36, 2021.

[11] Sudhakar Rao, Minh Tang, Chih-Chien Hsu, and Jim Wang. Advanced antenna technologies for satellite communication payloads. In *2006 First European Conference on Antennas and Propagation*, pages 1–6, 2006.

[12] J. Tronc, P. Angeletti, N. Song, M. Haardt, J. Arendt, and G. Gallinaro. Overview and comparison of on-ground and on-board beamforming techniques in mobile satellite service applications. *International Journal of Satellite Communications and Networking*, 32(4):291–308, 2014.

[13] Marko Höyhtyä, Sandrine Boumard, Anastasia Yastrebova, Pertti Järvensivu, Markku Kiviranta, and Antti Anttonen. Sustainable satellite communications in the 6g era: A european view for multilayer systems and space safety. *IEEE Access*, 10:99973–100005, 2022.

[14] Yaomin Zhang, Haijun Zhang, Huan Zhou, Keping Long, and George K. Karagiannidis. Resource allocation in terrestrial-satellite-based next generation multiple access networks with interference cooperation. *IEEE Journal on Selected Areas in Communications*, 40(4):1210–1221, 2022.

[15] Nazli Ahmad Khan Beigi and Mohammad Reza Soleymani. Interference management using cooperative noma in multi-beam satellite systems. In *2018 IEEE International Conference on Communications (ICC)*, pages 1–6, 2018.

[16] Alessandro Ugolini, Giulio Colavolpe, Martina Angelone, Alessandro Vanelli-Coralli, and Alberto Ginesi. Capacity of interference exploitation schemes in multibeam satellite systems. *IEEE Transactions on Aerospace and Electronic Systems*, 55(6):3230–3245, 2019.

[17] Alessandro Ugolini, Yuri Zanettini, Amina Piemontese, Alessandro Vanelli-Coralli, and Giulio Colavolpe. Efficient satellite systems based on interfer-

ence management and exploitation. In *2016 50th Asilomar Conference on Signals, Systems and Computers*, pages 492–496, 2016.

[18] Baofeng Ji, Yanan Wang, Kang Song, Chunguo Li, Hong Wen, Varun G Menon, and Shahid Mumtaz. A survey of computational intelligence for 6g: Key technologies, applications and trends. *IEEE Transactions on Industrial Informatics*, 17(10):7145–7154, 2021.

[19] Hong-Yunn Chen, Cheng-Fu Chou, and Leana Golubchik. Joint iwmmse-based channel estimation and finsler-manifold-based codebook for the design of v2x fdd massive mimo systems. In *2019 IEEE 89th Vehicular Technology Conference (VTC2019-Spring)*, pages 1–6. IEEE, 2019.

[20] DP Gaillot, Pierre Laly, N Dahmouni, Gauthier Delbarre, Matthias Van den Bossche, Günter Vermeeren, Emmeric Tanghe, EP Simon, Wout Joseph, Luc Martens, et al. Measurement of the v2i massive radio channel with the mamimosa sounder in a suburban environment. In *2021 15th European Conference on Antennas and Propagation (EuCAP)*, pages 1–4. IEEE, 2021.

[21] Gaurang Naik, Biplav Choudhury, and Jung-Min Park. Ieee 802.11 bd & 5g nr v2x: Evolution of radio access technologies for v2x communications. *IEEE access*, 7:70169–70184, 2019.

[22] Shibiao He, Jieru Du, and Yong Liao. Multi-user scheduling for 6g v2x ultra-massive mimo system. *Sensors*, 21(20), 2021.

[23] Hayder Al-Hraishawi, Houcine Chougrani, Steven Kisseleff, Eva Lagunas, and Symeon Chatzinotas. A survey on non-geostationary satellite systems: The communication perspective. *IEEE Communications Surveys & Tutorials*, pages 1–1, 2022.

[24] Alessandro Guidotti, Alessandro Vanelli-Coralli, Alberto Mengali, and Stefano Cioni. Non-terrestrial networks: Link budget analysis. In *ICC 2020 - 2020 IEEE International Conference on Communications (ICC)*, pages 1–7, 2020.

[25] et al. Vazquez, Miguel. Precoding in multibeam satellite communications: Present and future challenges. *IEEE Wireless Commun Mag*, 23, 06 2015.

[26] Vincenzo Icolari, Alessandro Guidotti, Daniele Tarchi, and Alessandro Vanelli-Coralli. An interference estimation technique for satellite cognitive radio systems. In *2015 IEEE International Conference on Communications (ICC)*, pages 892–897. IEEE, 2015.

[27] Symeon Chatzinotas, Barry Evans, Alessandro Guidotti, Vincenzo Icolari, Eva Lagunas, Sina Maleki, Shree Krishna Sharma, Daniele Tarchi, Paul Thompson, and Alessandro Vanelli-Coralli. Cognitive approaches to enhance spectrum availability for satellite systems. *International Journal of Satellite Communications and Networking*, 35(5):407–442, 2017.

[28] Konstantinos Liolis, Gerald Schlueter, Jens Krause, Frank Zimmer, Laurent Combelles, Joel Grotz, Symeon Chatzinotas, Barry Evans, Alessandro Guidotti, Daniele Tarchi, et al. Cognitive radio scenarios for satellite communications: The corasat approach. In *2013 Future Network & Mobile Summit*, pages 1–10. IEEE, 2013.

[29] R. F. E. Guy. Potential benefits of dynamic beam synthesis to mobile satellite communication, using the inmarsat 4 antenna architecture as a test example. *International Journal of Antennas and Propagation*, 2009:1–5, 2009.

[30] Bertrand Grau Richard Swinford. High throughput satellites: Delivering future capacity needs. *ARTHUR D LITTLE*, July 2015.

[31] Robert T Schwarz, Thomas Delamotte, Kai-Uwe Storek, and Andreas Knopp. Mimo applications for multibeam satellites. *IEEE Transactions on Broadcasting*, 65(4):664–681, 2019.

[32] Miguel Ángel Vázquez, Ana Perez-Neira, Dimitrios Christopoulos, Symeon Chatzinotas, Björn Ottersten, Pantelis-Daniel Arapoglou, Alberto Ginesi, and Giorgio Taricco. Precoding in multibeam satellite communications: Present and future challenges. *IEEE Wireless Communications*, 23(6):88–95, 2016.

[33] Nick Letzepis and Alex J Grant. Capacity of the multiple spot beam satellite channel with rician fading. *IEEE Transactions on Information Theory*, 54(11):5210–5222, 2008.

[34] Wenjin Wang, Ao Liu, Qian Zhang, Li You, Xiqi Gao, and Gan Zheng. Robust multigroup multicast transmission for frame-based multi-beam satellite systems. *IEEE Access*, 6:46074–46083, 2018.

[35] Li You, Ao Liu, Wenjin Wang, and Xiqi Gao. Outage constrained robust multigroup multicast beamforming for multi-beam satellite communication systems. *IEEE Wireless Communications Letters*, 8(2):352–355, 2018.

[36] Giuseppe Caire, Merouane Debbah, L Cottatellucci, R De Gaudenzi, R Rinaldo, R Mueller, and G Gallinaro. Perspectives of adopting interference mitigation techniques in the context of broadband multimedia satellite systems. In AIAA, editor, *ICSSC 2005, 23rd AIAA International Communications Satellite Systems Conference, 25-28 September, 2005, Rome, Italy*, Rome, 2005.

[37] Laura Cottatellucci, Merouane Debbah, E Casini, R Rinaldo, R Mueller, M Neri, and G Gallinaro. Interference mitigation techniques for broadband satellite system. In AIAA, editor, *ICSSC 2006, 24th AIAA International Communications Satellite Systems Conference, 11-15 June 2006, San Diego, USA*, San Diego, 2006.

[38] Pantelis-Daniel Arapoglou, Konstantinos Liolis, Massimo Bertinelli, Athanasios Panagopoulos, Panayotis Cottis, and Riccardo De Gaudenzi. Mimo over satellite: A review. *IEEE Communications Surveys & Tutorials*, 13(1):27–51, 2011.

[39] Hien Quoc Ngo, Alexei Ashikhmin, Hong Yang, Erik G. Larsson, and Thomas L. Marzetta. Cell-free massive mimo versus small cells. *IEEE Transactions on Wireless Communications*, 16(3):1834–1850, 2017.

[40] S. M. Riazul Islam, Nurilla Avazov, Octavia A. Dobre, and Kyung-sup Kwak. Power-domain non-orthogonal multiple access (noma) in 5g systems: Potentials and challenges. *IEEE Communications Surveys & Tutorials*, 19(2):721–742, 2017.

[41] Alan Barbieri, Dario Fertonani, and Giulio Colavolpe. Time-frequency packing for linear modulations: spectral efficiency and practical detection schemes. *IEEE Transactions on Communications*, 57(10):2951–2959, 2009.

[42] Giulio Colavolpe, Andrea Modenini, Amina Piemontese, and Alessandro Ugolini. Multiuser detection in multibeam satellite systems: Theoretical analysis and practical schemes. In *2015 IEEE 16th International Workshop on Signal Processing Advances in Wireless Communications (SPAWC)*, pages 525–529, 2015.

[43] Kai Yuan Zhong, Yu Jian Cheng, Hai Ning Yang, and Bin Zheng. Leo satellite multibeam coverage area division and beamforming method. *IEEE Antennas and Wireless Propagation Letters*, 20(11):2115–2119, 2021.

[44] Hanan Weingarten, Yossef Steinberg, and Shlomo Shitz Shamai. The capacity region of the gaussian multiple-input multiple-output broadcast channel. *IEEE transactions on information theory*, 52(9):3936–3964, 2006.

[45] Alex B Gershman, Nicholas D Sidiropoulos, Shahram Shahbazpanahi, Mats Bengtsson, and Bjorn Ottersten. Convex optimization-based beamforming. *IEEE Signal Processing Magazine*, 27(3):62–75, 2010.

[46] Christian B Peel, Bertrand M Hochwald, and A Lee Swindlehurst. A vector-perturbation technique for near-capacity multiantenna multiuser communication-part i: channel inversion and regularization. *IEEE Transactions on Communications*, 53(1):195–202, 2005.

[47] Harsh Tataria, Peter J Smith, Larry J Greenstein, and Pawel A Dmochowski. Zero-forcing precoding performance in multiuser mimo systems with heterogeneous ricean fading. *IEEE Wireless Communications Letters*, 6(1):74–77, 2016.

[48] Quentin H Spencer, A Lee Swindlehurst, and Martin Haardt. Zero-forcing methods for downlink spatial multiplexing in multiuser mimo channels. *IEEE transactions on signal processing*, 52(2):461–471, 2004.

[49] Runhua Chen, Zukang Shen, Jeffrey G Andrews, and Robert W Heath. Multimode transmission for multiuser mimo systems with block diagonalization. *IEEE Transactions on Signal Processing*, 56(7):3294–3302, 2008.

[50] Zukang Shen, Runhua Chen, Jeffrey G Andrews, Robert W Heath, and Brian L Evans. Low complexity user selection algorithms for multiuser

mimo systems with block diagonalization. *IEEE Transactions on Signal Processing*, 54(9):3658–3663, 2006.

[51] Emil Björnson, Marios Kountouris, Mats Bengtsson, and Björn Ottersten. Receive combining vs. multi-stream multiplexing in downlink systems with multi-antenna users. *IEEE Transactions on Signal Processing*, 61(13):3431–3446, 2013.

[52] Qiang Hu, Meixiang Zhang, and Renzheng Gao. Key technologies in massive mimo. In *ITM Web of Conferences*, volume 17, page 01017. EDP Sciences, 2018.

[53] Emil Björnson, Mats Bengtsson, and Björn Ottersten. Optimal multiuser transmit beamforming: A difficult problem with a simple solution structure [lecture notes]. *IEEE Signal Processing Magazine*, 31(4):142–148, 2014.

[54] Mahmoud A. Albreem, Alaa H. Al Habbash, Ammar M. Abu-Hudrouss, and Salama S. Ikki. Overview of precoding techniques for massive mimo. *IEEE Access*, 9:60764–60801, 2021.

[55] Alessandro Guidotti and Alessandro Vanelli-Coralli. Design trade-off analysis of precoding multi-beam satellite communication systems. In *2021 IEEE Aerospace Conference (50100)*, pages 1–12, 2021.

[56] Taek Keun Lyu. Capacity of multi-user mimo systems with mmse and zf precoding. In *2016 IEEE Conference on Computer Communications Workshops (INFOCOM WKSHPS)*, pages 1083–1084, 2016.

[57] Sourjya Bhaumik, Shoban Preeth Chandrabose, Manjunath Kashyap Jataprolu, Gautam Kumar, Anand Muralidhar, Paul Polakos, Vikram Srinivasan, and Thomas Woo. Cloudiq: A framework for processing base stations in a data center. In *Proceedings of the 18th annual international conference on Mobile computing and networking*, pages 125–136, 2012.

[58] Yuanyuan Dong, Zhenyu Zhang, Chen Liang, Xiaoxiao Yin, Xiyuan Wang, Runmin Zou, and Xiaoming Dai. A low-complexity precoding method based on the steepest descent algorithm for downlink massive mimo systems. In *2018 IEEE/CIC International Conference on Communications in China (ICCC)*, pages 17–21. IEEE, 2018.

[59] Xu Qiao, Yao Zhang, and Longxiang Yang. Conjugate gradient method based linear precoding with low-complexity for massive mimo systems. In *2018 IEEE 4th International Conference on Computer and Communications (ICCC)*, pages 420–424. IEEE, 2018.

[60] Nusrat Fatema, Guang Hua, Yong Xiang, Dezhong Peng, and Iynkaran Natgunanathan. Massive mimo linear precoding: A survey. *IEEE systems journal*, 12(4):3920–3931, 2017.

[61] Yimeng Bai, Zhonghua Liang, Chenhui Zhai, Yue Xin, and Wei Li. Joint precoding using successive over-relaxation matrix inversion and newton iteration for massive mimo systems. In *2019 11th International Conference on Wireless Communications and Signal Processing (WCSP)*, pages 1–5. IEEE, 2019.

[62] Mahmoud A Albreem, Markku Juntti, and Shahriar Shahabuddin. Massive mimo detection techniques: A survey. *IEEE Communications Surveys & Tutorials*, 21(4):3109–3132, 2019.

[63] Subuh Pramono, Eddy Triyono, and Budi Basuki Subagio. Performance of leakage based precoding scheme for minimizing interference. *J. Commun.*, 15(2):214–220, 2020.

[64] Ehab Ali, Mahamod Ismail, Rosdiadee Nordin, and Nor Fadzilah Abdulah. Beamforming techniques for massive mimo systems in 5g: overview, classification, and trends for future research. *Frontiers of Information Technology & Electronic Engineering*, 18:753–772, 2017.

[65] M. Mahdi Azari, Sourabh Solanki, Symeon Chatzinotas, Oltjon Kodheli, Hazem Sallouha, Achiel Colpaert, Jesus Fabian Mendoza Montoya, Sofie Pollin, Alireza Haqiqatnejad, Arsham Mostaani, Eva Lagunas, and Bjorn Ottersten. Evolution of non-terrestrial networks from 5g to 6g: A survey. *IEEE Communications Surveys & Tutorials*, 24(4):2633–2672, 2022.

[66] Puneeth Jubba Honnaiah, Eva Lagunas, Nicola Maturo, and Symeon Chatzinotas. Demand-aware beam design and user scheduling for precoded multibeam geo satellite systems. In *WSA 2021; 25th International ITG Workshop on Smart Antennas*, pages 1–6, 2021.

[67] Alessandro Guidotti, Carla Amatetti, Fabrice Arnal, Baptiste Chamaillard, and Alessandro Vanelli-Coralli. Location-assisted precoding in 5g leo systems: architectures and performances. In *2022 Joint European Conference on Networks and Communications & 6G Summit (EuCNC/6G Summit)*, pages 154–159, 2022.

[68] Li You, Ke-Xin Li, Jiaheng Wang, Xiqi Gao, Xiang-Gen Xia, and Björn Ottersten. Massive mimo transmission for leo satellite communications. *IEEE Journal on Selected Areas in Communications*, 38(8):1851–1865, 2020.

[69] Hlib Cheporniuk, Robert T. Schwarz, Thomas Delamotte, and Andreas Knopp. Mimo throughput performance analysis in leo communication scenario. In *2021 IEEE 94th Vehicular Technology Conference (VTC2021-Fall)*, pages 01–06, 2021.

[70] Ke-Xin Li, Li You, Jiaheng Wang, Xiqi Gao, Christos G. Tsinos, Symeon Chatzinotas, and Björn Ottersten. Downlink transmit design for massive mimo leo satellite communications. *IEEE Transactions on Communications*, 70(2):1014–1028, 2022.

[71] Xinping Yi and Edward K. S. Au. User scheduling for heterogeneous multiuser mimo systems: A subspace viewpoint. *IEEE Transactions on Vehicular Technology*, 60(8):4004–4013, 2011.

[72] Alessandro Guidotti and Alessandro Vanelli-Coralli. Geographical scheduling for multicast precoding in multi-beam satellite systems. In *2018 9th Advanced Satellite Multimedia Systems Conference and the 15th Signal Processing for Space Communications Workshop (ASMS/SPSC)*, pages 1–8, 2018.

[73] Yang Liu, Changqing Li, Jiong Li, and Lu Feng. Joint user scheduling and hybrid beamforming design for massive mimo leo satellite multigroup multicast communication systems. *Sensors (Basel, Switzerland)*, 22(18):6858, September 2022.

[74] Dimitrios Christopoulos, Symeon Chatzinotas, and Björn Ottersten. Multicast multigroup precoding and user scheduling for frame-based satellite communications. *IEEE Transactions on Wireless Communications*, 14(9):4695–4707, 2015.

[75] Puneeth Jubba Honnaiah, Eva Lagunas, Danilo Spano, Nicola Maturo, and Symeon Chatzinotas. Demand-based scheduling for precoded multibeam high-throughput satellite systems. *2021 IEEE Wireless Communications and Networking Conference (WCNC)*, pages 1–6, 03 2021.

[76] Ashok Bandi, Bhavani Shankar M. R, Symeon Chatzinotas, and Björn Ottersten. A joint solution for scheduling and precoding in multiuser miso downlink channels. *IEEE Transactions on Wireless Communications*, 19(1):475–490, 2020.

[77] Kai-Uwe Storek and Andreas Knopp. Fair user grouping for multibeam satellites with mu-mimo precoding. In *GLOBECOM 2017 - 2017 IEEE Global Communications Conference*, pages 1–7, 2017.

[78] Roberto P. Antonioli, Gábor Fodor, Pablo Soldati, and Tarcisio F. Maciel. User scheduling for sum-rate maximization under minimum rate constraints for the mimo ibc. *IEEE Wireless Communications Letters*, 8(6):1591–1595, 2019.

[79] Giorgio Taricco. Linear precoding methods for multi-beam broadband satellite systems. In *European Wireless 2014; 20th European Wireless Conference*, pages 1–6, 2014.

[80] Vahid Joroughi, Miguel Ángel Vázquez, and Ana I. Pérez-Neira. Generalized multicast multibeam precoding for satellite communications. *IEEE Transactions on Wireless Communications*, 16(2):952–966, 2017.

[81] Miguel Ángel Vázquez, M. R. Bhavani Shankar, Charilaos I. Kourogiorgas, Pantelis-Daniel Arapoglou, Vincenzo Icolari, Symeon Chatzinotas, Athanasios D. Panagopoulos, and Ana I. Pérez-Neira. Precoding, scheduling, and link adaptation in mobile interactive multibeam satellite systems. *IEEE Journal on Selected Areas in Communications*, 36(5):971–980, 2018.

[82] Dénes König. Theory of finite and infinite graphs. In *Theory of Finite and Infinite Graphs*, pages 45–421. Springer, 1990.

[83] Karen Hunger Parshall. America's first school of mathematical research: James joseph sylvester at the johns hopkins university 1876–1883. *Archive for History of Exact Sciences*, 38(2), 1988.

[84] Ahmed Douik, Hayssam Dahrouj, Tareq Y. Al-Naffouri, and Mohamed-Slim Alouini. A tutorial on clique problems in communications and signal processing. *Proceedings of the IEEE*, 108(4):583–608, 2020.

[85] Jerzy A. Filar, Michael Haythorpe, and Richard Taylor. Linearly-growing reductions of karp's 21 np-complete problems. *ArXiv*, abs/1902.10349, 2018.

[86] Richard M Karp. Reducibility among combinatorial problems. In *Complexity of computer computations*, pages 85–103. Springer, 1972.

[87] R Duncan Luce and Albert D Perry. A method of matrix analysis of group structure. *Psychometrika*, 14(2):95–116, 1949.

[88] Béla Bollobás. *Modern graph theory*, volume 184. Springer Science & Business Media, 1998.

[89] John Adrian Bondy, Uppaluri Siva Ramachandra Murty, et al. *Graph theory with applications*, volume 290. Macmillan London, 1976.

[90] Daniel Gaetano Riviello, Bilal Ahmad, Alessandro Guidotti, and Alessandro Vanelli-Coralli. Joint graph-based user scheduling and beamforming in leo-mimo satellite communication systems. In *2022 11th Advanced Satellite Multimedia Systems Conference and the 17th Signal Processing for Space Communications Workshop (ASMS/SPSC)*, pages 1–8, 2022.

[91] Malek Khammassi, Abla Kammoun, and Mohamed-Slim Alouini. Precoding for high throughput satellite communication systems: A survey, 2022.

[92] 3GPP. Solutions for nr to support non-terrestrial networks (ntn) (release 16). Rec. TR 38.821 V16.1.0, 3GPP, May 2021.

[93] 3GPP. Service requirements for the 5g system; stage 1 (release 18). Technical Report TS 22.261 V18.2.0, 3GPP, March 2021.

[94] ITU-R. Itu-r radiocommunication sector of itu, "modelling and simulation of imt networks and systems for use in sharing and compatibility studies". Technical Report M.2101-0), ITU-R, February 2017.

[95] Kuangming Jiang, Xiaoyong Wang, Yanliang Jin, Asad Saleem, and Guoxin Zheng. Design and analysis of high-capacity mimo system in line-of-sight communication. *Sensors*, 22(10), 2022.

[96] Coen Bron and Joep Kerbosch. Algorithm 457: Finding all cliques of an undirected graph. *Commun. ACM*, 16(9):575–577, sep 1973.

[97] Dewayne Rocky Aloysius. *Bron-Kerbosch Algorithm.* PopulPublishing, 2012.

[98] F. Cazals and C. Karande. A note on the problem of reporting maximal cliques. *Theoretical Computer Science*, 407(1):564–568, 2008.

[99] David Eppstein, Maarten Löffler, and Darren Strash. Listing all maximal cliques in sparse graphs in near-optimal time. *CoRR*, abs/1006.5440, 2010.

[100] J Gary Augustson and Jack Minker. An analysis of some graph theoretical cluster techniques. *Journal of the ACM (JACM)*, 17(4):571–588, 1970.

[101] Robert E Osteen and Julius T Tou. A clique-detection algorithm based on neighborhoods in graphs. *International Journal of Computer & Information Sciences*, 2(4):257–268, 1973.

[102] Robert E Osteen. Clique detection algorithms based on line addition and line removal. *SIAM Journal on Applied Mathematics*, 26(1):126–135, 1974.

[103] J. W. Moon and L. Moser. On cliques in graphs. *Israel Journal of Mathematics*, 3(1):23–28, 1965.

[104] Eralp Abdurrahim Akkoyunlu. The enumeration of maximal cliques of large graphs. *SIAM Journal on Computing*, 2(1):1–6, 1973.

[105] HC Johnston. Cliques of a graph-variations on the bron-kerbosch algorithm. *International Journal of Computer & Information Sciences*, 5(3):209–238, 1976.

[106] Leonhard Gerhards and Wolfgang Lindenberg. Clique detection for nondirected graphs: Two new algorithms. *Computing*, 21(4):295–322, 1979.

[107] Emmanuel Loukakis and Constantine Tsouros. A depth first search algorithm to generate the family of maximal independent sets of a graph lexicographically. *Computing*, 27(4):349–366, 1981.

[108] E Loukakis. A new backtracking algorithm for generating the family of maximal independent sets of a graph. *Computers & Mathematics with Applications*, 9(4):583–589, 1983.

[109] David S Johnson, Mihalis Yannakakis, and Christos H Papadimitriou. On generating all maximal independent sets. *Information Processing Letters*, 27(3):119–123, 1988.

[110] Ina Koch. Enumerating all connected maximal common subgraphs in two graphs. *Theoretical Computer Science*, 250(1-2):1–30, 2001.

[111] David Eppstein. Small maximal independent sets and faster exact graph coloring. *J. Graph Algorithms Appl*, 7(2):131–140, 2002.

[112] Eric Harley, Anthony Bonner, and Nathan Goodman. Uniform integration of genome mapping data using intersection graphs. *Bioinformatics*, 17(6):487–494, 2001.

[113] Eric Richard Harley. *Graph algorithms for assembling integrated genome maps*. PhD thesis, Ph. D. dissertation, University of Toronto, 2003, adviser-Anthony Bonner, 2003.

[114] David Eppstein. Small maximal independent sets and faster exact graph coloring. *J. Graph Algorithms Appl*, 7(2):131–140, 2002.

[115] Etsuji Tomita, Akira Tanaka, and Haruhisa Takahashi. The worst-case time complexity for generating all maximal cliques. In *International Computing and Combinatorics Conference*, pages 161–170. Springer, 2004.

[116] Etsuji Tomita, Akira Tanaka, and Haruhisa Takahashi. The worst-case time complexity for generating allmaximal cliques and computational experiments. *Theoretical computer science*, 363(1):28–42, 2006.

[117] Li Wan, Bin Wu, Nan Du, Qi Ye, and Ping Chen. A new algorithm for enumerating all maximal cliques in complex network. In *International Confer-*

*ence on Advanced Data Mining and Applications*, pages 606–617. Springer, 2006.

[118] Coen Bron and Joep Kerbosch. Algorithm 457: finding all cliques of an undirected graph. *Communications of the ACM*, 16(9):575–577, 1973.

[119] Frank Kose, Wolfram Weckwerth, Thomas Linke, and Oliver Fiehn. Visualizing plant metabolomic correlation networks using clique–metabolite matrices. *Bioinformatics*, 17(12):1198–1208, 2001.

[120] Janez Konc and Dušanka Janežič. An improved branch and bound algorithm for the maximum clique problem. In *An improved branch and bound algorithm for the maximum clique problem*, 2007.

[121] Steven Skiena. *Implementing discrete mathematics: combinatorics and graph theory with Mathematica*. Addison-Wesley Longman Publishing Co., Inc., 1991.

[122] Giorgio Ausiello, Pierluigi Crescenzi, Giorgio Gambosi, Viggo Kann, Alberto Marchetti-Spaccamela, and Marco Protasi. *Complexity and approximation: Combinatorial optimization problems and their approximability properties*. Springer Science & Business Media, 2012.

[123] Robert Endre Tarjan and Anthony E Trojanowski. Finding a maximum independent set. *SIAM Journal on Computing*, 6(3):537–546, 1977.

[124] Tang Jian. An o (2 0.304 n) algorithm for solving maximum independent set problem. *IEEE Transactions on Computers*, 100(9):847–851, 1986.

[125] John Michael Robson. Algorithms for maximum independent sets. *Journal of Algorithms*, 7(3):425–440, 1986.

[126] Fedor V Fomin, Fabrizio Grandoni, and Dieter Kratsch. A measure & conquer approach for the analysis of exact algorithms. *Journal of the ACM (JACM)*, 56(5):1–32, 2009.

[127] Kazuaki Yamaguchi and Sumio Masuda. A new exact algorithm for the maximum weight clique problem. In *ITC-CSCC: International Technical Conference on Circuits Systems, Computers and Communications*, pages 317–320, 2008.

[128] 3GPP. Study on new radio to support non-terrestrial networks release 15. Technical Report TR 38.811 V15.4.0, 3GPP, September 2020.

[129] Edy Winarno, Wiwien Hadikurniawati, and Rendy Nusa Rosso. Location based service for presence system using haversine method. In *2017 International Conference on Innovative and Creative Information Technology (ICITech)*, pages 1–4, 2017.

[130] Y. Saab and V. Rao. On the graph bisection problem. *IEEE Transactions on Circuits and Systems I: Fundamental Theory and Applications*, 39(9):760–762, 1992.